

Surface modification of nanofillers and encapsulation of healing agents for ROMP- and “click”-based self-healing polymer nanocomposites.

Dissertation
Zur Erlangung des
Doktorgrades
der Naturwissenschaften (Dr. rer. nat.)

der
Naturwissenschaftlichen Fakultät II
Chemie, Physik und Mathematik

der Martin-Luther-Universität Halle-Wittenberg

vorgelegt von
Herr M.Sc. Wilton Osim

geb. am 22.03.1983 in Usumutong.

Gutachter:
Prof. Dr. W. H. Binder

Prof. Dr. Liberata Guadagno

Verteidigung am 11.07.2018

Acknowledgement

Although this thesis is singularly authored, its completion was made possible by the timely contributions of key individuals to which I owe my utmost gratitude.

Firstly, my eternally unreserved thanks go to God for His boundless love and ability that pulled me through.

Special thanks to my Ph.D. supervisor, Prof. Wolfgang Binder for giving me the rare privilege to undertake my Ph.D. thesis in his highly esteemed research group and for duplicating his wealth of professional wisdom in me to the admiration of many. His support, encouragement, and personal guidance is second to none, and for this and lots more, I'll always be grateful.

Many thanks to my project partners Dr. Sravendra Rana, M.Sc. Philip Michael, and M.Sc. Ali Shaygan for being dear and rare.

My heart-felt appreciation to all my colleagues for their continued and unrelenting assistance, and for creating a very convenient environment that encouraged creativity. I would always be grateful for your love and friendliness. Of particular reference of gratitude are the following, Dr. Diana Döhler, Mrs. Susanne Tanner, Dr. Senbin Chen, Clement Appiah, Mrs. Anke Hassi for always being for me.

Finally, my love and thanks goes to my parents, siblings, and friends for believing in me to a fault. Thank you for always telling me I CAN.

Dedication

To my jewel of inestimable value.

Table of Contents

Chapter 1	
Introduction.....	1
1.1. Composites.....	1
1.2. Concept of self-healing materials.....	2
1.3. Self-healing nanocomposites and their applications.....	3
1.3.1. Carbon-based Self-healing nanocomposites.....	5
1.3.2. POSS-based self-healing nanocomposites.....	9
1.3.3. Clay-based self-healing nanocomposites.....	13
1.4. Modification of nanofillers and their self-healing nanocomposites.....	15
1.4.1. Nanoclays.....	15
1.4.1.1. Swelling of clay.....	16
1.4.1.2. Surface modification of clay materials.....	17
1.4.2. Polyhedral oligomeric silsesquioxanes.....	19
1.5. Enhancement of thermal and mechanical properties of polymers with POSS.....	21
1.6. Microencapsulation of healing agents for self-healing materials.....	21
1.6.1. General concept of microencapsulation.....	21
1.6.2. Supramolecular encapsulation.....	23
1.6.3. Emulsion Encapsulation.....	23
1.6.4. Miniemulsion/interfacial encapsulation.....	23
1.6.5. In-situ encapsulation.....	24
Chapter 2	
Aim and synthetic concept.....	25
2.1. Aim.....	25
2.2. Synthetic concept.....	26
Chapter 3	
Synthesis and characterization of Cu- and Ru-immobilized nanoclays.....	29
3.1. Modification of nanoclay with vinylbenzyl dodecyl ammonium chloride and subsequently with Grubbs catalyst.....	29
3.2. Modification of nanoclay with 5,6-di(11-(n,n,n-trimethylammonium)undecoxycarbonyl) norbornene and subsequently with Grubbs catalyst.....	32
3.3. Synthesis of modifiers for Cu (I) attachment.....	35

3.4. Modification of nanoclay with 3a , 3b , 5 and subsequent attachment of Cu (I).....	38
Chapter 4	
Synthesis and characterization of copper-immobilized POSS.....	42
4.1. Surface modification of glycidylisobutyl POSS for Cu (I) attachment.....	42
4.2. Surface modification of epoxycyclohexylisobutyl POSS for Cu (I) attachment.....	47
Chapter 5	
Performance evaluation of clays and POSS immobilized Cu and Ru catalysts.....	54
5.1. Kinetic investigation of Cu (I)-modified clay and POSS using DSC.....	54
Chapter 6	
Synthesis and encapsulation of multivalent alkynes and azides for click-based self-healing nanocomposites.....	61
6.1. Introduction.....	61
6.2. Synthesis of multivalent alkynes and azides.....	62
6.3. Encapsulation of trivalent compounds.....	64
Chapter 7	
Experimental part.....	68
7.1. Material.....	68
7.2. Measurements.....	68
7.3. Modification of nanoclay with VDAC and TAUN and subsequently with Grubbs catalyst	70
7.3.1. Synthesis of vinylbenzyl dodecyl ammonium chloride.....	70
7.3.2. Synthesis of 5-norbornene-2,3-dicarbonyl dichloride.....	71
7.3.3. Synthesis of 5-Norbornene diester.....	71
7.3.4. Synthesis of 5,6-di(11-(n,n,n-trimethylammonium)undecoxycarbonyl) norbornene	72
7.3.5. Surface modification of nanoclays with VDAC and subsequent attachment of Ru.....	72
7.3.6. Surface modification of nanoclays with 5,6-di(11-(n,n,n-trimethylammonium)undecoxycarbonyl) norbornene and subsequent attachment of Ru.....	73
7.4. Synthesis of modifiers for Cu (I) attachment and subsequent attachment of Cu carbenes....	73
7.4.1. Synthesis of 1-tert-butyl-1H-imidazole.....	74
7.4.2. Synthesis of tert-butyl-1-dodecylimidazolium bromide.....	74

7.4.3. Synthesis of 1-(2,4,6-trimethylphenyl)-1H-imidazole.....	74
7.4.4. Synthesis of 1-mesityl-1-dodecylimidazolium iodide.....	75
7.4.5. Synthesis of tertiary amino ligand.....	75
7.4.6. Surface modification of Na MMT with 6a and 6b and subsequent attachment of Cu (I).....	75
7.4.7. Surface modification of Na MMT with 5 and subsequent attachment of Cu (I).....	76
7.5. Synthesis of Cu-and Ru-modified POSS.....	76
7.5.1. Synthesis of azidohydrinisobutyl POSS	77
7.5.2.Synthesis of azidohydrincyclohexylisobutylPOSS.....	77
7.5.3.Synthesis of hexynylhydrincyclohexylisobutyl POSS via “click” chemistry.....	78
7.5.4. Synthesis of 1-methylimidazoliumhydrincyclohexylisobutyl POSS via “click” chemistry.....	78
7.5.5. Synthesis of hexynylhydrinisobutyl POSS via “click” chemistry.....	79
7.5.6. Synthesis of 1-methylimidazoliumhydringlycidylisobutyl POSS via “click” chemistry.....	79
7.5.7. Synthesis of 1,2,3-triazol-5-ylidene-copper(I) POSS complex.....	80
7.5.8. Synthesis of Cu(I)-imidazoliumcyclohexylisobutyl POSS complex.....	80
7.5.9. Synthesis of 1,2,3-triazol-5-ylidene-copper(I) POSS complex	81
7.5.10. Synthesis of Cu (I)-imidazoliumhydringlycidylisobutyl POSS complex.....	81
7.6. Synthesis and encapsulation of multivalent alkynes and azides.....	82
7.6.1. Azidation of trimethylolpropanetriglycidyl ether (TriAzOH).....	82
7.6.2. Synthesis of triazidomethylbenzopropanetriglycidyl ether.....	82
7.6.3. Synthesis of triazidomethyloctanopropanetriglycidyl ether.....	83
7.6.4. Synthesis of triazidomethylacetopropanetriglycidyl ether.....	83
7.6.5. Synthesis of trimethylethoxyprop-1-yne.....	84
Chapter 8	
Summary.....	85
8.0. References.....	90

List of figures

Figure 1.1: Schematic of the different structures of grapheme composite electrode material. All models refer to composites grapheme and the active material are synthesized through one-pot process.....	1
Figure 1.2: Classification of self-healing materials based on their mechanism. Source: Janet Sinn-Hanlon, Scott White, Ben Blaiszik.....	5
Figure 1.3: Synthesis of self-healing fatty acid rubber, its representative chemical structure rich of hydrogen bonds and the Young's modulus of self-healing fatty acid rubber/MWCNT nanocomposite as a function of MWCNT concentration. Source: Tongfei Wu and Biqiong Chen.....	7
Figure 1.4: Incorporation of glucose into fermented yeast. Source: Bonn et. al.....	8
Figure 1.5: (a) schematic PBS network cross-linked by boron/oxygen dative bonds, and (b) the pathway to the synthesis of polyborosiloxane (PBS) through modifying hydroxyl terminated polydimethylsiloxane (PDMS) using boric acid (BA) at ambient temperature, (c) schematic condensation of boric acid with one silanol end PDMS, (d) tensile strength and elongation at break and (e) Young's modulus. Source: Chen et. al.....	9
Figure 1.6: Na MMT structure containing <i>TOT</i> sheets and counterions in addition to the dispersion of these counterions in the clay gallery.....	18
Figure 1.7: The three sheet structure of a typical Na MMT clay material showing the penetration of water molecules at the interlayer of the clay gallery.....	19
Figure 1.8: Modification of Na MMT with cationic surfactants and the effect of the cationic exchange of counterions with organic molecules on the interlayer distance	20
Figure 1.9: Silsesquioxanes: (a) Q8 (Q = SiO _{2/2}), R = H, vinyl, epoxy, methacrylate, etc.; (b) R _x T _x (T = R-SiO _{3/2}), R = alkyl, alkene, acetylene, acrylate; (c) Typical sizes and volumes.....	23
Figure 2.0: General synthetic concept and pathways for the surface modification of clay and POSS, and subsequent attachment of metal catalysts on their surfaces.....	25
Figure 3.1.1: ¹ H NMR spectrum of vinylbenzyl dodecyl ammonium chloride.....	29
Figure 3.1.3 A: Thermogravimetric analysis of organoclay, and B: X-ray diffraction patterns of modified clay materials at different modification conditions.....	30
Figure 3.2.5: ¹ H spectra of 5,6-di(11-(n,n,n-trimethylammonium)undecoxycarbonyl) norbornene.....	33

Figure 3.2.7 A: Thermogravimetric analysis of Nmod clay, and B: X-ray diffraction patterns of modified clay materials at different modification conditions.....	33
Figure 3.3.1: ¹ H NMR spectrum of tert-butyl-1-dodecylimidazolium bromide.....	36
Figure 3.3.2: ¹ H NMR spectrum of 1-mesityl-1-dodecylimidazolium iodide.....	37
Figure 3.3.3: ¹ H NMR spectra of tertiary ammonium ligand.....	38
Figure 3.4.1: Thermogravimetric analysis, conducted under nitrogen atmosphere of modified clay: Na MT-TAL (11), Na MMT-TBIDBr (12a), Na MMT-TMPIDD (12b), and B: X-ray diffraction patterns of modified clay materials.....	39
Figure 3.4.5: X-ray photoemission spectroscopic analysis (XPS) measured at 200μ50W X-ray settings of NaMMT-TAL-Cu 12 showing the oxidation state of Cu.....	41
Figure 4.1.4: ¹ H NMR spectrum of hexynylhydrinisobutyl POSS 33a	44
Figure 4.1.8: ¹ H NMR spectrum of 1,2,3-triazol-5-ylidene-copper(I) POSS complex 35a	44
Figure 4.1.9: ¹ H NMR spectrum of 1-methylimidazoliumhydringlycidylisobutyl POSS 33b	45
Figure 4.1.10: ¹ H NMR spectrum of Cu (I)-imidazoliumhydringlycidylisobutyl POSS complex(35b).....	46
Figure 4.1.11: MALDI-TOF spectrum of hexynylhydrinisobutyl POSS 33a	47
Figure 4.2.4: ¹ H NMR spectrum of hexynylhydrincyclohexylisobutyl POSS 32a	49
Figure 4.2.7: ¹ H spectrum of Cu (I)-imidazoliumcyclohexylisobutyl POSS complex 34b	49
Figure 4.2.8: XPS analysis measured at 200μ50W X-ray settings for a) Ep-1H-Cu (34a) and b) Ep-1MIM-Cu 34b showing the observable shakeup satellites corresponding to Cu(I).....	50
Figure 4.2.9: MALDI-TOF spectrum of azidohdrincyclohexylisobutyl POSS 29	51
Figure 4.2.10: MALDI-TOF spectrum of hexynylhydrincyclohexylisobutyl POSS 32a	52
Figure 4.2.11: MALDI-TOF spectrum of 1-methylimidazoliumhydrincyclohexylisobutyl POSS 32b	52
Figure 5.1.1: DSC dynamic scan curves for trivalent alkyne, 37 and azide, 36 , systems (with 1 mol% Cu (I)-modified clay catalyst, 13b) at different heating rates of 5, 10, 15, and 20 °C/min- A , and DSC dynamic scan curves for trivalent alkynes and azides systems (with 1 mol% NaMMT 22 , NaMMT-TMPIDD 12b , and NaMMT-TMPIDD-Cu 13b , with trivalent azide, 42c , and alkyne, 38 curve as reference- B	55

Figure 5.1.2: DSC dynamic scan curves for trivalent alkyne, 37 and azide, 36 , systems (with 1 mol% Cu (I)-modified clay catalyst, 13a) at different heating rates of 5, 10, 15, and 20 °C/min- A , and DSC dynamic scan curves for trivalent alkynes and azides systems (with 1 mol% NaMMT 22 , NaMMT-TBIDBr 12a , and NaMMT-TBIDBr-Cu 13a , with trivalent azide, 42c , and alkyne, 38 curve as reference- B	56
Figure 5.1.3: DSC dynamic scan curves for trivalent alkyne, 37 and azide, 36 , systems (with 1 mol% Cu (I)-modified clay catalyst, 11) at different heating rates of 5, 10, 15, and 20 °C/min- A , and DSC dynamic scan curves for trivalent alkynes and azides systems (with 1 mol% NaMMT 22 , NaMMT-TAL 10 , and NaMMT-TAL-Cu 11 , with trivalent azide, 36 , and alkyne, 37 curve as reference B	57
Figure 5.1.4: DSC dynamic scan curves for trivalent alkyne, 37 and azide, 36 , systems (with 1 mol% Cu (I)-modified POSS catalyst, 34a) at different heating rates of 5, 10, 15, and 20 °C/min- A , and DSC dynamic scan curves for trivalent alkynes and azides systems (with 1 mol%, Ep-1H 32a , and Ep-1H-Cu 34a , with trivalent azide, 36 , and alkyne, 37 curve as reference- B	58
Figure 5.1.5: DSC dynamic scan curves for trivalent alkyne, 38 and azide, 42c , systems (with 1 mol% Cu (I)-modified POSS catalyst, 34b) at different heating rates of 5, 10, 15, and 20 °C/min- A , and DSC dynamic scan curves for trivalent alkynes and azides systems (with 1 mol% Ep-1MIM 32b , and Ep-1MIM-Cu 34b , with trivalent azide, 36 , and alkyne, 37 curve as reference- B	58
Figure 5.1.6: DSC dynamic scan curves for trivalent alkyne, 37 and azide, 36 , systems (with 1 mol% Cu (I)-modified POSS catalyst, 35a) at different heating rates of 5, 10, 15, and 20 °C/min- A , and DSC dynamic scan curves for trivalent alkynes and azides systems (with 1 mol% OH-1H 33a , and OH-1H-Cu 35a , with trivalent azide, 36 , and alkyne, 37 curve as reference- B	59
Figure 6.3.2: FE-SEM images of TriAzB (42a), TriAzM (42b), and TriAzAc (42c), measured under gas mode.....	65
Figure 6.3.3: FE-SEM images of TriMEP (31), measure under gas mode	65
Figure 6.3.4: FE-SEM images of TriMEP (38) +TriAzAc (42c), measured under gas mode....	65
Figure 8.1:General synthetic concept and pathways for the surface modification of clay and POSS, and also the encapsulation of trivalent alkynes and azides	78

List of tables

Table 1: Self-healing performance of PBS and MWCNT/PBS nanocomposites	8
Table 2: Healing results obtained from the scratch profiles before and after healing process....	11
Table 3: Names and structures of surfactants used for nanoclay modification.....	13
Table 4: Chemical, physic-chemical, and physico-mechanical microencapsulation processes and applications.....	22
Table 5: Effect of temperature and time on the loading of vinylbenzyl dodecyl ammonium chloride on NaMMT.....	31
Table 6: Influence of reaction time on the cationic exchange reaction of 21 with NaMMT 22 at 60 °C.....	34
Table 7: Flame atomic absorption spectrometric measurements of Grubbs-modified clay nanomaterials.....	35
Table 8: Interlayer d-spacing of modified clay materials measured by XRD using Ni filter CuK α radiation in transmission at a sample-detector distance of 9.85 cm.....	40
Table 9: Interlayer d-spacing of modified clay materials measured by XRD using Ni filter CuK α radiation in transmission at a sample-detector distance of 9.85 cm.....	53
Table 10: Summary of the enthalpies of the reaction per functional group, conversion, peak temperature and other kinetic parameters evaluated using DSC.....	60
Table 11: Thermal stability and vibrational peaks of multivalent alkynes and azides measured by IR.....	63
Table 12: Amount of encapsulated compounds calculated from ^1H NMR using naphthalene as internal standard.....	65
Table 13: Thermal stabilities of compounds and microcapsules determined by thermogravimetric analysis under nitrogen atmosphere.....	66
Table 14: Amount of Cu on the surface of various POSS catalysts synthesized, as determined by FAAS.....	88

List of schemes

Scheme 1: Synthesis of PU microcapsules using a prepolymer (BD-TDI prepolymer) and a chain extender (BD).....	3
Scheme 2: Molecular structure of compounds. Source: Guadagnoet. al.....	6
Scheme 3: Schematic procedure for the preparation of functionalized graphenenanosheets (FGNS). Source: Wu et. al.....	8
Scheme 4: Synthesis of rGO-POSS. Source: Namvariet. al.....	9
Scheme 5: Synthetic route to hyperbranchedsilsesquioxane polymer grafted graphene oxide (HPP-GO). Source: Zhang et. al.....	10
Scheme 6: (a) Schematic representation of the synthetic route from graphite to ApPOSS-graphene and ApPOSS-graphene/EP, and photographic images manifesting the dispersion of samples in solvent and cured EP nanocomposites. (b) Synthesis of poly(1,8-octanediol- ω -critic acid)-POSS prepolymers. Source: Duet. al.....	11
Scheme 7: Chemical structure of UPyNCO, UPCL, and nanocomposite preparation. Source: Neikirket. al.....	12
Scheme 2.1.1: Step by step synthetic rout for the successful synthesis of organic modifiers with potential sites for the immobilization of Cu(I), subsequent modification of nanoclays with modifiers and immobilization of Cu metal catalyst.....	26
Scheme 2.1.2: Step by step reaction pathways for the synthesis of organic modifiers with potential sites for the immobilization of Ru catalyst, subsequent modification of nanoclays and immobilization of Rucatalyst	27
Scheme 2.1.3: Surface modification of different POSS compounds with low molecular weight compounds with potential bonding sites for the immobilization of metal catalyst.....	28
Scheme 2.1.4: Synthetic representation of the synthesis of multivalent alkynes and azides with subsequent modifications.....	28
Scheme 3.1.1: Synthesis of vinylbenzyl dodecyl ammonium chloride (16) and subsequent modification of nanoclay with 16 and thereafter with Grubbs catalyst I.....	30
Scheme 3.2.1: Synthesis of 5,6-di(11-(n,n,n-trimethylammonium)undecoxy carbonyl) norbornene (21) followed by the modification of nanoclay with 21 and thereafter with Grubbs catalyst II.....	32

Scheme 3.3.1: Synthesis of the different organic modifiers with potential sites for Cu I attachment.....	35
Scheme 3.4.1: Synthetic representation of nanoclay modification and subsequent attachment of Cu(I).....	38
Scheme 4.1.1: Synthetic representation of glycidylisobutyl POSS modification with 1-hexyne and 1-propargyl-3-methylimidazole bromide, and subsequent attachment of Cu(I).....	42
Scheme 4.2.1: Synthetic representation of epoxycyclohexylisobutyl POSS modification and subsequent immobilization of Cu (I).....	47
Scheme 5.1.1: Schematic representation for ‘click’ cross linking reaction.....	54
Scheme 5.1.2: Chemical structures of modified catalysts used for kinetic investigation.....	55
Scheme 6.2.1: Schematic representation of multivalent alkynes and azides synthesized via azidation, nucleophilic and acetylation reactions.....	62
Scheme 7.3.1: Step by step reaction pathways for the synthesis of organic modifiers with potential sites for the immobilization of Rucatalyst.....	70
Scheme 7.4.1: Step by step synthetic rout for the successful synthesis of organic modifiers with potential sites for the immobilization of Cu(I).....	73
Scheme 7.5.1: Surface modification of different POSS compounds with low molecular weight compounds with potential bonding sites for the immobilization of metal catalyst	77
Scheme 7.6.1: Schematic representation of multivalent alkynes and azides synthesized via azidation, nucleophilic and acetylation reactions.....	82
Scheme 8.1: Step by step reaction pathways for the synthesis of organic modifiers with potential sites for the immobilization of Ru catalyst.....	85
Scheme 8.2:Synthetic representation for the modification of nanoclays with synthesized organic modifiers with metal-active binding sites followed by the subsequent immobilization of Ru catalyst.....	86
Scheme 8.3: Synthetic representation for the modification of nanoclays with the synthesized organic modifiers for the immobilization of metal catalyst and the subsequent immobilization of Cu(I) onto clay surface.....	87
Scheme 8.4: Surface modification of different POSS compounds with low molecular weight compounds with potential bonding sites for the immobilization of metal catalyst.....	88

Abbreviations

DCM	Dichloromethane
TGA	Thermogravimetric Analysis
POSS	Polyhedral oligomeric silsesquioxanes
Na MMT	Na-montmorillonite clay
VDAC	Vinylbenzyl dodecyl ammonium chloride
NMR	Nuclear magnetic resonance
Na MMT-TMPIDDD	Na-montmorillonite modified 1-mesityl-1-dodecylimidazolium iodide
NbnN ₂ +	5,6-di(11-(n,n,n-trimethylammonium)undecoxycarbonyl) norbornene
Na MMT-TBIDBr	Na-montmorillonite modified tert-butyl-1-dodecylimidazolium bromide
Na MMT-TAL	Na-montmorillonite modified tertiary ammonium ligand
MALDI-TOF	Matrix Assisted Laser Desorption/Ionization Time of Flight
IR	Infrared spectroscopy
ESI-TOF	Electrospray Ionization Time of Flight
LiTFA	Lithium trifluoromethanesulfonate
NaTFA	Sodium trifluoromethanesulfonate
OH-c-1H-Cu	1,2,3-triazol-5-ylidene-copper(I) POSS complex
OH-c-1MIM-Cu	Cu (I)-imidazoliumhydrinisobutyl POSS complex
Ep-1MIM-Cu	Cu (I)-imidazoliumcyclohexylisobutyl POSS complex
DCPD/ENB	Dicyclopentadiene/5-ethylidene-2-norbornene
TriAzAc	triazidomethylacetopropanetriglycidyl ether
TriAzB	triazidomethylbenzopropanetriglycidyl ether
TriAzM	triazidomethylcyclohexylisobutyl POSS complex
TBAB	Tetra-n-butylammonium bromide
TriMEP	1-(prop-2-ynyloxy)-2,2-bis((prop-2-ynyloxy)methyl)butane
BHT	Butylated hydroxytoluene
TBTA	Tris(benzyltriazolylmethyl)amine
DIPEA	N,N-Diisopropylethylamine

Abstract (English)

Self-healing systems have attracted lots of interest in recent times because of their ability to autonomously repair damages, caused when a material is exposed to some physical and chemical phenomena, including any mechanical rupture. The damage on the material creates a vent for the (encapsulated) healing agent to flow into contact with catalysts, thus forming a network that seals the cracked plane. Different self-healing systems have been reported but this thesis targets the surface modification of nanomaterials such as nanoclays and polyhedral oligomeric silsesquioxanes (POSS) with special organic modifiers, and subsequent attachment of specific metal particles/catalysts (Ru and Cu) onto their surfaces, which can be used subsequently for the activation of self-healing chemistry at room temperature. The synthesis of the organic modifiers (vinylbenzyl dodecyl ammonium chloride (VDAC), 5,6-di(11-(n,n,n-trimethylammonium)undecoxycarbonyl) norbornene (TAUN), 1-mesityl-1-dodecylimidazolium iodide (TMPIDD), 1-tertiary-butyl-1-dodecylimidazolium bromide (TBIDBr), and tertiary amino ligand (TAL)), having cationic sites necessary for cationic exchange reactions with nanoclays is achieved through a series of reaction steps followed by the attachment of Ru (for VDAC- and TAUN-modified clay) and Cu (for TMPIDD-, TAL- and TBIDBr-modified clay) catalysts. X-ray Photoelectron Spectroscopy (XPS), Flame Atomic Absorption Spectroscopy (FAAS), and Energy-dispersive X-ray Spectroscopy (EDX) have been used to quantify the amount and type of Ru and Cu-carbenes formed on the surface of the organoclay and the POSS. The quantitative amount and the thermal stability of the modifiers on the surface of the nanomaterials have been calculated via TGA, resulting in surface loading of the produced organoclay in the range 0.32×10^{-3} – 0.72×10^{-3} (mmol/mg).

The purity of the organic modifiers is investigated using Nuclear Magnetic Resonance (NMR)

and the molecular weight of the different POSS molecules is proven using Mass-assisted laser desorption/ionization-time of flight (MALDI-TOF) and the results found were consistent with theoretical calculations. Differential Scanning Calorimetry (DSC) measurement is conducted to investigate the catalytic activity of the metal particle-modified nanomaterials (with respect to the enthalpy of the cross linking reaction, the peak temperature and the temperature at which crosslinking starts). The obtained results demonstrate a high activity of immobilized Cu and Ru particles and the resulting particle-catalysts could be used to prepare “click”- and ROMP-based self-healing composites.

Abstract (German)

Selbstheilungssysteme haben in letzter Zeit viel Interesse auf sich gezogen, da sie in der Lage sind, Schäden, die verursacht werden, wenn ein Material physikalischen und chemischen Phänomenen ausgesetzt ist, einschließlich mechanischer Brüche, autonom zu reparieren. Die Beschädigung des Materials erzeugt eine Entlüftung für das (eingekapselte) Heilmittel, das mit Katalysatoren in Kontakt kommt und so ein Netzwerk bildet, das die gerissene Ebene abdichtet. Es wurden verschiedene Selbstheilungssysteme beschrieben, aber diese Dissertation zielt auf die Oberflächenmodifizierung von Nanomaterialien wie Nanoclays und polyedrischen oligomeren Silsesquioxanen (POSS) mit speziellen organischen Modifizierungsmitteln und die anschließende Befestigung spezifischer Metallpartikel / Katalysatoren (Ru und Cu) auf ihren Oberflächen ab, die anschließend zur Aktivierung der Selbstheilungschemie bei Raumtemperatur verwendet werden kann. Die Synthese der organischen Modifizierungsmittel (vinylbenzyl-dodecyl ammonium chloride (VDAC), 5,6-di(11-(n,n,n-trimethylammonium)undecoxycarbonyl) norbornene (TAUN), 1-mesityl-1-dodecylimidazoliumiodide (TMPIDD),), 1-tertiary-butyl-1-dodecylimidazolium bromide (TBIDBr), and tertiary amino ligand (TAL)), mit kationischen Zentren, die für Kationenaustauschreaktionen mit Nanotonen erforderlich sind, wird durch eine Reihe von Reaktionsschritten erreicht, gefolgt von der Anlagerung von Ru (für VDAC- und TAUN-modifizierten Ton) und Cu (für TMPIDD-, TAL- und TBIDBr -modifizierte Ton) Katalysatoren. Röntgen-Photoelektronenspektroskopie (XPS) - Flammenatomabsorptionsspektroskopie (FAAS) und energiedispersive Röntgenspektroskopie (EDX) wurden zur Quantifizierung der Menge und des Typs von auf der Oberfläche des Organotons und des Organos gebildetem Ru und Cu-Carbenen und POSS verwendet. Die quantitative Menge und die thermische Stabilität der Modifikatoren auf der Oberfläche der Nanomaterialien wurden über TGA berechnet, was zu einer Oberflächenbelastung des erzeugten Organotons im Bereich von $0,32 \times 10^{-3}$ bis $0,72 \times 10^{-3}$ (mmol / mg) führte. Die Reinheit der organischen Modifizierungsmittel wird mit Kernspinresonanz (NMR) untersucht.

Das Molekulargewicht der verschiedenen POSS-Moleküle wird mit einem massengestützten Laser nachgewiesen Desorptions- / Ionisations-time of flight (MALDI-TOF) und die gefundenen Ergebnisse stimmten mit überein theoretische Berechnungen. Das Differential Scanning Calorimetry (DSC) -Messung wird durchgeführt, um die katalytische Aktivität der Metallpartikel-modifizierten Nanomaterialien zu untersuchen (in Bezug auf die Enthalpie der Vernetzungsreaktion, die Peaktemperatur und die Temperatur, bei der die Vernetzung beginnt). Die erzielten Ergebnisse zeigen eine hohe Aktivität von immobilisierten Cu- und

Ru-Partikeln, und die resultierenden Partikelkatalysatoren könnten zur Herstellung von "click" - und ROMP-basierten selbstheilenden Composites verwendet werden.

Keywords (English)

Self-healing composites, nanofillers, encapsulation, surface modification, surface loading, enthalpy, cross linking, peak temperature, catalytic activity, immobilized metal catalysts.

Keywords (German)

Selbstheilende Composites, Nanofüllstoffe, Verkapselung, Oberflächenmodifizierung, Oberflächenbelastung, Enthalpie, Vernetzung, Peaktemperatur, katalytische Aktivität, immobilisierte Metallkatalysatoren.

Chapter 1

Introduction

1.1.Composites

The overall demand for the improvement of materials performance to meet specific technical needs with negligible disadvantages is the underlying motivation for modern engineering undertakings^{1,2}. Laudable improvements in performance in engineering structures such as materials development, testing, analysis, design, maintenance and production, are direct results of the advancements in materials technologies which by itself is a major factor that determines the reliability, cost effectiveness, and performance of such systems^{3,4}.

Composite materials are basically unique materials made from the combination of two or more constituents possessing significantly distinct physical and chemical properties such that the formed material possesses, on the one hand, the combined properties of the constituent materials, and on the other hand, additional properties that are independent of the starting materials⁵. This is the advantage composite material has over other multi-component systems such as blends and alloys. These composite materials find application in diverse areas such as construction, consumer products, and transportation due to their unusual combinations of unique component properties including permeability, electrical conductivity, weight, strength, stiffness, and optical properties which is difficult to attain separately by individual components^{6,7,8,9,10}. The material properties of composites can be tailored to meet specific need or special requirements.

Composite materials are made up of two phases: the continuous phase, otherwise called the matrix and the dispersed phase called the filler. The classification of any composites is based on the matrix phase, and can be classified as polymeric^{11,12}, ceramic^{13,14} and metallic⁹.

Polymers have great advantage over metals and ceramics because there are light weight and ductile in addition to their ease of production. Nevertheless, they have lower mechanical, modulus and strength properties when compared with metals and ceramics, however the properties varies with respect to used filler (carbon black, CNT, graphene, clay, POSS, etc)¹⁵. Nanocomposites (howbeit, composite materials having constituents at the nanometer range), have been developed to meet more technical needs with improved properties that composite materials¹⁶ do not possess. The level of dispersion of these nanofillers (even at small nanoparticle loading) in the epoxy or polymer matrix enhances special properties such as the

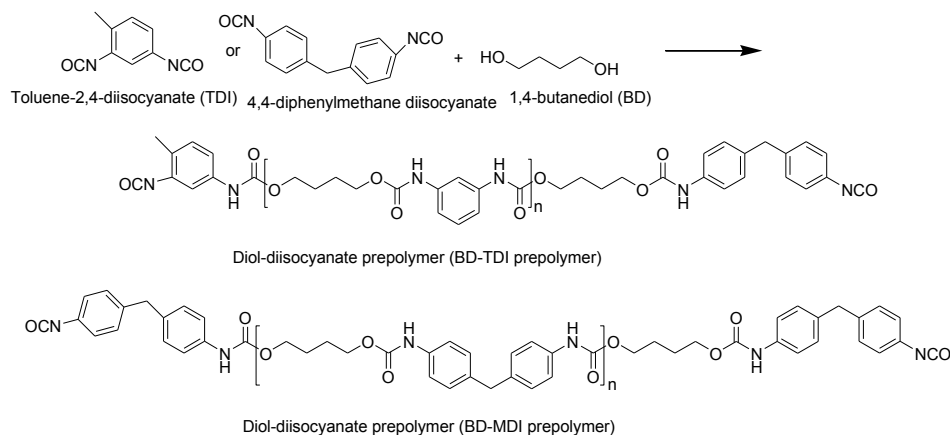
mechanical, thermal, flame resistance, and optical properties etc¹⁷, making nanocomposites more advantageous. However, further advances in materials applications was made, duplicating the self-healing properties of biological systems pioneered and reported by White et. al¹⁸. They working group was the first to prove the autonomic self healing of a structural polymeric material which incorporates a microencapsulated healing agent that is released upon crack intrusion. The encapsulated healing agent is released during crack formation, and when in contact with the embedded Grubbs catalyst, polymerization occurs thus healing the crack plan. This advances lead to the concept of self-healing nanocomposites where materials are developed with special functionalities that promote self-healing behavior, particularly relevant in aerospace engineering where material recovery is of utmost important with the guarantee of safety.

1.2. Concept of self-healing materials

Self-healing materials are synthetically-created or artificial substances that have inert ability to automatically repair damage to themselves without any external intervention¹⁹. These materials can be classified based on their self-healing mechanisms and chemistries. Notable among them are intrinsic self-healing materials, which are based on supramolecular bonding interactions and reversible reactions^{20,21,22,23,24}, extrinsic self-healing materials which require the embedding of microcapsules filled with healing agents in a matrix system or vascular networks^{25,26,27,28} and a metal catalyst²⁹ that can activate the self-healing process when the healing agent is released from the capsules. Self-healing can also be achieved by a self-assembly process using a dialkyl cationic surfactant as reported by Shimojima et. al³⁰ as well as by Π - Π stacking as reported by Burattini et. al³¹ and Hart et. al³². Another examples of self-healing by pi-pi stacking have been shown³³ which exploit non-covalent cross linking of polymer chains generated through pi-pi stacking interactions involving the intercalation of pyrenyl end groups into polyimide chain-folds.

Of particular interest in this work is the capsule-based self-healing systems. The capsule-based self-healing system (an approach that releases the confined healing agent through the rupture of the microcapsule), and microvascular networks, are the two pathways frequently used in the preparation of extrinsic self-healing materials^{34,35,36}. Different polymerization techniques³⁷ and polymers, including poly (melamine-formaldehyde) (PMF); poly (urea-formaldehyde) (PUF); and poly (melamine-urea-formaldehyde), have been used to prepare the capsules and to form the

shell walls of the capsules^{38,39,40,41,42}. Capsule-based self-healing technique has found vast applications including coating industries^{43,44}, adhesive industries⁴⁵, paint industries⁴⁶, amongst others. The potential for polyurethane (PU) microcapsules containing hexamethylene diisocyanate (HDI) as a core material in polymeric composites to achieve self-healing properties thus improving the corrosion resistance of coatings, was demonstrated by Huang et. al^{47,48}. Amine⁴⁹, epoxy resins⁵⁰, and inorganic particles⁵¹ have been used independently as core healant of capsules in self-healing polymeric composites.



Scheme 1: Synthesis of PU microcapsules using a prepolymer (BD-TDI prepolymer) and a chain extender (BD)⁴⁶

Kim et al. synthesized a diol-diisocyanate prepolymer based on 1,4-butanediol that was reacted with toluene-1,4-diisocyanate or 4,4-diphenylmethane diisocyanate (MDI) to prepare PU microcapsule shell as seen in **Scheme 1**⁴⁶. The characterization of the capsules and its core healing loadings was done. They discovered that the protection coating evaluation from scratch test of PU capsules on paint coatings displayed excellent protection performance with a repairing efficiency in the range of 47-100%.

However, the microencapsulation method particularly suffers from two major drawbacks amongst others, such as (i) the cost of the catalyst, particularly the Grubbs catalyst, and (ii) the self-healing process is irreversible, implying that the healing of the materials can only occur once and when crack occur at the same point as previously healed region, healing would not occur because the amount of the healing agent is depleted in the previously healed region. Nonetheless, several reviews have been reported with suggested solutions to overcome these drawbacks^{52,53,54}.

1.3. Self-healing nanocomposites and their applications

The concept of self-healing nanocomposites for industrial applications was inspired by biological systems. They form a new class of materials with inherent ability to heal themselves spontaneously or autonomously, thus mimicking the self-healing behavior exhibited by living organisms.

Self-healing polymers/polymer composites have been categorized based on their chemistries, into two major groups: (i) autonomic and (ii) nonautonomic self-healing materials⁵⁵. The autonomic self-healing materials releases the chemical potential trapped in the material to facilitate the healing upon damage, while the nonautonomic self-healing material relies on external aid to promote self repair upon damage (Figure 1.2).

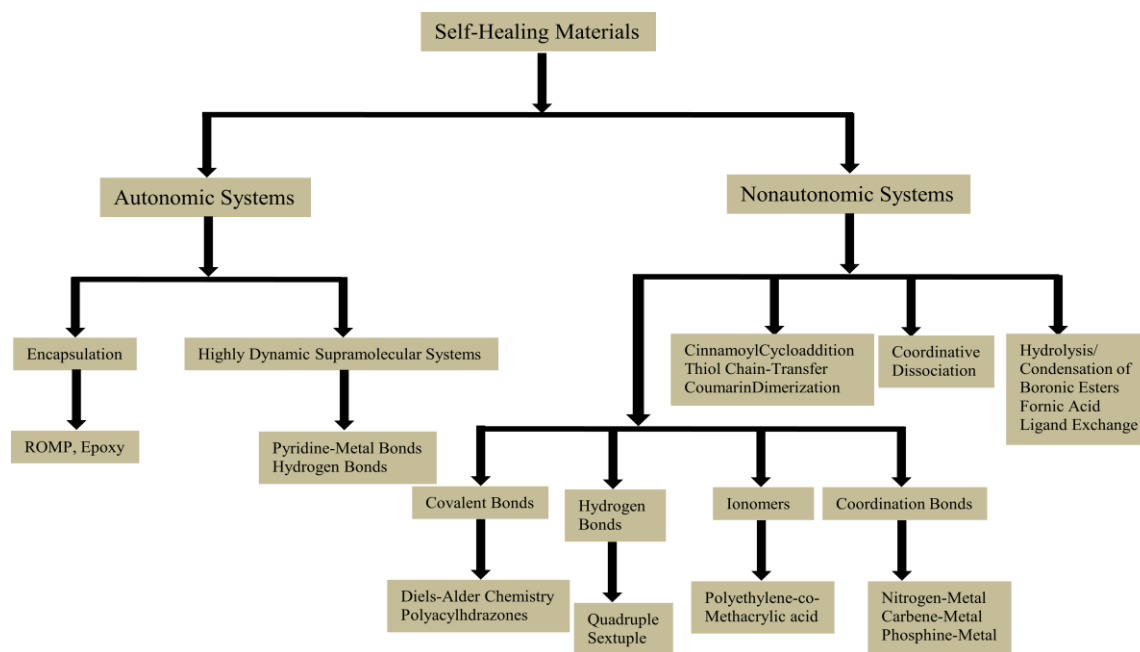


Figure 1.1: Classification and organization of materials based on their self-healing chemistry

Polymer composites, amongst other materials, are arguably leading in materials applications in terms of sustainability and efficiency, having better properties including strength, cost, stiffness, lightweight, and thermal stability^{56,57,58,59,60}. Unfortunately, many of these materials exhibit low mechanical properties such as lower modulus and strength, when compared with metals and ceramics^{58,61} in addition to a few drawbacks such as micro-cracks and cavitation, degradation, and surface stitches⁵⁵. Gordon et al.⁶², amongst others^{63,64} have demonstrated that the incorporation of nanomaterials has great effect on the physical and mechanical properties of

different polymers. Therefore, embedding of nanomaterials into host matrix yields material properties, typically caused by the materials interaction with the matrix that cannot be achieved by either phase independently^{65,66}. The combination of polymer and nanomaterials at the nanometer regime in nanocomposites, give rise to a new breed of highly homogeneous materials with excellent properties, having a major disadvantage, being crack formation, which is comparable to that seen in polymer and polymer composite systems⁵⁵. An attempt to resolve this problem gave rise to self-healing polymer nanocomposites. The development of these healable polymer nanocomposites which has the ability to heal itself at the instance of a crack makes it possible for such materials to find widespread industrial applications^{67,68}.

Several nanofillers or nanomaterials have been incorporated into different surfaces to achieve specific applications. Notable amongst others are multiwalled carbon nanotubes, graphene, silica, nanoclays, and polyhedral oligomeric silsesquioxanes.

1.3.1. Carbon-based self-healing nanocomposites

Carbon nanomaterials (CNMs; CNT, graphene) have attracted an enormous interest to prepare self-healing nanocomposites due to their fascinating properties, including good mechanical and electrical conductivity, high aspect ratio, and unique thermal properties⁵⁵. Another excellent property of these nanomaterials is that they can be used as nanoreservoirs for the healing agents, trapped within the confinements of the SWCNTs thus, creating the possibility for making self-healing materials with improved mechanical properties without use of nanocapsules²⁵. Carbon-based nanomaterials have the slightest affinity to interact with the polymer matrix material either covalently or non-covalently. Graphene-based composites having shape memory and self-healing properties were prepared by Xiao et al⁶⁹, where the authors observed an enhancement of the scratch resistance of epoxy-based graphene. Based upon thorough experimental investigations, the enhanced scratch resistance was due to the in-plane fracture toughness of the individual sheets of graphene. Hence, it was concluded that the overall properties of the graphene-based shape memory polymer composites were greatly improved upon when compared with their pristine counterpart. Shape memory polymers were also used to prepare self-healing foams, reported by Li et al⁷⁰, where different materials such as shape memory polystyrene, multi-walled carbon nanotubes (MWCNTs), VARIM (Vacuum assisted resin infusion molding) technology, and glass micro-balloons were introduced to produce composites sandwich plates with foam

core. The study not only indicated the possibility to heal the impact damage created in foams but also confirmed the enhanced strength, stiffness and shape memory behavior.

Tongfei Wu and Biqiong Chen⁷¹ explored extensively the effect of incorporating multiwalled carbon nanotube (MWCNTs) in self-healing fatty acid rubber matrix. They observed that the electrical conductivity of self-healing fatty acid rubber was improved with increased concentration of MWCNTs (19.7 vol%).

The piezoresistive effect was also observed particularly for the nanocomposite with 19.7 vol% MWCNT which makes it potentially applicable in pressure sensing devices. Chen et al.⁷¹ further observed that the elongation at break was dramatically reduced due to the effect of the rigid nanofillers on the flexibility of polymer chains. In their work, Guadagno et. al⁷² studied the effect of carbon nanofillers (carbon nanotubes, carbon nanofibres, and graphene based nanoparticles) on the cure kinetics of epoxy-amine resin by DSC. They proved that the reactive diluents causes a decrease in the activation energy for $\alpha > 0.7$ for which it is considered that the reaction of the secondary amine is active.

It was also shown that for TGMDA_DDS diluents system, the inclusion of the 1D filler in the resin does not lead to a big difference in the cure kinetics when compared with the unfilled epoxy mixture (TGMDA_DDS_DILUENT). Studies by Bon et. al⁷³ showed the possibility to achieve self-healing by the incorporation of graphene nanoparticles into fermented yeast. It was observed that the incorporation of graphenes into fermented yeast resulted in improved mechanical and electrical properties of the formed nanocomposite in addition to its ability to convert the light stimulus in the electrical signal. It was also observed that the surface of the stressed cell was repaired, partially restoring the pristine electrical and mechanical properties. They claim that this method is potentially relevant in the development of self-healable bioelectronic devices and microorganism-based strain and chemical biosensors.

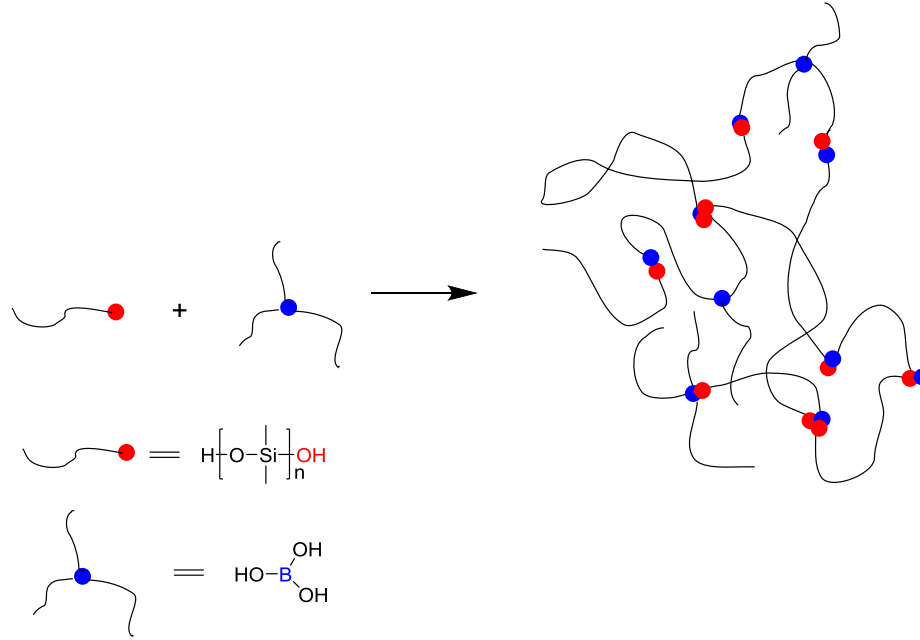


Figure 1.2: (a) schematic PBS network cross-linked by boron/oxygen dative bonds⁷⁴.

Chen et. al⁷⁴ made efforts to investigate the intrinsic self-healing behavior of polyborosiloxane (PBS) reinforced with multiwalled carbon nanotube, exemplified in **Figure 1.4**. It was observed that MWCNT-reinforced PBS showed excellent electrical and mechanical self-healing properties, moldability and adhesion to PDMS elastomer substrate. These properties makes it possible for the fabrication of self-healing MWCNTs-PBS electronic circuits on PDMS elastomer substrate.

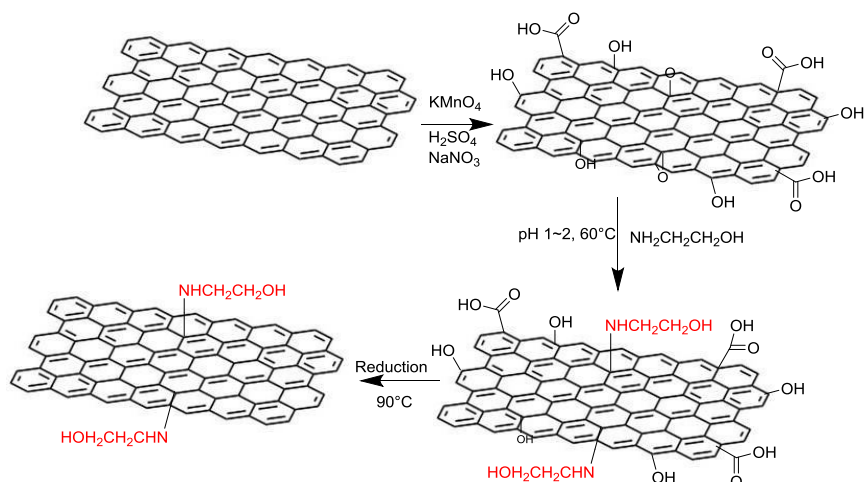
Table 1: Self-healing performance of PBS and MWCNT/PBS nanocomposites^{a74}.

Sample	Self-healing efficiency, %				
	10 min	Mechanical 30 min	2 h	4 h	Conductive 10 s
PBS	99.6 ± 0.4				
MWCNT/PBS 3.0%	39.5 ± 3.3	86.3 ± 2.8			98.1 ± 0.8
MWCNT/PBS 6.2%	26.2 ± 2.7	66.0 ± 3.1			98.7 ± 0.7
MWCNT/PBS 13.3%	13.9 ± 1.5, 96.7 ± 2.1 (w) ^b , 98.4 ± 0.9 (m) ^b	52.5 ± 2.9	84.4 ± 2.2	96.7 ± 1.3	97.9 ± 0.8

^aUnless otherwise noted, the values presented in this table represent the results of the samples healed under ambient conditions.

^bw = healed with water vapor; m = healed with methanol vapor.

Furthermore, it was noticed that MWCNTs at higher concentrations acted as continuous electrical channel in PBS offering electrical conductivity which was up to 1.21 S/cm for the nanocomposite containing 13.3wt% MWCNTs, with the conducting healing efficiency calculated as high as 98% for all MWCNT/PBS nanocomposites (**table1**).



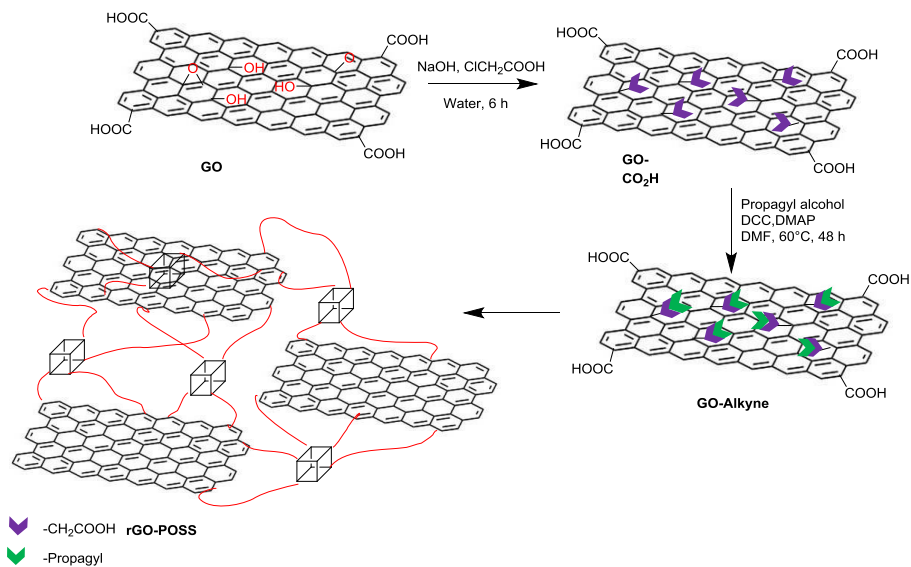
Scheme 2: Schematic procedure for the preparation of functionalized graphene nanosheets (FGNS)⁷⁵

In their work, Wong et. al⁷⁵ described a composite material made up of a polyurethane based on Diels-Alder reaction linked with functionalized graphene nanosheets covalently, which shows robust mechanical properties and infrared (IR) laser self-healing properties at ambient conditions making it suitable for flexible substrate applications (**Scheme 3**). The results show the breaking strength as high as 36 MPa with only 0.5 wt% FGNS loading. It was also shown that the initial mechanical properties were restored upon rupture with more than 96 % healing efficiency after 1 min irradiation time by 980 nm IR laser.

1.3.2. POSS-based self-healing nanocomposites

Similar in characteristics to nanoclays, polyhedral oligomeric silsesquioxanes (POSS) are useful building blocks in the formulation of organic-inorganic polymer hybrid materials due to its high heat resistivity, high mechanical properties, and easy introduction of desired functional groups in the side chain. Cubic polyhedral oligomeric silsesquioxanes, are usually preferred amongst other types of oligosilsesquioxanes because of their novel contributions when used as filler in nanocomposites and finds a lot of interesting applications in material sciences and in the field of catalysis. The structural integrity of cubic POSS caused by its rigid and bulky core and the non-conjugated nature of the siloxane bond makes cubic POSS competitively advantageous⁷⁶. The substituent on the cage silicon atom can be a reactive or non-reactive group. The reactive organic group has unique properties that make POSS materials potential candidates for the formulation of nanocomposites with the inorganic POSS core molecularly dispersed in the matrix⁷⁷. POSS nanocomposites have been proven to have superior properties such as high use temperature,

oxidation resistance, improved mechanical properties, lower dielectric constant, flammability and heat evolution, when compared with their polymeric counterpart^{78,79,80,81}. Zhiguang et al.⁸² explored the thermal properties of mendable POSS nanocomposites by directly cross-linking a POSS that brings eight furan-end functional groups with bismaleimide molecules via Diels-Alder reaction. The authors observed that the POSS nanocomposites was stiff at room temperature but could excellently heal thermally repeatedly.



Scheme 3: Synthesis of rGO-POSS⁸³

In their work, Stadler et. al synthesized graphene oxide-based silsesquioxane-crosslinked networks (**Scheme 4**)⁸³. They observed that the rGO-POSS composites show a greater tendency to percolate rheologically, suggesting that the functionalization of rGO with POSS has a positive effect on the filler efficiency, thus making rGO-POSS more efficient than rGO rheologically.

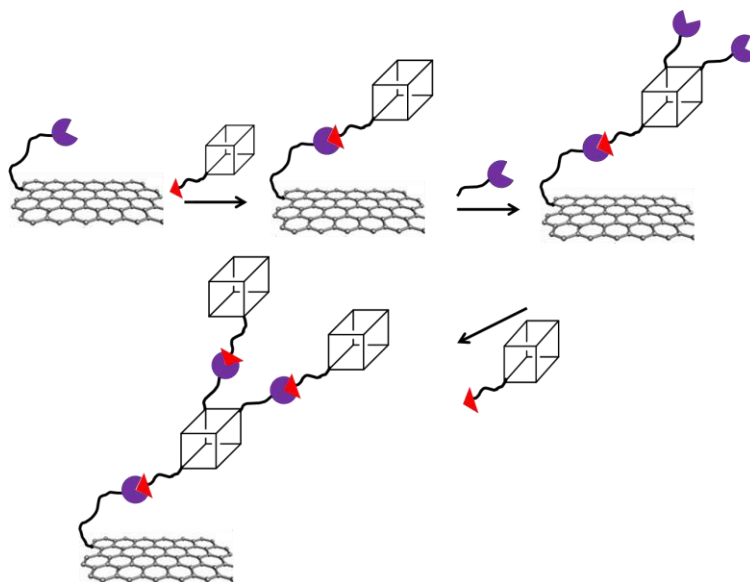


Figure 1.4: Schematic representation of a hyperbranched silsesquioxan polymer grafted graphene oxide (HPP-GO)⁸⁴

In the same vein, Liu et. al⁸⁴ successfully fabricated a hyperbranched silsesquioxan polymer grafted graphene oxide (**Figure 1.4**). The authors went further to investigate systematically the effect of HPP-GO on the mechanical, dynamic mechanical, dielectric and thermal properties of dicyclopentadiene bisphenol cyanate ester resin (DCPDCE). They observed that the appropriate content of HPP-GO enhanced the mechanical properties as well as the flexural and impact strengths of the DCPDCE resin even with 0.6 wt% of HPP-GO. Also, Deng et. al proposed an approach in studying the effect of aminopropylisobutyl polyhedral oligomeric silsesquioxanes (ApPOSS) functionalized graphene on the thermal conductivity and electrical insulation properties of epoxy composites⁸⁵. The authors observed that, as compared to pristine GO/enhanced epoxy (EP), the interfacial interaction between ApPOSS-graphene and the epoxy matrix through covalent and non-covalent bonding promotes very good dispersibility, compatibility and interfacial quality in composites which improves the thermal conductivity through the formation of networks that conduct heat and decrease thermal interfacial resistance.

Deng et. al concluded that ApPOSS-graphene is a preferred filler for the enhancement of the thermal conductivity and electrical insulation with potential application in electronics and microelectronic industries. An effective method for the preparation of functionalized poly(cyclotriphosphazene-co-4,4'-sulfonyldiphenol) (PZS) nanotube reinforced UV-curable materials was developed by Hu et. al⁸⁶. They observed that the storage modulus of POPZS/EA-

3.0 nanocomposite was increased by 16 °C compared to those of pure epoxy acrylate (EA). The reason for this, according to the authors is due to the high stiffness of POPZS and the formation of strong interfacial interactions⁸⁶. In their work, Messori et. al modified typical acrylic melamine clearcoat with hyperbranched polymer and polyhedral oligomeric silsesquioxane nanostructures to simultaneously enhance its scratch resistance and healing ability⁸⁷. They observed that while the enhanced scratch resistance was due to the increased elastic recovery of the clearcoats in the presence of nanostructured modifiers, the healing ability was a result of the partial replacement of covalent cross-links with H-bonding (**table 2**)⁸⁷.

Table 2: Healing results obtained from the scratch profiles before and after healing process⁸⁷.

Sample	Mean y (bef.) (µm)	Max. depth (bef.) (µm)	Mean y (aft.) (µm)	Max depth (aft.) (µm)	Healing according to mean y (%)	Healing according to max. depth (%)
HOPO	-4.36	10.06	-2.06	6.75	52.7	32.9
H5P5	-2.06	6.65	-1.06	17.13	48.5	Not definable
H5P15	-5.19	10.33	-1.23	3.39	76.3	67.1
H5P25	-4.06	8.04	-0.24	0.95	94.0	88.1
H10P5	-2.58	8.01	2.1	11.8	Not definable	Not definable
H10P15	-6.11	11.45	1.31	4.73	Not definable	58.6
H10P25	-3.63	8.07	-0.7	1.19	80.7	85.2

The superior healing ability of modified clearcoats was assigned to the reduced functional reactivity, increased polarity and more globularity of hyperbranched polymers and POSS nanostructures⁸⁷.

POSS materials used as fillers have equally found applications in the development of special hybrid systems for biological applications. In the light of this, Lei et. al⁸⁸ developed a biocompatible elastomer using functionalized POSS having great mechanical stability, very high tunable behavior and osteogenic differential activity, thus extending the applications of such materials in bone tissue regeneration (**Scheme 6b**). This development overcame the traditional limitations of other bioelastomers due their low mechanical stability at hydrated state and poor osteogenic differential activity. The authors show that the POC-POSS possessed significantly improved stiffness and ductility in either dry or hydrated conditions, as well as good antibiodegradable ability (20-50% weight loss in 3 months) thus making POC-POSS a promising hybrid elastomer in the development of scaffolds and nanoscale vehicles for bone tissue regeneration and drug delivery⁸⁸.

The effect of silica nanoparticles in supramolecular polymers have been reported. This studies was reported by Priestley et. al⁶⁵ in an attempt to overcome the inferior creep mechanical properties supramolecular polymers usually have when compared to traditional polymers due to the absence of aggregation or crystalline domains. Although progress was made in the improvement of the mechanical properties of supramolecular polymers via strong interchain interactions limited to few examples of ureidopyrimidinone (UPy) stacking to form supramolecular thermoplastic elastomers⁸⁹, Priesley et. al discovered a more effective and alternative route which requires the inclusion of silica particles⁶⁵ (**Figure 1.5**).

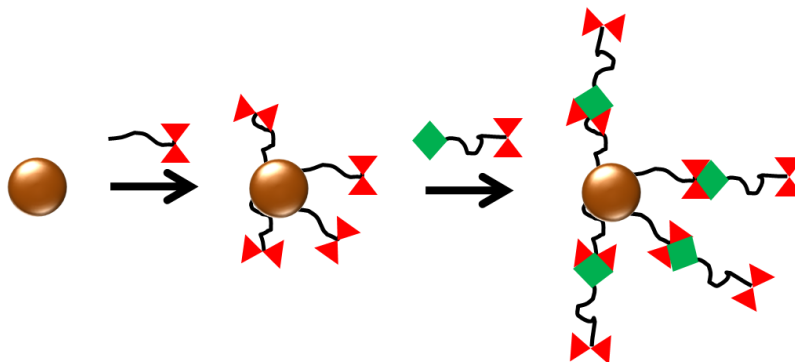


Figure 1.5: Modification of silica nanoparticles and its effect in nanocomposite preparation⁶⁵

The result of this investigation show a huge impact of nanofiller loading and surface functionality on the mechanical properties and suggest that the network formation of the nanofiller may play a key role, the understanding of which will be vital in the development of advanced stimuli-responsive nanocomposite material.

1.3.3. Clay-based self-healing nanocomposites

Multifunctional resins designed from thermosetting structural materials possess outstanding potentials that impact the structural performance of these materials by reducing cost, weight, size, and power consumption while ultimately improving versatility, safety and efficiency. In the field of aeronautic engineering, successful strategies intended to reduce the flame retardance of the resin material while simultaneously increasing the electrical conductivity is very crucial.

The flame retardance of nanofilled resin materials can be improved upon by the inclusion of nanofillers such as nanoclays, polyhedral oligomeric silsesquioxanes or new phosphorous hardeners. Layered silicates such as montmorillonite, etc have been used as reinforcing agents

due to their high aspect ratio^{90,91}. Nanoclays are very important fillers in the preparation of self-healing composites not only because of their exfoliated arrangements in the polymer but also the flame-retardant property introduced into the self-healing nanocomposite as a result of their inclusion into the polymer matrix^{92,93,94,95,96}. Mechanical and fracture properties such as stiffness are improved upon even though a few drawbacks still exist when manufacturing those exfoliated structures^{97,98}. However, Lau et.al⁹⁹ provides an innovative pathway to overcoming such drawbacks. It has been documented that the interfacial shear strength of epoxy is remarkably improved upon by the inclusion of nanoclays in the epoxy resin¹⁰⁰. The properties of the resin material are greatly improved upon by the large surface to volume ratio of nanoclays. In epoxy resin, the large exposed surface area is interacted with a large number of tiny nanoparticles much more than larger particles having the same net microscopic volume¹⁰¹. The macroscopic properties of the material is generally enhanced by increasing the interfacial area of the small nanoparticles at lower concentrations, even though a well dispersed interfacial area between the nanoclay and the resin leads to further improvement in barrier properties, electrical properties and thermal stability¹⁰².

For better dispersion of the nanoclays in the epoxy matrix, nanoclays are modified with organic molecules. This modification not only causes an increase in the interlayer spacing of the clay platelets, but also provides an opportunity for functional groups to interact with the epoxy matrix. Also, the modification of nanoclays causes an increase in the interfacial gap and reduces the surface energy making it more compatible with the epoxy matrix. Clay layers can either be intercalated when dispersed in a polymer matrix with the insertion of the polymer chains in the clay layers that retains their lateral order, or exfoliated when the clay platelets are completely delaminated and dispersed individually in the polymer matrix. The intercalation or exfoliation of clay platelets causes the platelets to interact more effectively with the epoxy matrix, thus increasing the properties of the nanocomposites. But nevertheless, complete exfoliation is readily achieved in an epoxy matrix because clay exfoliation is enhanced by a series of factors, ranging from curing agents and conditions, the cationic exchange capacity of the clay and the property of the clay modifier^{103,104,105,106}.

Tensile properties, enhanced barrier properties, increase in thermal stability, increase in flame retardance, and enhanced barrier properties are all improved upon by the exfoliation of nanoclays^{91,107}.

Several studies which have been carried out to integrate nanoclays into the polymer matrix show that the orientation of the clay platelets occurring usually along the loading direction, causes an increase in the Young's modulus^{108,109}. Also, it has been noted that addition of nanoclays to epoxy matrix improves wettability in fibre-epoxy composite, hence the need for a well dispersed nano reinforcement in the matrix¹¹⁰. This addition of the inorganic clay also (depending on the area of application of final material) prolongs, by tortuosity the pathways of diffusing molecules (water or gas molecules), thereby reducing the material permeability and improving the life span of the polymer-based material^{111,112,113}. In addition to the barrier properties that is usually improved when inorganic clay is incorporated into the polymer matrix, the overall mechanical and thermal properties of the final resin material is also significantly improved upon even at low nanoparticle loading^{114,115}. It is important to note that the tortuosity effect created by the inclusion of nanoparticles into polymer matrix is directly related to the effective dispersion of these clay particles in the polymer matrix and by extension, the amount of matrix/nanoclay interfacial region. This is very crucial because the degree of nanoclay delamination into the polymer matrix is a function of the chemical modification on the clay surface, which is in practice, intended to facilitate great affinity with the polymer matrix and also improve the processing conditions of nanocomposites¹¹⁶. In the work of Safi et. al¹¹⁷ the addition of nanoclay to the epoxy matrix led to a nano-reinforced matrix with the expectation that such reinforcement will further strengthen the interfacial adhesion by different mechanisms such as being a razor to direct crack path through different constituents alternatively. It was also found that the nanoclay was capable of crack deviation¹¹⁷.

1.4. Modification of nanofillers(nanoclays and POSS) and their self-healing nanocomposites

1.4.1.Nanoclays

Clays minerals, generally called layered silicates, such as montmorillonite (MMT), mica, or pyrophyllite are very important category of materials because there are abundantly available in soil and other sediments¹¹⁸. There have vast range of applications such as additives, mud drilling, catalysis and construction material^{119,120}, in addition to their usefulness as rheology control agents¹²¹, reinforcements in nanocomposites¹²², and substrates for nanopatterning^{123,124}. The application of clay minerals in biogeochemical processes to retain and release metal nutrients in soil¹²⁰ has also been explored likewise. Clay minerals, made up of a layer-like shape with a comparatively high mechanical strength¹²⁵, are considered as nano materials (or nanoplatelets)

because the diameter of the clay platelets are in the nano meter range ($<100\text{ nm}$)¹²⁵. When the particles are tubular in shape and within the nano meter range, there are called nano fibers (e.g. carbon nanotubes and graphenes) and when the particles are circular, there are considered as nanoparticles.

Montmorillonite clay material, used in this work, for example, is a layered 2:1 dioctahedral phyllosilicate composed of an octahedral sheet (*O*) sandwiched between tetrahedral sheets (*T*), thus giving a *TOT* structure¹²⁶ as illustrated in **Figure 1.5** below. The *T* sites are made up of SiO_4 units and the *O* sites are made up of AlO_6 units in the absence of any substitutions. The coordination sphere also contains structural hydroxyl groups. Meanwhile, one of the three symmetrically unique octahedral sites is not occupied by a cation in dioctahedral 2:1 phyllosilicates¹²⁶. Cationic substitutions frequently occurs in dioctahedral 2:1 phyllosilicates, with isomorphous substitutions of Al^{3+} ions by Mg^{2+} ions in the *O* sheets being particularly peculiar to MMT. This substitutions results in a net negative charge for the clay layer, which is balanced by existing cations at the interlayer such as Na^+ , Li^+ and Ca^{2+} ¹²⁶. Na MMT is the most preferred clay mineral for wide range of applications as mentioned earlier because it possesses excellent cation exchange capacity (between 70-95 meq/100 g) and a high surface area¹²⁷.

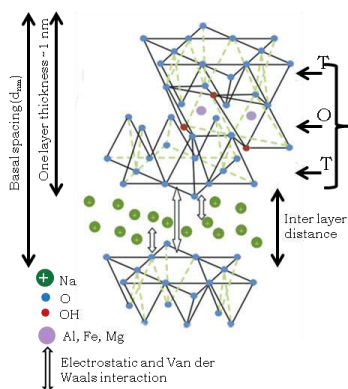


Figure 1.6: Na MMT structure containing *TOT* sheets and counterions in addition to the dispersion of these counterions in the clay gallery.

Perhaps the most characteristic property of clay materials is their ability to adsorb water molecules between the layers which results in strong repulsive forces with clay expansion as consequence.

1.4.1.1. Swelling of clay

The ability of clay materials to swell in the direction perpendicular to the silicate platelets by the intake of water, polymers, salts, and other materials in the interlayer region is what makes it useful as a colloidal model¹²⁸. Consequently, the clay gel formed represents a one-dimensional colloidal system that is appropriate for studies in electrostatic interactions as well as interlayer structure in polyelectrolyte solutions and colloidal suspensions¹²⁸. Swelling strongly depends on the molecular packing of intercalated water¹²⁹ and the type of interlayer counter-ion¹³⁰. For instance, clay materials containing K^+ as the interlayer counter-ion shows fewer propensities to swell, compared to clay materials having Na^+ as its counter-ion. Li^+ -containing clays, on the other hand swell better than their Na^+ -containing counterparts. For K^+ -containing clays, the intermolecular interaction that exist with water molecules is too weak, leading to the formation of inner sphere complexes which does not depend on the location of the layer charge¹²⁰.

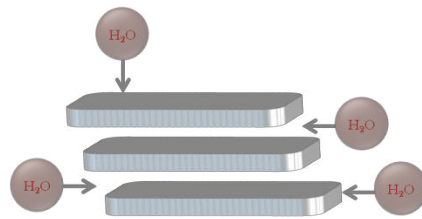


Figure 1.7: The three sheet structure of a typical Na MMT clay material showing the penetration of water molecules at the interlayer of the clay gallery.

Figure 1.6 illustrates the positioning of the water molecules in a three sheet clay material. The sodium counter-ion coordinates to the water oxygen while the oxygen atoms on the clay surface are bonded to the water hydrogen atoms. When the water vapor in the clay gallery increases, the clay platelets swell but the complexes already formed in the inner sphere are preserved, and their distance to the clay surface remains almost constant. The consequence of this phenomenon is the formation of a double layer by the water molecules.

1.4.1.2. Surface modification of clay materials

Clay materials basically contains Na^+ or K^+ ions and are only compatible with hydrophilic polymers such as poly (vinyl alcohol). Rendering them compatible with non-polar polymers requires further reactions to make them organophilic. Achieving this requires ion exchange reactions between existing counter ions and long chain primary, secondary, tertiary and quaternary alkylammonium cations which contain various substituents¹²⁵. In order for the

organophilic clay to be compatible with the polymer, at least one of its substituent must be a long carbon chain of 12 carbon atoms or more¹³¹. The resulting clay with a nonpolar surface, therefore, possesses the very important property of being able to swell and disperse in certain organic solvents, which has been a major setback for pristine clay materials. In the light of this, Zhu et al. reported the structure and adsorption properties of zwitterionic surfactants when used to modify clay material¹³². They reported that the loading, chain length and concentration of the surfactants mainly affected the properties and structure of modified clay¹³². A few other surfactants have been used as modifiers for cationic exchanged reactions and reported as well, as contained in **table3**. With the successful cationic exchange reactions of certain montmorillonite, the organophilic clays extends its application to cover wide range of industrial applications and are, for example, an important constituent of oil-well drilling fluids, paints, plastics, greases, detergents, thin films, rubber, and plastics^{133,90,134,135,136,137,138,139,140,141,142}. Organophilically modified clays have been thoroughly studied over the last few decades, but neither the structure nor the mechanisms by which swelling and dispersion occur in organic solvents are deeply understood yet.

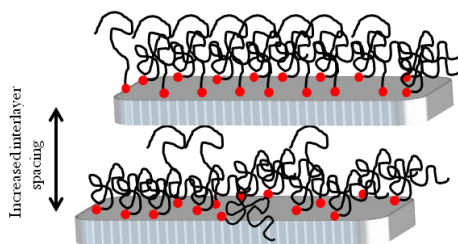


Figure 1.8: Modification of Na MMT with cationic surfactants and the effect of the cationic exchange of counterions with organic molecules on the interlayer distance.

However, the structure of the organic layers formed at the interface of organophilic clays depends on the nature of the modifier and its content^{133,143,144}. Of great scientific and industrial relevance is the knowledge of the behavior of organic molecules embedded into clay galleries. In as much as the fabrication of polymer-clay nanocomposites is concerned, for instance, the surface modification of clay allows the penetration of polymers into the clay galleries, which is why knowing the structure of the organophilic layer in the modified clay is of great importance.

Table 3: Names and structures of surfactants used for nanoclay modification

Name of surfactant	Structure	Name of surfactant	Structure
N,N,N,N',N',N'-hexamethylhexamethylene diammonium dibromide ¹⁴⁵		Dodecyltrimethylammonium chloride ¹⁴⁶	
N,N,N,N',N',N'-hexabutylhexamethylenediammonium dihydroxide solution ¹⁴⁵		N,N-trimethyl-6-(4-vinylbenzyl)hexane-1-aminium ¹⁴⁶	
N,N,N',N'',N''-pentamethyldiethylenetriamine ¹⁴⁵		N,N-trimethyl-6-(4-vinylphenyl)dodecan-1-aminium ¹⁴⁶	
N,N-dimethyl-N-(4-vinylbenzyl) hexan-1-aminium ¹⁴⁶		N-(4-ethylbenzyl)-N,N-dimethyldodecan-1-aminium ¹⁴⁶	
N,N-dimethyl-N-(4-vinylbenzyl) dodecan-1-aminium ¹⁴⁶		5,6-di(11-(N,N,N-trimethylammonium)undecoxycarbonyl)norbornene	
1-methyl-3-decahexylimidazolium ¹⁴⁷		1-mesityl-1-dodecylimidazolium iodide ¹⁴⁸	
Tertiary amino ligand ¹⁴⁹		1-tertiary-butyl-1-dodecylimidazolium bromide ¹⁴⁸	
Alkylmethyl dipolyoxyethylene ammonium cation ¹⁵⁰		Tallow-based ammonium cation ¹⁵⁰	
Alkylmethyl dipolyoxyethylene ammonium cation ¹⁵⁰		3-(N,N-dimethylmyristylammonio) propane sulfonate ¹³²	
3-(N,N-dimethyldodecylammonio) propane sulfonate ¹³²		3-(N,N-dimethylpalmitylammonio) propane sulfonate ¹³²	

The surface modification of Na MMT with quaternary ammonium cations, as shown in **Figure 1.7 and table 3**, can be achieved under mild conditions and allows broad range of functionality

in these hybrid systems. Added to the industrial importance of the organophilic clay, mechanical properties such as higher moduli^{133,134,135}, increase heat resistance and increased strength^{134,135}, decreased flammability¹³⁸, decreased gas permeability¹⁴², have been shown to greatly improve as well as improved biodegradability¹⁵¹. Hence, macroscopic properties which depend on the choice of the clay mineral and the surfactant can be engineered over a wide range.

1.4.2. Polyhedral oligomeric silsesquioxanes

Resins have been intensely applied in wide range of applications attributed to their excellent physical and chemical properties including high tensile strength, thermal stability, and compression strength¹⁵². However, as a prospective material for widely considered applications together with high performance purposes for instance in automobile parts and turbine blade,¹⁵³ further enhancement in mechanical properties are extremely required. To achieve this goal, the addition of nanofillers into resins is highly advantageous, where addition of small amount of nanofillers (*e.g.* POSS, clays, CNTs, graphene, etc.)^{72, 154} provide excellent mechanical properties, thus enhancing the strength of the material significantly.

At the molecular level, polysilsesquioxanes are organic-inorganic hybrid materials with the molecular formula $(\text{RSiO}_{1.5})_n$ ^{155,156}. Silsesquioxanes, typified in **Figure 1.8**, have a general formula $(\text{RSiO}_{1.5})_a(\text{H}_2\text{O})_{0.5b}$, where *a* and *b* are integer numbers and *R* is a hydrogen atom or an organic group¹⁵⁷. They are basically composed of rigid crystalline silica-like core that has a perfect definition spatially (0.5-0.7 nm)¹⁵⁷. Silsesquioxanes have several structures such as ladder^{158,159}, random^{160,161,155}, and cage^{162,163}, with the cage structure having 8 silicon atoms at the vertices of the cube. Based on the number of silicon atoms present in the cubic structures of silsesquioxanes (completely and incompletely condensed silsesquioxanes), different designations such as T₆, T₇, T₈, T₁₀ and T₁₂ are used^{76,164}.

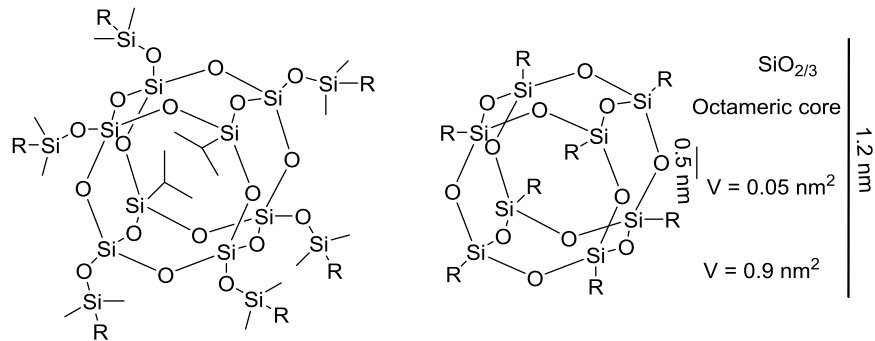


Figure 1.9: Silsesquioxanes: (a) Q8 ($Q = \text{SiO}_{2/2}$), $R = \text{H}$, vinyl, epoxy, methacrylate, etc.; (b) RxTx ($T = \text{R-SiO}_{3/2}$), $R = \text{alkyl}$, alkene, acetylene, acrylate; (c) Typical sizes and volumes.

The highly symmetrical and star-shaped structures formed by POSS materials, makes it possible for POSS materials to have unique characteristics that are distinctly different from planar molecules^{165,166}, and as a result, the solid polyhedral oligomeric silsesquioxanes have received considerable attention as building blocks for the formation of functional molecules as well as nanomeric materials in nanocomposites^{167,168,169,170,171}. Physical properties such as processability, toughness, thermal and oxidative stability are expected to be enhanced as a result of the incorporation of an inorganic component into an organic polymer matrix.

Incorporation of polyhedral oligomeric silsesquioxane (POSS) into polymer matrix dramatically improves their mechanical properties as well as reduces their flammability, heat evolution, and viscosity during processing¹⁵⁵⁻¹⁵⁶. In addition, generally POSS molecules are soluble in monomer mixtures; therefore, they can be incorporated as true molecular dispersions in the resulting polymer matrix, an advantage over their carbon counterparts¹⁷². POSS have been used to modify polymers¹⁷³, nanoparticles¹⁷⁴ and carbon nanotubes¹⁷⁵. The most common reaction till date, for crosslinking POSS for capillary liquid chromatography application is the thiol-ene reaction¹⁷⁶. Alves et al. reported to have obtained hydrogels with enhanced and largely varied physicochemical characteristics from the crosslinking of vinyl-POSS and homotelechelic thiol polyethylene glycol di-ester macromonomers¹⁷⁷. POSS molecules have also been grafted together with graphene to produce materials possessing high electrical and sensing properties in addition to its solubility property caused by the presence of POSS¹⁷⁸.

1.4.2.1. Enhancement of thermal and mechanical properties of polymer nanocomposites with POSS

The use of fillers to enhance the mechanical and thermal properties of conventional polymers is a simple and effective pathway that has dissolved the growing concerns of such material properties in recent past. To this end therefore, silica and siloxanes are considered practical fillers which improve the material properties of polymers significantly^{179,180,181}, in addition to POSS which has also been reported^{182,183,184}. The cage-like structures of POSS materials having eight organic functionalities, makes it suitable as a crosslinking molecule since it is soluble in a wide range of organic solvents. Researchers have shown that the reinforcement of polyimide aerogels can be achieved by cross linking with POSS derivatives than with polymers¹⁸². And as a consequence, very porous materials with high modulus, large surface area and low thermal conductivity were obtained. Enhancement of thermal and mechanical properties can also be derived by covalently incorporating POSS materials into polymer chains and terminals. Even with little amount of POSS materials, the pyrolysis of the polymer¹⁸⁵ or hybrid materials¹⁸⁶ is considerably suppressed. Additionally, the end-capping by POSS materials can effectively enhance the rigidity of the polymers¹⁸⁷.

1.5. Microencapsulation of healing agents for self-healing materials

1.5.1. General concept of microencapsulation

The concept of encapsulation has been utilized in pharmaceutical and other companies for drug delivery¹⁸⁸, cell encapsulation¹⁸⁹, catalysis^{190,191}, and food additives¹⁹² before now, but has been adopted in recent past for the formulation of self-healing composites where special healing agents of interest are enclosed in a capsule.

Microencapsulation is profoundly regarded as a preservation technique of sensitive compounds with special characteristics for the production of materials with desired and valuable properties³⁸. It protects the solids, liquid droplets or gases from the inert shell which directly protects the enclosed compound from the external environment.

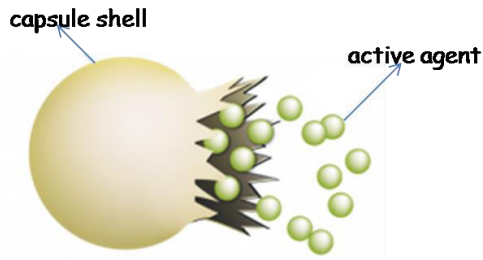


Figure 1.10: Release of active agents from microcapsules during mechanical rupture of the embedded microcapsule in composite material.

The product of the microencapsulation process is either regarded as microspheres, micro particles, or microcapsules depending on the size and morphology. When the size is below 1 μ m the particles are considered as nanoparticles, and when the size is between 3-800 μ m, are called microcapsules. Macrocapsules with particle size greater than 1000 μ m. The microcapsule is made up of two distinct parts: the microcap and the active agent as seen in **Figure 1.9**. Several approaches have been developed and reported for microencapsulation ranging from colloidosomes¹⁹³, self-assembled polymersomes^{194,195}, vesicles¹⁹⁶ and polymer microcapsules^{197,198,199,200,201}. The fabrication of these capsules through these approaches often require an experimentally laborious multiple steps^{202,203,204}. Generally, encapsulation is done to (i) protect sensitive substances from harsh environmental conditions, (ii) protect organoleptic properties like colour, taste, and odour of the substance, (iii) for safe handling of toxic materials, (iv) to achieve target release of active component, (v) and to avoid adverse effects that the encapsulated compound could cause²⁰⁵.

Broadly, there are three major categories of encapsulation techniques based upon their applicability. These are: chemical methods, physico-chemical methods, and physico-mechanical methods. The difference in their processabilities and applicabilities are listed in table 4 below²⁰⁵.

Table 4: Chemical, physic-chemical, and physico-mechanical microencapsulation processes and applications.

Chemical processes	Physico-chemical processes	Physico-mechanical processes
Interfacial polymerization	Coacervation and phase separation	Spray drying and congealing
In situ polymerization	Sol-gel encapsulation	Fluid bed coating
Polycondensation	Supercritical CO ₂ assisted microencapsulation	Pan coating and Solvent evaporation

However, emerging industrially relevant techniques for the encapsulation of desired compounds have been developed²⁰⁶ and for the purpose of clarity and conciseness, emphasis would be on three major aspects of organic encapsulation methods.

1.5.2. Supramolecular encapsulation

Supramolecular chemistry, in an extended form, also encapsulates the inclusion of small molecules within organic structural cavities which basically consist of macrocyclic oligomeric materials. Conversely, their inorganic counterpart are based on metal-organic frameworks or mesoporous silica^{207,208,209,210,211}. The weak enthalpic intermolecular interactions and a favorable entropy that results in the evaporation of trapped solvent in the molecular compartments constitutes the driven force for the mode of encapsulation for this approach²¹².

1.5.3. Emulsion Encapsulation

Emulsion encapsulation differs from other encapsulation techniques discussed herein in that it relies on covalent shell-wall formation that provides a robust encapsulation unlike the previously discussed encapsulation methods that are driven by inter-/intramolecular non-covalent interactions. Emulsion-based technique has been strategically applied extensively to produce microcapsules^{40, 213} for different applications including food and nutrition, coatings, utilizing triggerable microcapsules, micro-reactors, synthetic cellular structures, and self-healing materials^{214,215,216,217}. With respect to preparation, amphiphiles known as emulsifiers are usually introduced to stabilize the immiscible multiphase mixtures by lowering the interfacial energy of the discontinuous phase. Macromolecular amphiphiles which often serve as stabilizers due to their hydrophobic and hydrophilic states as well as surfactants, have been widely used as emulsifiers^{218,218b,219}.

1.5.4. Miniemulsion/Interfacial encapsulation

Miniemulsion technique has been developed to overcome the challenges of encapsulating special healing agents for self-healing materials, having good dispersion of the capsules in the polymer matrix²²⁰. While miniemulsion encapsulation process guarantees the efficient encapsulation of healing agents, it is likewise a method of choice for encapsulating various low molecular weight materials that can either be solid²²¹, hydrophilic or hydrophobic^{202,222,223,224,225} or liquid^{224,225}. The encapsulation of liquid substances is necessary for self-healing materials since the healing

materials is expected to be mobile enough to diffuse to the cracked plane for healing to take effect.

Miniemulsions are generally considered to be relatively stable droplets (with size range between 50-500 nm) prepared by either oil-in-water or water-in-oil emulsion techniques where the emulsion generated consist of water, oil, surfactant, and a stabilizer²²⁶. The latex particles formed from the polymerization process have the same size as the initial droplets. The concept of “nanoreactors” is usually applied in miniemulsion polymerization technique. This allows the formation of polymer latex particles. It has been successfully shown that the miniemulsion encapsulation method is suitable in the production of stable latexes as well as in reactions involving dispersed media where the same principle of miniemulsion polymerization can be transferred to polyadditions^{227,228}.

The widely known Interfacial polymerization technique of encapsulation, on the other hand, can be applied to dispersed systems and is used to encapsulate varieties of materials such as live cells, enzymes, agrochemicals, flavors, fragrance, drugs and dyes²²⁹. Other compounds that have been successfully encapsulated are osmium tetroxide²³⁰, palladium (II) acetate, and Pd (0) (20-250 μm) in a polyurea matrix²³¹. The polyurea was synthesized at the interface of the oil droplets by polycondensation.

1.5.5. *In-situ* encapsulation

The precipitation of polymeric materials at the oil-in-water interface during the production of polymer capsules or hollow capsules, causes the droplets to be enclosed in a polymeric shell. In *in-situ* polymerization technique, the conditions are predominantly driven by interfacial energy criteria. Several compounds have been encapsulated by *in-situ* polymerization method for specific applications. Sondi et al.²³² successfully encapsulated nanosized silica coated with *tert*-butyl acrylate polymer by *in-situ* technique. They showed that the stable dispersions of the capsules where in the size between 8 and 11 nm with potential relevance in photoresist applications. Mukkaram et al.²³³ also reported the *in-situ* ATRP of a cross-linked terpolymer designed to migrate to the oil-water interface giving rise to hollow polymer particles.

Chapter 2

Aim and synthetic concept

2.1.Aim

The overall aim of this dissertation is to systematically develop catalytically active nanofillers with desirable catalytic activity capable of activating self-healing functions at low temperatures (**Figure 2.0**). This thesis is also targeted at synthesizing and encapsulating multifunctional azides and alkynes which can act as healing agents for the activation of ROMP- and click-based self-healing systems.

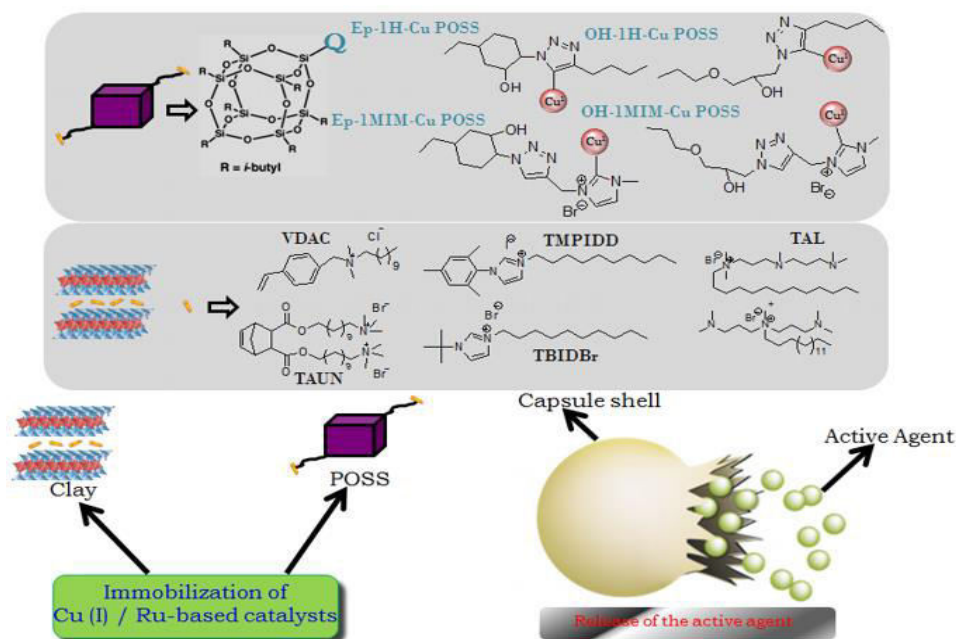


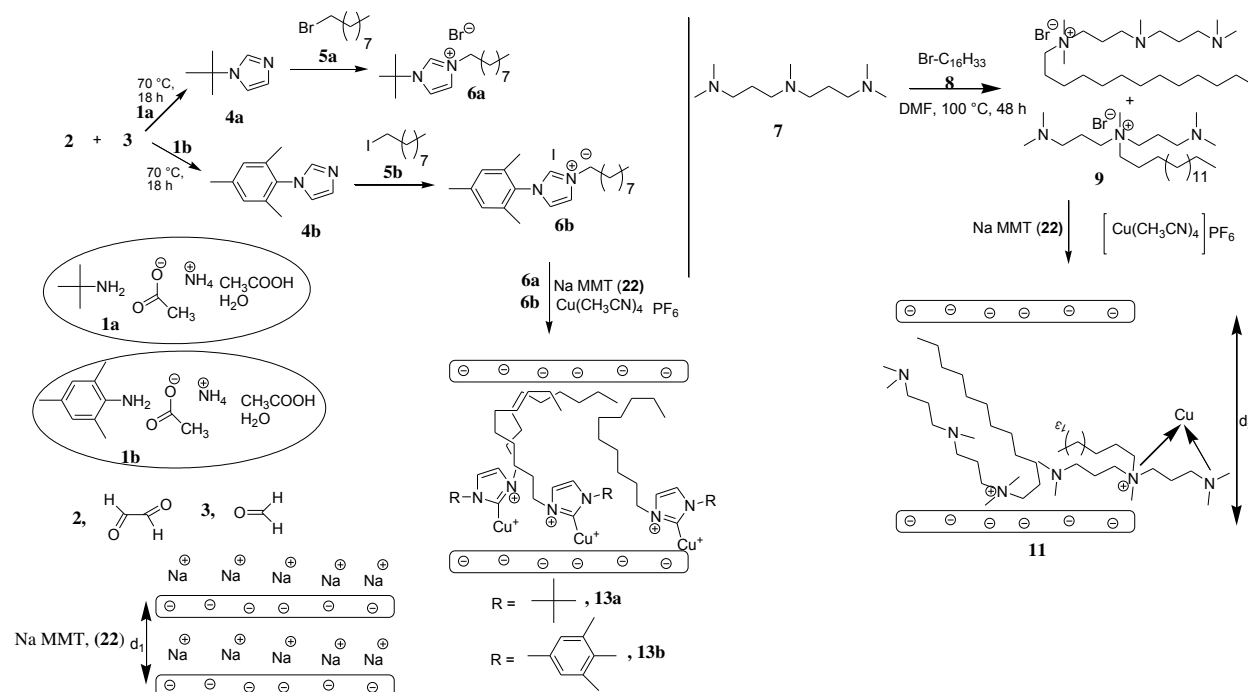
Figure 2.0: General synthetic concept and pathways for the surface modification of clay and POSS, and subsequent attachment of metal catalysts on their surfaces.

For the surface modification of the nanoclays by cationic exchange reaction, different modifiers with potential binding sites for the immobilization of Cu- and Ru-based catalysts have been synthesized (**6a**, **6b**, **9**, **16**, and **21**). The developed catalytically active nanofillers are expected to initiate Ring Opening Metathesis Polymerization (ROMP), in the case of Ru-modified clays and POSS, and “click” reactions in the case of Cu-modified clays and POSS, while improving the overall mechanical and thermal properties of the final material.

Kinetic investigations are to be carried out in order to quantify the catalytic activity of the nanofillers modified with Ru/Cu (I)-based catalyst using differential scanning calorimeter (DSC), rheology and FTIR.

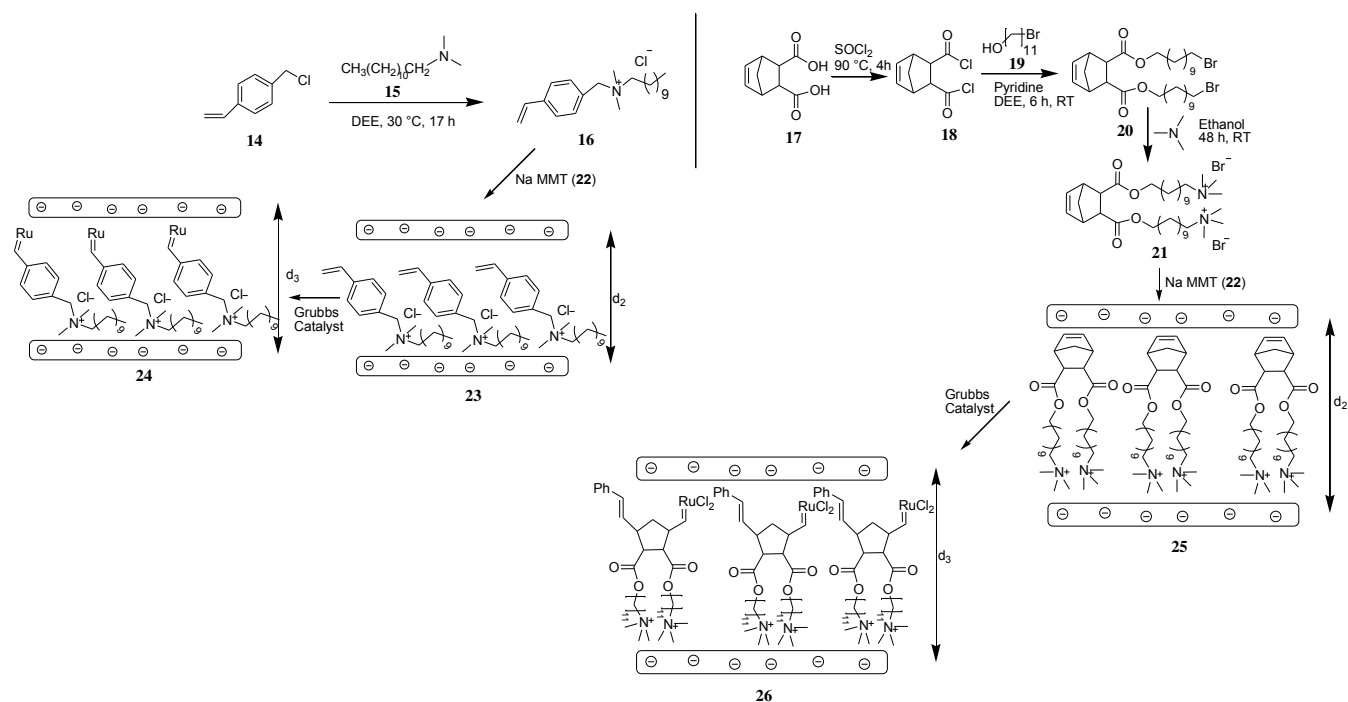
2.2.Synthetic Concept

The approach is to immobilize Cu-andRu-basedmetal catalysts on the surface of clay and POSS materials. This can be achieved by first modifying the pristine clay materials with organic ligands (**6a**, **6b**, **9**, **16**, and **21**).



Scheme 2.1.1: Step by step synthetic route for the successful synthesis of organic modifiers with potential sites for the immobilization of Cu(I), subsequent modification of nanoclays with modifiers and immobilization of Cu metal catalyst.

Scheme 2.1.1 illustrates the possibility through which Cu (I) can be attached onto the surface of pristine clay (Na MMT). It gives the pathways that allow the surface modification of Na MMT with specific ligand that can form a Cu-carbene through covalent bond formation (**13a**, **13b**), and also presents a pathway that allows modification of Na MMT with a non-specific ligand that doesn't really make a Cu-carbene but forms a Cu complex in certain ways with different complexing sites (**11**).



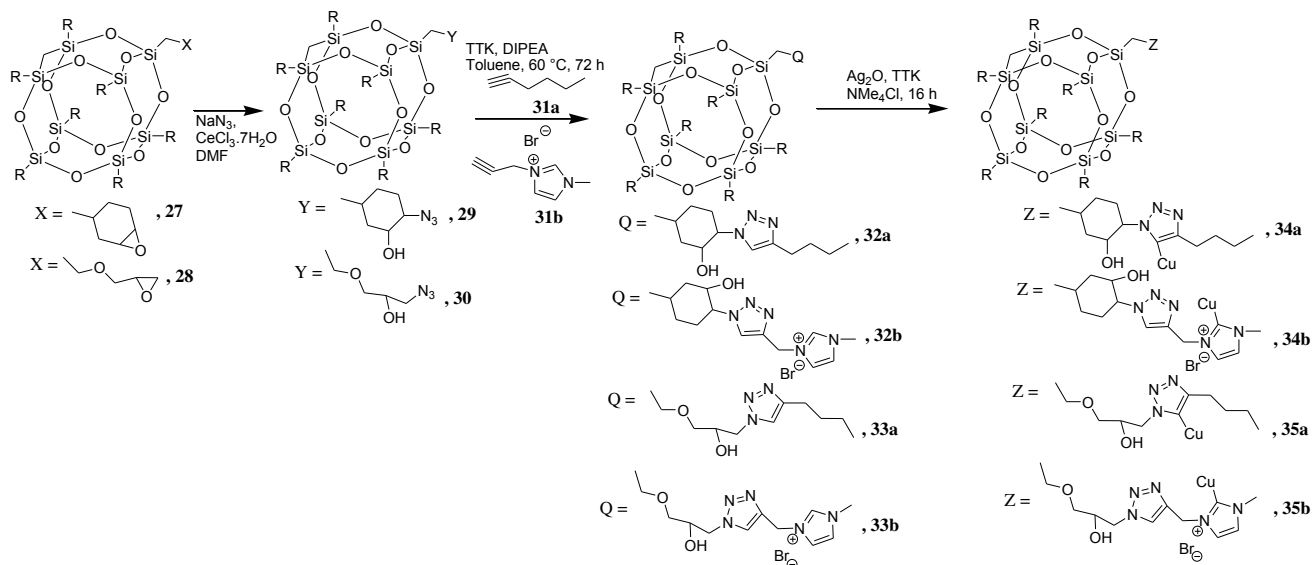
Scheme 2.1.2: Step by step reaction pathways for the synthesis of organic modifiers with potential sites for the immobilization of Ru catalyst, subsequent modification of nanoclays and immobilization of Ru catalyst.

It is expected that the interlayer distance d_1 , for pristine clay would be enhanced when the modifications and subsequent attachment of copper is completed, giving rise to new interlayer distances d_2 and d_3

The proposed pathway for the attachment of Ru catalyst onto clay galleries in this thesis can be seen in **scheme 2.1.2**. The increase in the interlayer distance of the clay material, which is proof of complete exfoliation or intercalation of the surfactants, is expected.

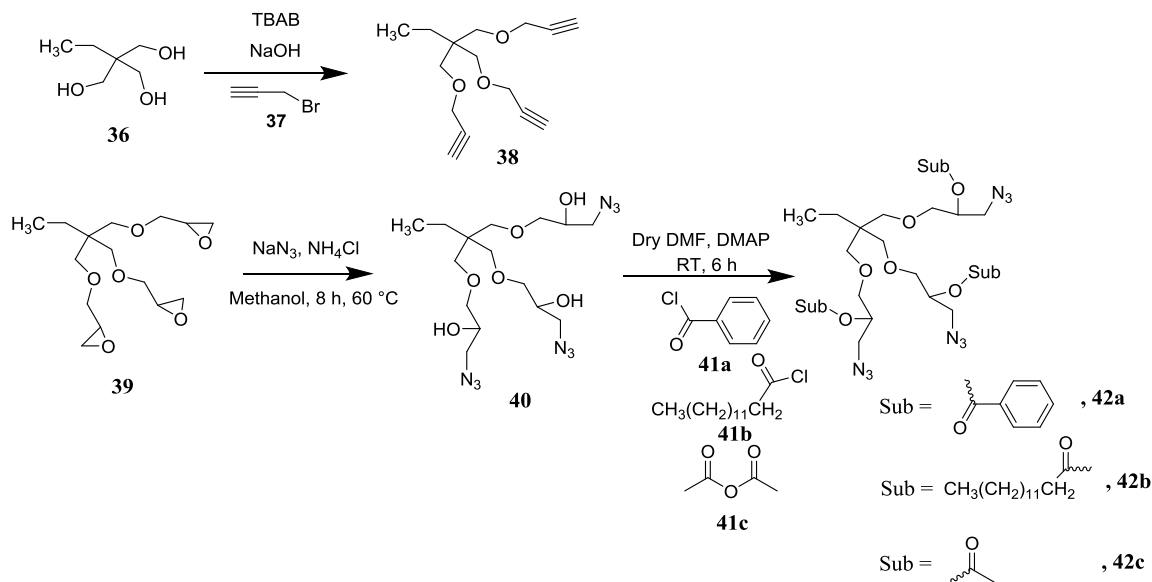
However, the approach for the attachment of Cu and Ru catalyst on POSS materials is different and the proposed reaction pathway is shown in **scheme 2.1.3**. One approach is to make a Cu-carbene on the triazole ring formed by click chemistry, however, in a second approach the Cu-carbene is formed by covalent linkage.

To evaluate the performance of the synthesized Cu-immobilized nanoparticles (clay/POSS), trivalent azide and alkynes could be useful where a “click” network develops during a cross-linking reaction, analyzed via DSC.



Scheme 2.1.3: Surface modification of different POSS compounds with low molecular weight compounds with potential bonding sites for metal catalyst.

Consequently, the synthesis and encapsulation of the multivalent low molecular weight alkynes and azides by *in situ* polymerization with poly (Urea-Formaldehyde) (PUF) as the shell could be achieved and the synthesized capsules would be used to prepare self-healing composites in the future.



Scheme 2.1.4: Synthetic representation of the synthesis of multivalent alkynes and azides with subsequent modifications.

Chapter 3

Synthesis and characterization of Cu and Ru immobilized nanoclays

Sodium montmorillonite (Na-MMT) which is a special type of clay minerals, is abundantly available having great swelling capacities, high cationic exchange capacities and a high surface area²³⁴. These interesting properties of Na-MMT makes it a preferred option for researchers seeking to use nanofillers that can be engineered at the nanometer regime for making materials with fire retardant properties. The hydrophilic nature of nanoclays however, hinders the homogeneous dispersion of these clay minerals in a hydrophobic polymer matrix²³⁵. Therefore, modifying the nanoclay surface with organic modifiers creates a hydrophobic environment that enhances its compatibility with the polymer matrix. Herein, the modification of clay was done using different types of synthesized alkylammonium and tertiary ammonium modifiers. The choice of these modifiers lie in their ability to form a stronger dipolar bond with the hydroxonium ion in the clay gallery in addition to their ability to exhibit catalytic effect in epoxy systems²³⁶. This was followed by the immobilization of Ru and Cu metal catalysts onto the clay surface. The choice of these metal catalysts (Ru and Cu) was because of their ability to activate ROMP and “click’-based reactions respectively. This organically-modified clay with catalytically active sites not only play a vital role in the delamination of the organoclay in polymer matrix, but can also act as catalyst for the activation of self-healing functions at low temperatures.

3.1.Modification of nanoclay with vinylbenzyl dodecyl ammonium chloride (VDAC) and subsequently with Grubbs first generation catalyst

The modification of nanoclays began with the synthesis of vinylbenzyl dodecyl ammonium chloride (VDAC)**16**, which was according to the procedure from Qutubuddin²³⁷. It was just a one step quaternization reaction with a yield of 79 %. The purity of the quaternization reaction was proven by ¹H NMR.

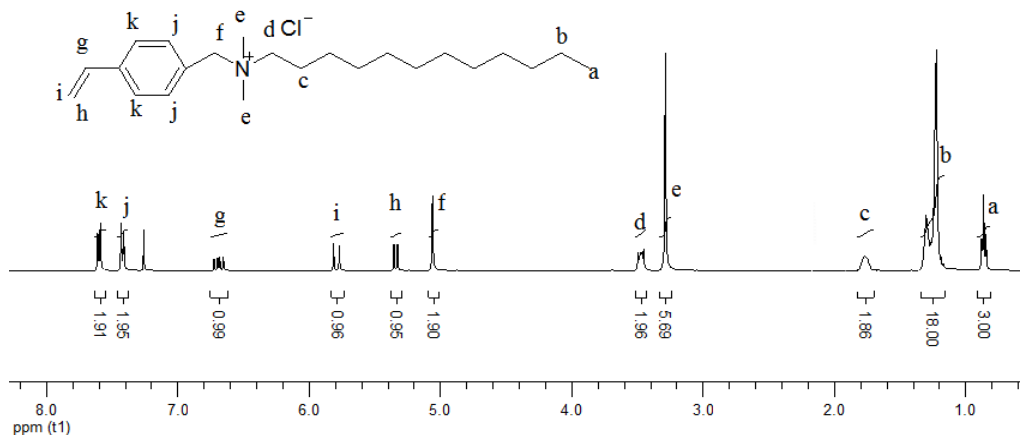
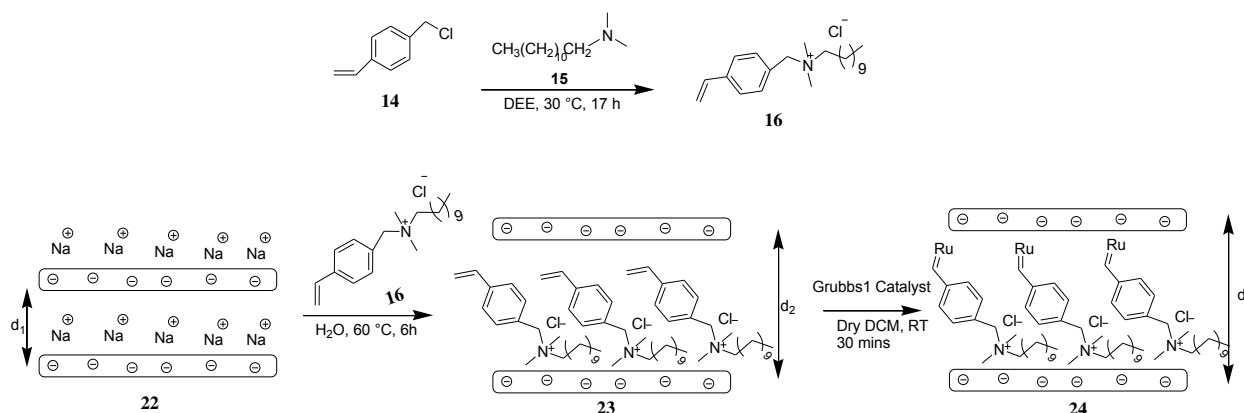


Figure 3.1.1: ^1H NMR spectrum of vinylbenzyldecyl ammonium chloride (**16**).

As can be seen in **Figure 3.1.1**, the protons at position “f” appeared as a singlet at 5.06 ppm and that at position “d” appeared as a doublet with J-coupling constant of 17.16 Hz. The presence of these protons and the other protons that have been successfully assigned proved that the quaternization reaction was successful. All signals were properly assigned, thus proven the purity of the compound.



Scheme 3.1.1: Synthesis of vinylbenzyldecyl ammonium chloride (**16**) and subsequent modification of nanoclay with **16** and thereafter with Grubbs catalyst I.

Subsequently, the preparation of organoclay **23** was achieved by cationic exchange reaction where the sodium ions at the interlayer of the clay galleries were replaced with VDAC (**16**). Further details about the synthetic procedure have been explained in the experimental section. As a prove of successful intercalation or exfoliation, the interlayer distance was increased significantly (see **table 5**). However, the interlayer distance (d_3) of clay **24** (23.0 d/A) was

slightly higher than clay **23** (22.8 d/A) as determined by XRD. This result was expected giving that the Ru catalyst doesn't have any significant impact on the interlayer distance.

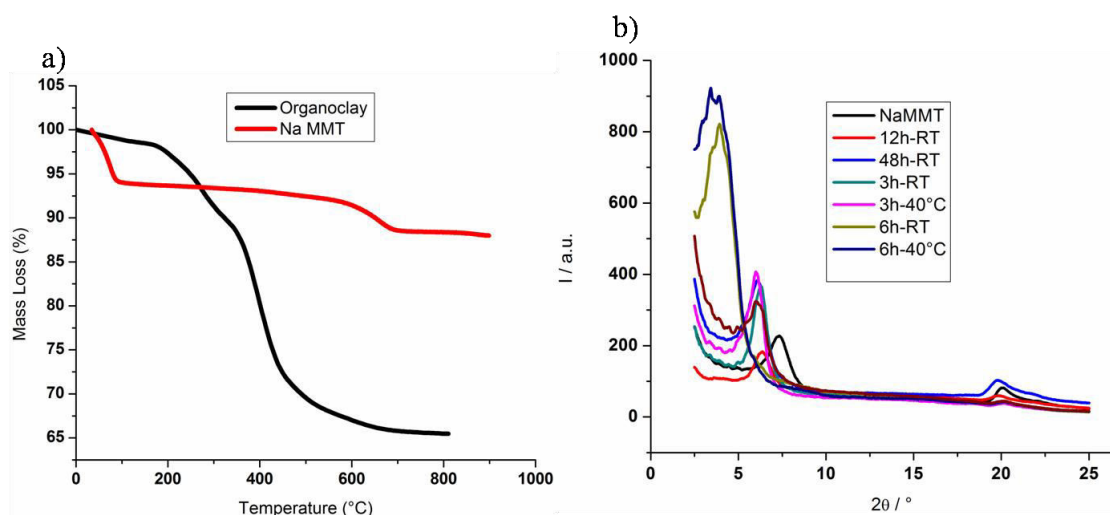


Figure 3.1.3a): Thermogravimetric analysis of organoclay, and b): X-ray diffraction patterns of modified clay materials at different modification conditions.

Table 5: Effect of temperature and time on the loading of vinylbenzyldecyl ammonium chloride on NaMMT.

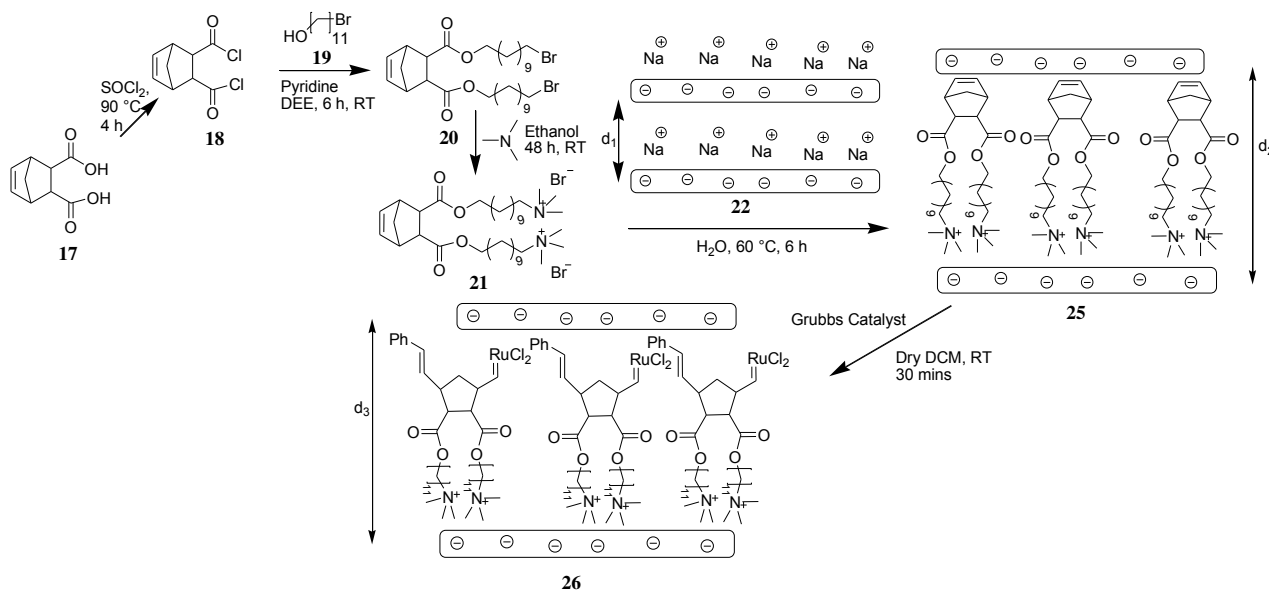
S/N	Organoclay	Reaction Condition	d/A (d ₂)	Amount of Na ⁺ exchanged (%)	Mass Loss (%)	Loading of surfactant ^a	
						mmol/mg	mg/mg
1	NaMMT	-	12.1	-	-	-	-
2	NaMMT:VDAC	3h, 40°C	14.8	87.8	29.40	0.72 *10 ⁻³	0.258
3	NaMMT:VDAC	3h, RT	13.9	82.9	26.21	0.68 *10 ⁻³	0.244
4	NaMMT:VDAC	6h, 40°C	22.0	93.9	33.51	0.77 *10 ⁻³	0.276
5	NaMMT:VDAC	6h, RT	22.8	93.4	32.91	0.77 *10 ⁻³	0.276
6	NaMMT:VDAC	12h, RT	14.6	85.4	28.12	0.70 *10 ⁻³	0.251
7	NaMMT:VDAC	48h, RT	14.6	87.8	29.34	0.72 *10 ⁻³	0.258

a: value calculated from TGA

Thermogravimetric analysis of the organoclays was carried out to investigate their thermal stabilities. It can be seen in **Figure 3.1.3a** that the organoclay was more thermally stable up to 200 °C. The analysis also showed the percentage decomposition of organic phase as well as the inorganic phase. Further modification parameters are outlined in **table 5**. Entry 4 and 5 shows the right condition for obtaining the maximum loading on the surface of nanoclays with the value

of the interlayer distance of the modified clay doubled when compared to the pristine clay and the amount of the Na^+ ions exchanged almost at maximum. X-ray diffraction patterns were done to underscore the effect of the cationic exchange reactions with regards to the interfacial distance (**Figure 3.1.3b**). The interlayer distance, d_2 was almost doubled after the complete modification for entry 4 and 5, compared to the pristine clay (NaMMT), entry 1.

3.2. Modification of nanoclay with 5,6-di(11-(n,n,n-trimethylammonium)undecoxycarbonyl) norbornene(**21**) and subsequently with Grubbs catalyst



Scheme 3.2.1: Synthesis of 5,6-di(11-(n,n,n-trimethylammonium)undecoxycarbonyl) norbornene (**21**) followed by the modification of nanoclay with **21** and thereafter with Grubbs catalyst II.

A second surfactant with the ability to bond Ru metal catalyst onto itself at the interlayer of clay galleries was synthesized according to several procedures (**scheme 3.2.1**). The surfactant, 5,6-di(11-(n,n,n-trimethylammonium)undecoxycarbonyl) norbornene **21**, was prepared in three steps. Firstly, bicyclo(2,2,1)-hept-5-ene-2,3-dicarboxylic acid **17**, was converted to bicyclo(2,2,1)-hept-5-ene-2,3-dicarbonyl chloride **18**, by esterification reaction by treating it with thionyl chloride according to the procedure from Binder et al.^{238,239}. Then the chloride derivative was reacted with bromoundecanol in pyridine followed by dropwise addition of diethylether to give 5-norbornene

diester **20**, as adopted from Harsha²⁴⁰ and Behling²⁴¹. Finally, the norbornene diester was mixed with trimethylamine in ethanol and stirred for 48 h under argon to give 5,6-di(11-(n,n,n-trimethylammonium)undecoxycarbonyl) norbornene **21**.

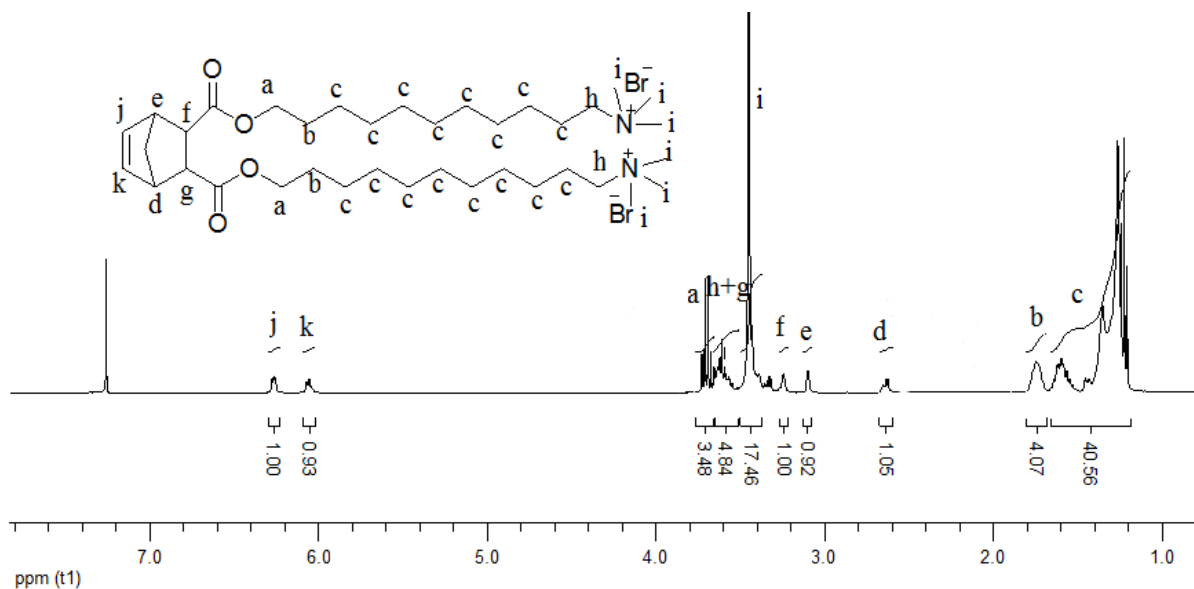


Figure 3.2.5: ¹H NMR spectrum of 5,6-di(11-(n,n,n-trimethylammonium)undecoxycarbonyl) norbornene (**21**).

Figure 3.2.5 shows the purity of 5,6-di(11-(n,n,n-trimethylammonium)undecoxycarbonyl) norbornene. All peaks were properly assigned, thus proving the structure of the compound.

The cationic exchange reaction of **21** with Na MMT **22**, was according to the procedure from Harsha²⁴⁰ by mixing norbornene surfactant **21**, with Na MMT clay **22** in distilled water and stirred under reflux for 96 hours to achieve maximum grafting density. The modified clay was recovered by filtration and further dried under vacuum at room temperature for 24 hours.

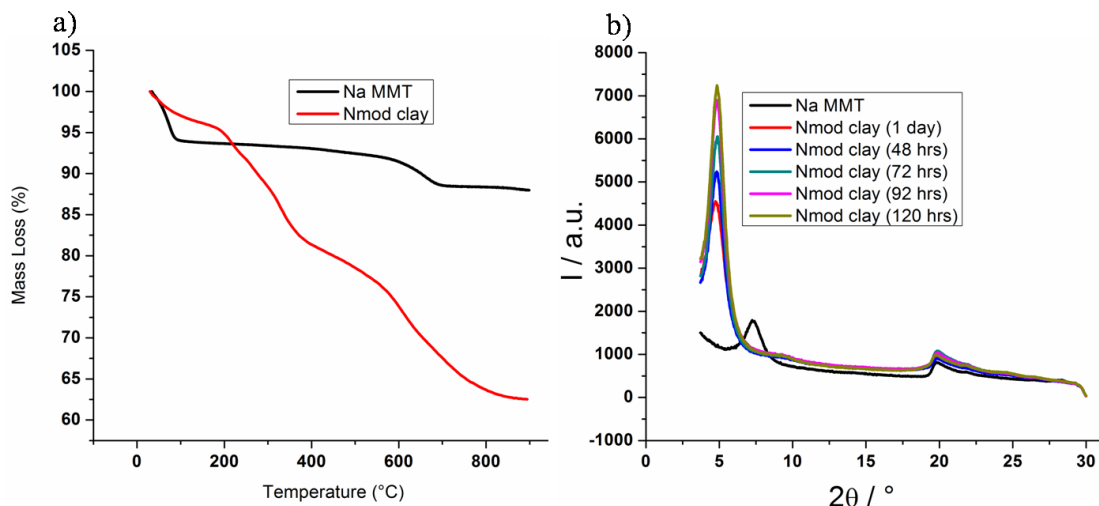


Figure 3.2.7 a): Thermogravimetric analysis of Nmod clay²⁵, and b): X-ray diffraction patterns of modified clay materials at different modification conditions.

The thermogravimetric analysis of the modified clay **20**(**Figure 3.2.7a**), showed two degradation peaks at 194.0 °C and 561.6 °C where the first degradation temperature corresponds to the Hoffmann decomposition peak caused by the decomposition of the surfactant molecule while the second degradation peak corresponds to the decomposition of the hydroxonium ions in the clay galleries. The X-ray patterns (**Figure 3.2.7b**) were measured and **table 6** below contains interfacial spacing of the modified clay materials at different reaction conditions. There wasn't any major difference in the interfacial distance with respect to the reaction conditions.

Table 6: Influence of reaction time on the cationic exchange reaction of **21** with NaMMT²² at 60 °C.

S/N	Organoclay	Reaction Time (hrs)	d/A	Amount of Na ⁺ exchanged (%)	Mass Loss (%)	Loading of surfactant ^a	
						mmol/mg	mg/mg
1	Nmod clay 01	120	18.1	52.3	23.33	0.43 *10 ⁻³	0.233
2	Nmod clay 02	96	18.5	70	31.00	0.57 *10 ⁻³	0.309
3	Nmod clay 03	72	18.3	56.6	25.19	0.46 *10 ⁻³	0.251
4	Nmod clay 04	48	18.2	51	22.61	0.42 *10 ⁻³	0.228
5	Nmod clay 05	24	18.2	50	21.97	0.40 *10 ⁻³	0.219

a: value calculated from TGA

From **table 6**, it can be seen that the highest grafting density of the modifier in the clay gallery was obtained at 96 hours with the amount of Na⁺ ions exchanged being 70 %. This modification was repeated to prove its reproducibility, and the results proved positive implying that the amount of Na⁺ ions exchanged are reproducible. After 96 hours, the grafting is drastically

reduced suggesting that the strength of the electrostatic bond that exists between the modifier and the hydronium ions in the clay gallery is weakend, and the already bonded modifiers are cleaved off.

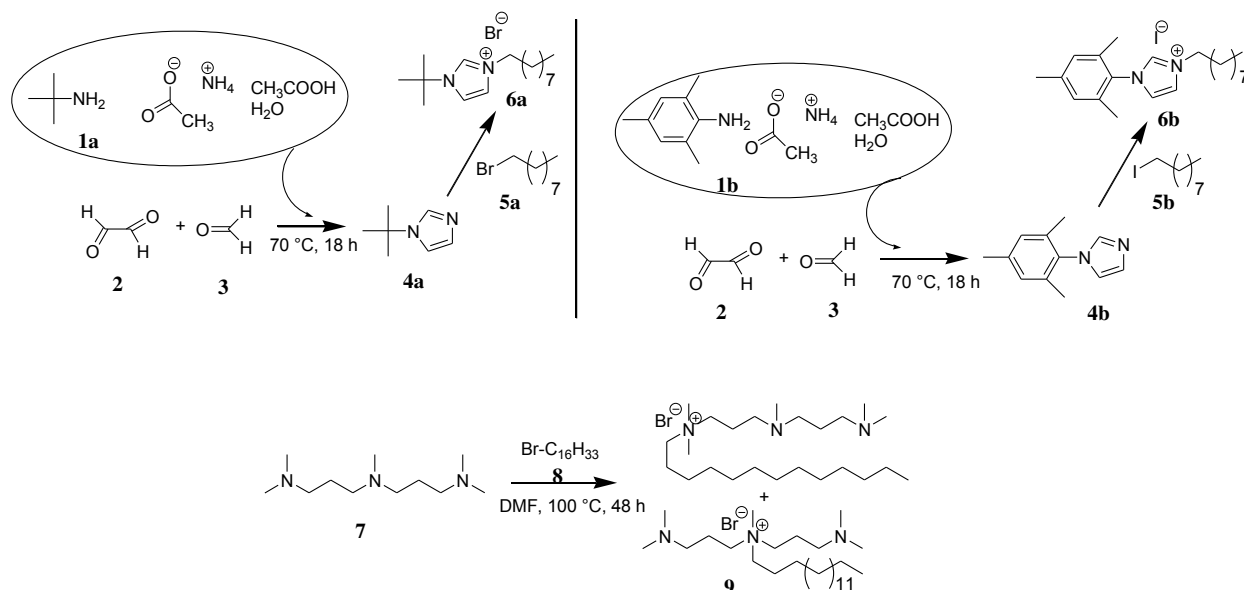
ROMP active Nmod-MMT substrate**26**, was prepared by the dispersion of Nmod-MMT**25** in dichloromethane for 4 hours with rigorous stirring at room temperature, and followed by the addition of Grubbs catalyst (first generation). The mixture was rigorously stirred for 1 hour at room temperature, thereafter filtered and the Ru-modified clay surface was dried under inert conditions. The G1-modified clay was thoroughly washed with dry DCM (50 mL, three times) to remove unreacted catalyst. Flame atomic absorption spectrometry was done to quantify the amount of Ru carbens formed on the surface. From the obtained FAAS results (**table 7**), it was found that the G1-modified Nmod clay contained more Ru (0.015 mg/mg) than the G2-modified Nmod clay (0.007 mg/mg).

Table 7: Flame atomic absorption spectrometric measurements of Grubbs-modified clay nanomaterials.

S/N	Grubbs-modified clay	Amount of Ru (mmol/mg)	Amount of Ru (mg/mg)
1	G1-mClay (24)	$0.27 * 10^{-4}$	0.022
2	G2-mClay (24)	$0.15 * 10^{-4}$	0.013
3	G1-Nclay (26)	$0.18 * 10^{-4}$	0.015
4	G2-Nclay (26)	$0.82 * 10^{-5}$	0.007

3.3.Synthesis of modifiers for Cu (I) attachment¹⁴⁸

Three different modifiers were prepared requiring a few steps, for the attachment of Cu(I)(required for “click” chemistry) unto clay galleries as illustrated in **scheme 3.3.1** according to the procedure from Giovanni²⁴² with modification. For the synthesis of 1-tertiary-butyl-1-dodecylimidazolium bromide **6a**, two reaction pathways were followed. In the first step, a solution of glacial acetic acid, ammonium acetate in water and 2-methylpropane-2-amine were added drop-wise to a flask containing glacial acetic acid, aqueous formaldehyde and aqueous glyoxal.



Scheme 3.3.1: Synthesis of the different organic modifiers with potential sites for Cu I attachment.

In the second step, 1-tert-butyl-1H-imidazole **4a** was reacted with 1-bromodecane to obtain the desired product. 1-Mesityl-1-dodecylimidazolium iodide, **6b** was synthesized under the same reaction conditions as **6a**. Firstly, a stock solution of mesitylamine **1b**, glacial acetic acid, ammonium acetate in water was added drop-wise to a flask containing glacial acetic acid, aqueous formaldehyde and aqueous glyoxal. Subsequently, 1-mesityl-1-dodecylimidazolium iodide **4b**, and 1-iodododecane were reacted in THF to give the desired product. The synthesis of the third modifier (tertiary amino ligand) **9**, was based on nucleophilic substitution of the bromine atom in 1-bromohexadecane by one amino group. This was accomplished according to the procedure from Stein, et.al¹⁴⁹ where N¹-(3-(dimethylamino)propyl)-N¹,N³,N³-trimethylpropane-1,3-diamine **7** was added to DMF, and with the protection of nitrogen, the mixture was heated to high temperatures followed by the drop-wise addition of 1-bromohexadecane **8**. The large excess of amine (**7**) (molar ratio of **7** to **8** is 4:1) and drop-wise addition of **8** ensured that the desired product should be mono-quaternized predominantly. The excess amine was removed, to a large extent by distillation under high vacuum without further purification because amine impurities would not affect further cation exchange reactions since these impurities do not carry charges. Besides, the impurities would be largely removed during the washing of the modified clay with warm water and ethanol.

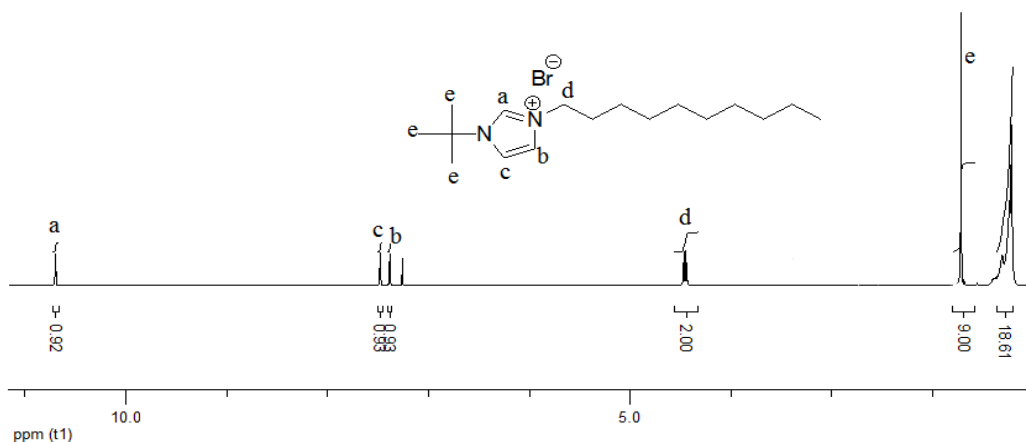


Figure 3.3.1: ^1H NMR spectrum of tert-butyl-1-dodecylimidazolium bromide **6a**.

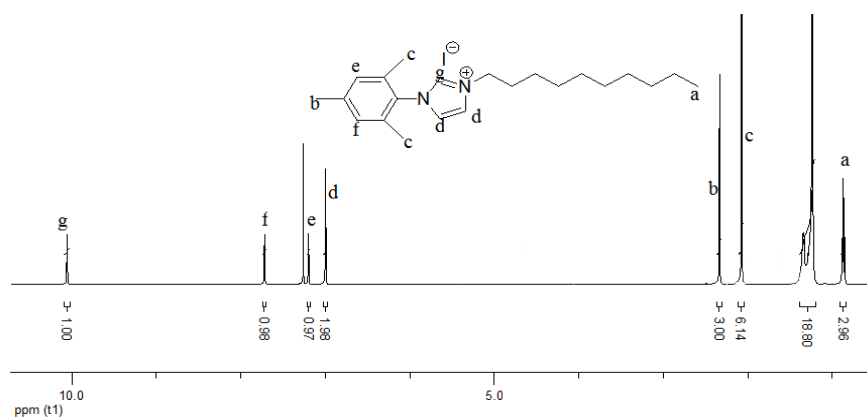


Figure 3.3.2: ^1H NMR spectrum of 1-mesityl-1-dodecylimidazolium iodide **6b**.

Figure 3.3.1 shows a signal at 4.46 ppm (t, $J = 7.46\text{Hz}$) belonging to protons at position 'd' confirming the completion as well as the purity of the reaction. In **Figure 3.3.2**, the appearance of the signal at 0.87 ppm (which is a triplet with J -coupling constant of 6.78 Hz) confirms the successful completion of the reaction as well as its purity.

The proton NMR spectra of the tertiary amine ligand (**9**), shown in **Figure 3.3.3** confirm the successful quaternization of the desired compound proven by the appearance of NMR peaks around 3.45 ppm, originating from the H atoms within the vicinity of the quaternized N atom. Quaternization can occur at terminal or central nitrogen atoms not exempting the possibility at multiple nitrogen atoms¹⁴⁹. The peak at 2.19, 2.29, and 2.38 ppm in the spectrum below is coming from a side product where both the central nitrogen and one/all terminal nitrogen atom(s) where quaternized at the same time by the long alkyl chain. Such products are usually obtained

as mixtures, hence the position of quaternization doesn't really matter for the subsequent clay modification process. As long as quaternization takes place, cationic sites are created in the modifier, making cationic exchange reactions of clay materials possible. Other peaks were properly assigned as can be seen in the NMR spectra below (**Figure 3.3.3**).

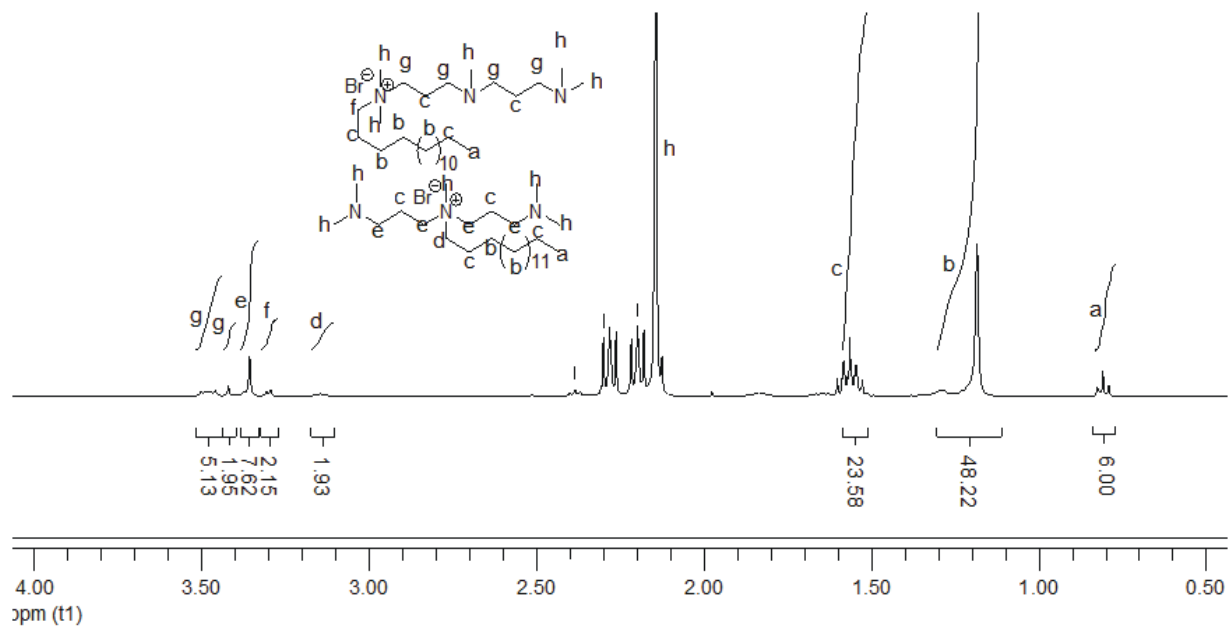
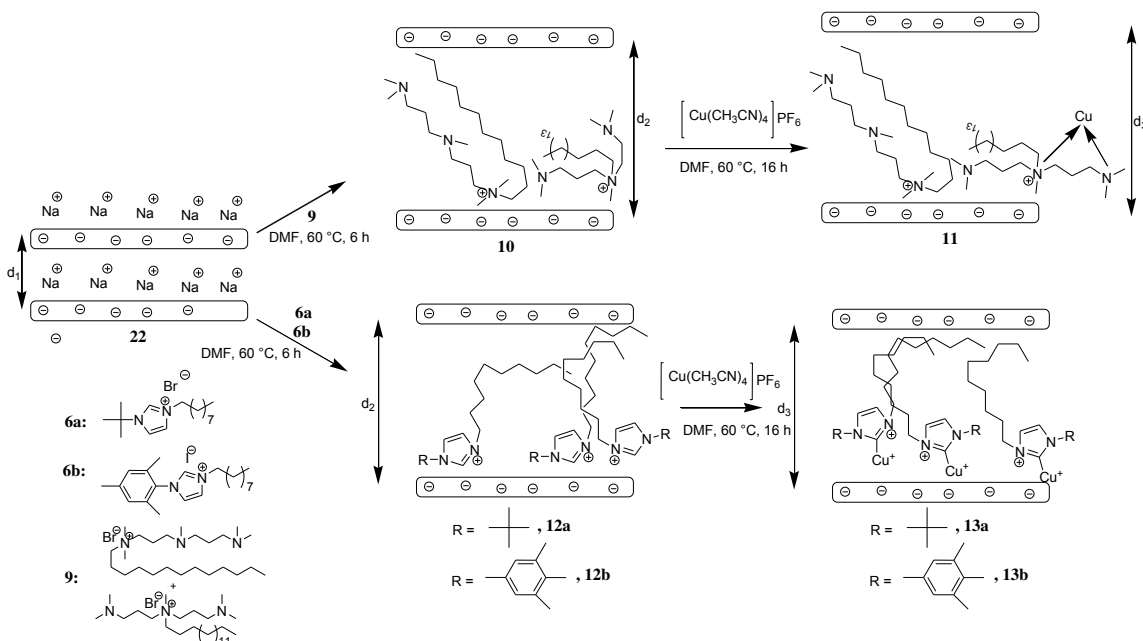


Figure 3.3.3: ^1H NMR spectra of tertiary ammonium ligand **9**.

3.4. Modification of nanoclay with **6a**, **6b**, **9** and subsequent attachment of Cu(I)



Scheme 3.4.1: Synthetic representation of nanoclay modification and subsequent attachment of Cu(I).

The modification of Na-MMT **22**, with 1-tertiary-butyl-1-dodecylimidazolium bromide **6a**, 1-mesityl-1-dodecylimidazoliumiodide **6b** and tertiary amino ligand **9** was done according to the procedure from Qutubuddin²⁴⁰ with modification. Na MMT was dispersed in a 50:50 mixture of water and methanol and the solution was allowed to stir for 1 hour to allow the clay to swell. The respective modifiers **6a**, **6b**, and **9** were dissolved in minimal amount of methanol and the resultant mixture was allowed to stir for further 5 hours while slowly cooling down to room temperature to give **11**, **12a** and **12b**.

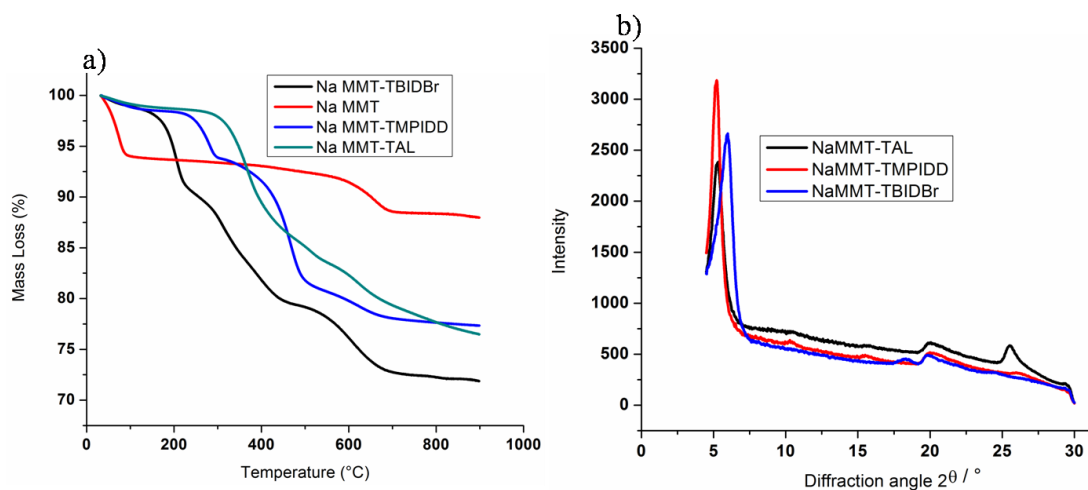


Figure 3.4.1: a) Thermogravimetric analysis, conducted under nitrogen atmosphere of modified clay: Na MT-TAL (**11**), Na MMT-TBIDBr (**12a**), Na MMT-TMPIDD (**12b**), and b): X-ray diffraction patterns of modified clay materials.

Thermogravimetric analysis was conducted under nitrogen atmosphere to determine the extent to which the material can resist heat. It can be seen from the graph (**figure 3.4.1A**) that the attachment of **9**, **6a**, and **6b** to the organoclay caused an increase in the thermal strength of the organoclay with values tabulated in **table 5**.

To the best of our knowledge, this is the first attempt made to attach copper (I) covalently unto modified clay surfaces both specifically (**12a and 12b**) and non-specifically (**11**). To achieve successful attachment of Cu(I), the modified clay, **13a/13b**, was dissolved in dry DMF and stirred for few hours at room temperature to allow the clay to swell. Thereafter, tetrakis(acetonitrile)copper(I) was added and the resultant solution was allowed to stir for some hours. After several failed attempts to remove the soluble excess copper, washing the obtained

Cu(I)-modified clay with dry DMF for several times with centrifuge gave the desired product, having no trace of soluble copper still present as proven by XPS.

Although Girard et al.²⁴³, made attempts to attach copper (1) unto clay galleries, the method employed seem somewhat questionable because with just physical mixing of clay materials with copper compound, there is the possibility of having copper (1) trapped in the clay gallery without the required bonding that is needed. Besides, the electrostatic bond between the hydronium ion in the clay gallery and the presupposed copper (1) is too labile, and hence can break easily.

Furthermore, the amount of copper attached on the surface was determined by Flame Atomic Absorption Spectroscopy as (see table 8). When compared with the amount of the potentially active sites before the attachment of copper, it can be seen that not all active sites had copper bonded to them which gives the possibility for further improvement on the reaction conditions for the formation of more copper carbenes.

X-ray diffraction measurements can be used to determine a number of parameters for any given sample. Of practical relevance to his work is the determination of the interlayer d-spacing (extrapolated from Bragg's equation) before and after modification of NaMMT. In principle, for complete exfoliation or intercalation of clay platelets, the interlayer d-spacing should increase significantly owing to the fact that the Na⁺ ions initially present at the interlayer of the pristine clay are replaced with bulkier organic molecules.

Table 8: Interlayer d-spacing of modified clay materials measured by XRD using Ni filter CuK_α radiation in transmission at a sample-detector distance of 9.85 cm.

Catalyst	Td (°C) ^a	d/A	Catalyst	Amt of Cu (I) (mg of Cu/mg of clay) ^a	Amt of Cu (I) (mmol of Cu/mg of clay) ^a
NaMMT (22)	-	12.1			
NaMMT-TAL (10)	308.6	16.7	NaMMT-TAL-Cu (11)	0.138	0.15 x 10 ⁻³
NaMMT-TMPIDD (6b)	240.8	20.9	NaMMT-TMPIDD-Cu (12b)	0.043	0.52 x 10 ⁻⁴
NaMMT-TBIDBr (6a)	174.6	17.1	NaMMT-TBIDBr-Cu (12a)	0.077	0.1 x 10 ⁻³

a: Values measured by FAAS.

The peak position, peak width, and peak intensity are critical parameters to be considered when calculating the d-spacing, bearing in mind that the most accurate is calculated from the high-angle peaks. **Table 8** above summarizes the interlayer d-spacing and the increase in interlayer distance as prove that some or most of the cations have been successfully exchanged. The lowest angle peaks originate from the (001) plane diffraction. After the modification, the same peaks shifted to lower angles indicating an increase in the interlayer d-spacing. The pristine clay showed two peaks and this could probably be due to a mixture of minerals. The modified clay materials also displayed two (001) peaks, strongly suggesting that the two d-spacings could be due to the heterogeneity of the pristine NaMMT as well as the different charge densities²⁴⁴.

To further confirm the attachment of copper, EDX (Electronic Dispersive using X-ray) analysis was done to prove the presence of copper (see **Figures 3.4.2, 3.4.3, 3.4.4** in appendix).

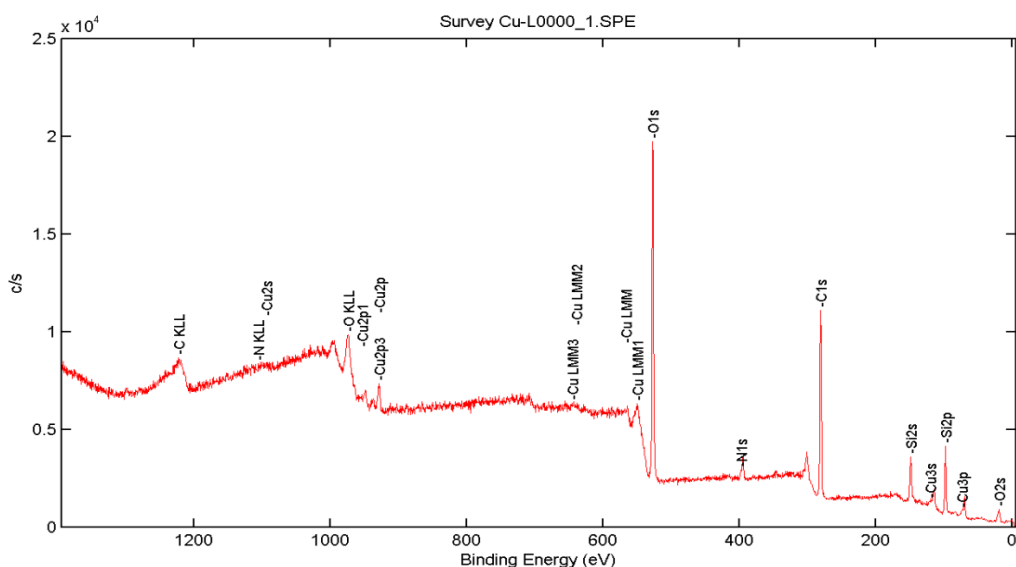


Figure 3.4.5: X-ray photoemission spectroscopic analysis (XPS) measured at 200 μ 50W X-ray settings of NaMMT-TAL-Cu (**11**) showing the oxidation state of Cu (I).

X-ray Photoemission Spectroscopy (XPS) was measured to investigate the state of copper present.

The analysis of NaMMT-TAL-Cu (**11**) shows the presence of C, O, N, Si, and Cu in the survey spectrum (**Figure 3.4.5**). In order to get the different Cu contributions, the shakeup satellites characteristic of the Cu oxidation states was taken into account. The result shows that the deconvolution of the Cu_{2p3/2} peak shows two different Cu contributions²⁴⁵. The contribution at

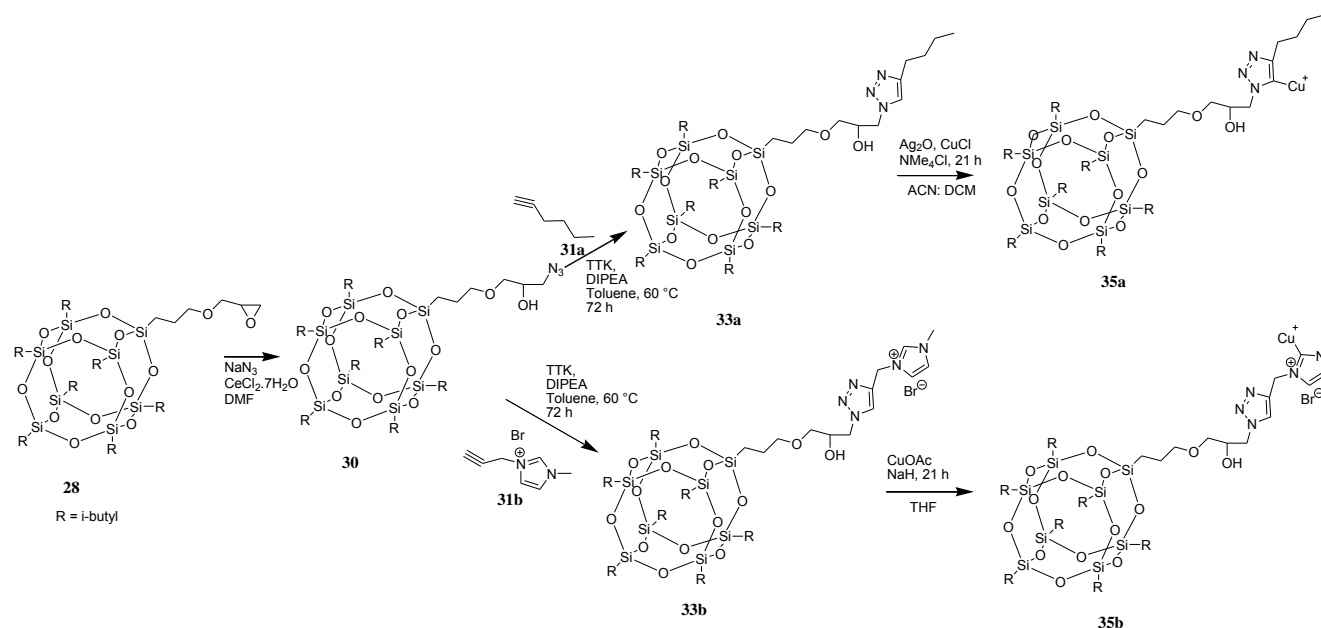
933.3 eV is related to Cu in +1 state and the one at 935.2 eV is related to Cu in +2 states. Based on the fitting of the peaks, the ratio of Cu (I) to Cu (II) is 50%/50%. The XPS analysis of Cu (I) in NaMMT-TBIDBr-Cu and NaMMT-TMPIDD-Cu at the time of writing this thesis wasn't accomplished due to time constrain; however, the catalytic activity was investigated (as would be seen in subsequent chapters) without the inclusion of a base. The exact amount of the copper catalyst present on the surface (estimated using FAAS) was taken into consideration while calculating the amount of the filler used in the mixture for the cross linking kinetics as seen in subsequent chapters.

Chapter 4

Synthesis and characterization of copper-immobilized POSS

To improve the mechanical properties and thermal properties of resin materials, surface modification of POSS molecules with subsequent attachment of metal catalysts (Cu and Ru) was done. This surface-modified POSS with catalytically active sites not only play a vital role in the enhancement of desired properties, but can also act as catalyst for the activation of self-healing functions at low temperatures.

4.1. Surface modification of glycidylisobutyl POSS for Cu (I) attachment



Scheme 4.1.1: Synthetic representation of glycidylisobutyl POSS modification with 1-hexyne and 1-propargyl-3-methylimidazole bromide, and subsequent attachment of Cu(I).

The attachment of Cu (I) onto POSS surface (**35a**, **35b**) was accomplished through two series of reaction pathways. Sodium azide was added to a mixture of glycidylisobutyl POSS (**28**) and cerium (III) chloride heptahydrate in a mixture of DMF and THF. The azido-hydroxyl POSS formed (**30**) was reacted separately with 1-hexyne (**31a**) and 1-propargyl-3-methylimidazole bromide (**31b**) by click reaction to give **33a**, and **33b**. Consecutively, treatment of **33a**, and **33b** separately with Ag_2O /ammonium chloride and then tetrakis(acetonitrile)copper(I)

hexafluorophosphate ($\text{Cu}(\text{MeCN})_4\text{PF}_6$) at room temperature²⁴⁶ successfully afforded the air-stable 1,2,3-triazole-5-ylidene-copper(I) complexes **35a** and **35b** characterized by ^1H NMR.

The characteristic signals of structure **30** at 3.9 ppm, assigned to the $-\text{CH}$ protons attached to the $-\text{OH}$ group, in the ^1H NMR, and the signals at 73.6 ppm (position “d”); 71.5 ppm (position “c”); 71.0 ppm (position “b”) and 53.4 ppm (position “a”) in the ^{13}C NMR prove the successful azidation reaction of the desired product (**Figures 4.1.1** below and **4.1.2** in appendix).

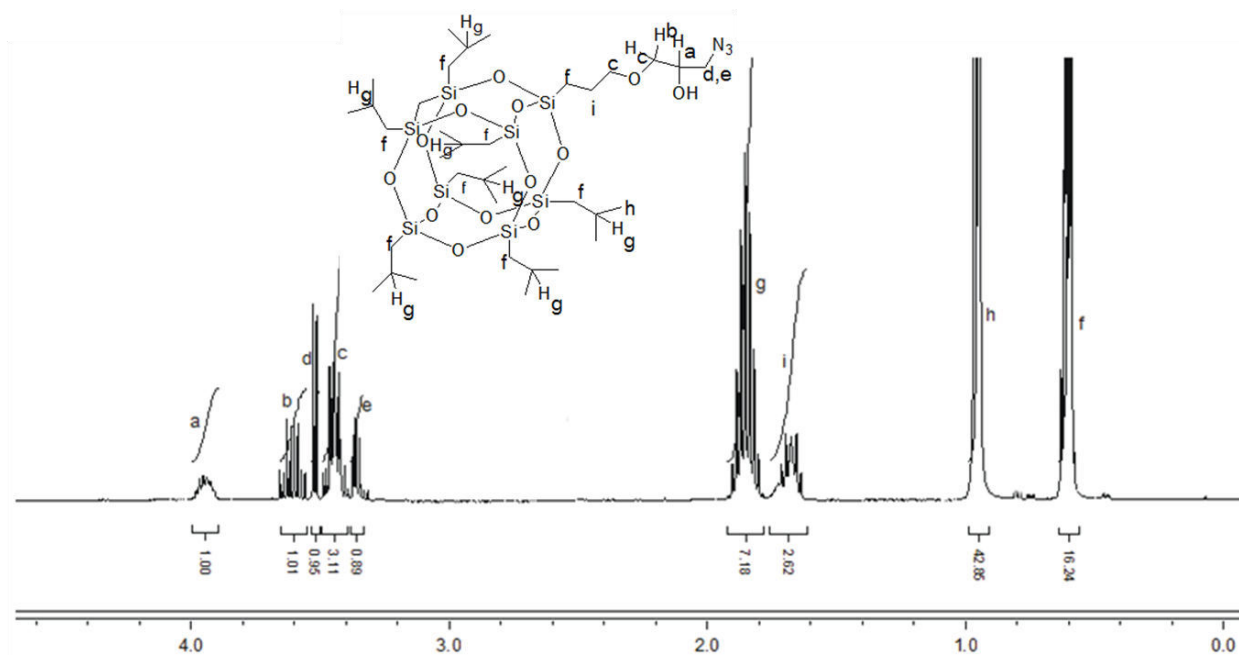


Figure 4.1.1: ^1H NMR spectrum of azidohydringlycidylisobutyl POSS **30**.

All other signals were properly assigned inclusive of the OH signal at 1.70 ppm (position “i”). Subsequently, the ^{29}Si NMR (**Figure 4.1.3**, see appendix) showed three characteristic peaks at 67.4 ppm, 67.6 ppm, and 67.8 ppm that can be assigned to silicons at position 1, 2, and 3 in **Scheme 4.1.1**.

In **Figure 4.1.4** all the characteristic signals of the protons of **33a** were properly assigned including the new peak at 7.41 ppm which is coming from the proton of the triazole ring, and the OH peak at 2.9 ppm. The ^{29}Si NMR (**Figure 4.1.5**, see appendix) shows distinctly three

characteristic peaks at 67.55 ppm, 67.69 ppm, and 67.89 ppm which can be assigned to silicon atoms at position 1, 2 and 3.

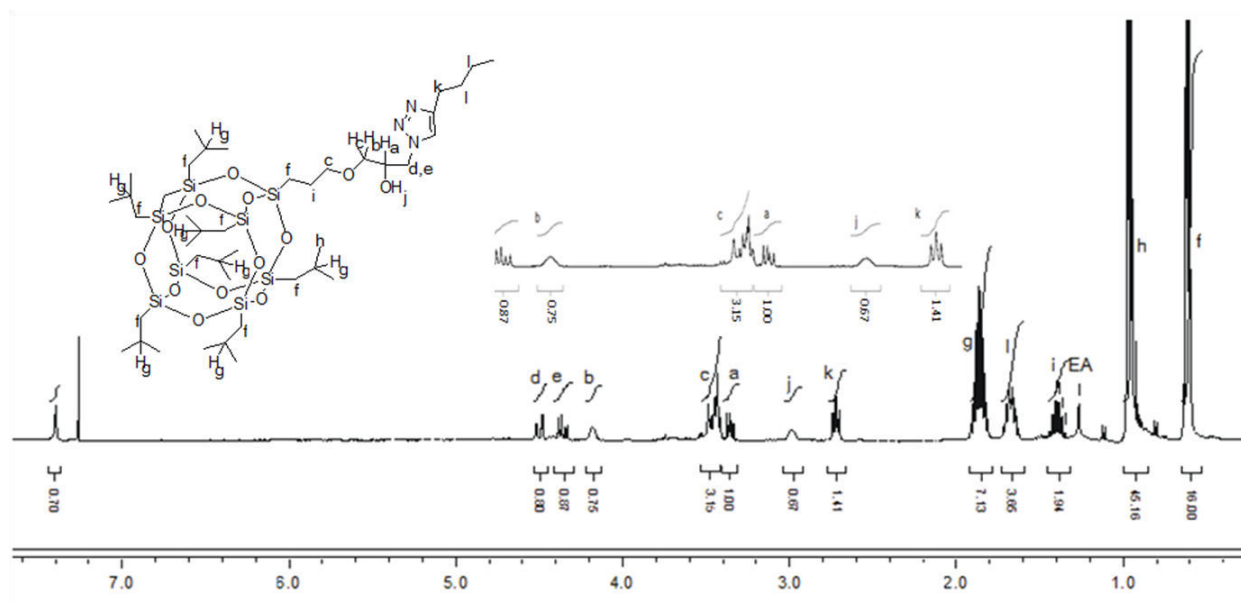


Figure 4.1.4: ^1H NMR spectrum of **33a**.

Figure 4.1.8 gives the ^1H NMR spectrum of **35a** confirming the successful attachment of Cu(I) onto **33a** with the disappearance of the triazole proton.

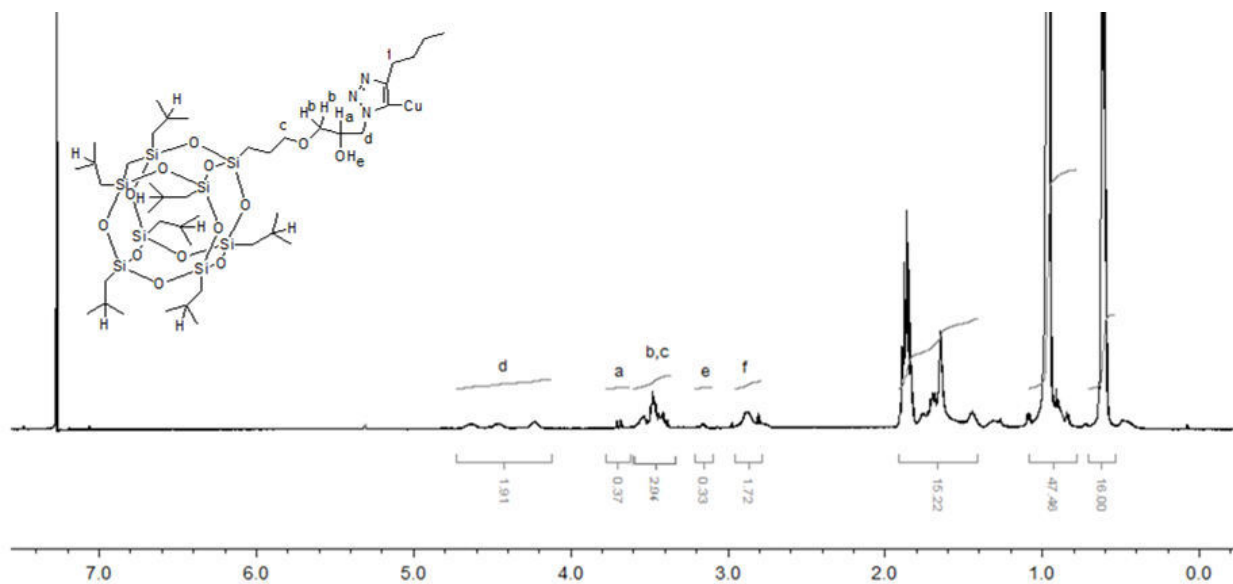


Figure 4.1.8. ^1H NMR spectrum of **35a**.

The ^1H NMR spectra of **33b** (see **Figure 4.1.9** in appendix) displays the characteristic signals of all the protons present in the molecule. As can be seen, the peak of the triazole proton appeared at 7.5 ppm. The protons at positions “o” and “p” (coming from the imidazolium molecule) appeared at 7.21 ppm and 7.1 ppm. Likewise the signal of the proton at position “k” which appears at 5.6 ppm. In the final structure **35b**, (**Figure 4.1.10**), it can be seen that peak coming from the triazole proton is not present anymore, which confirms the successful covalent bonding of Cu (I) onto the POSS surface.

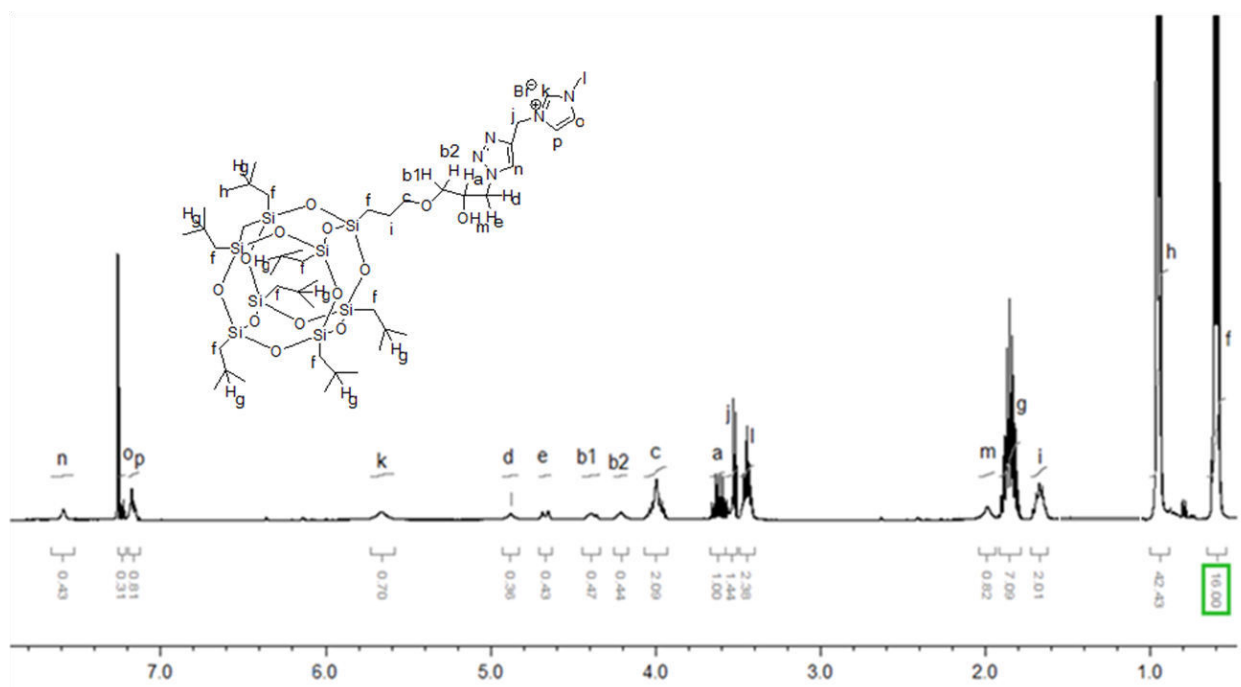


Figure 4.1.9. ^1H NMR spectrum of **33b**.

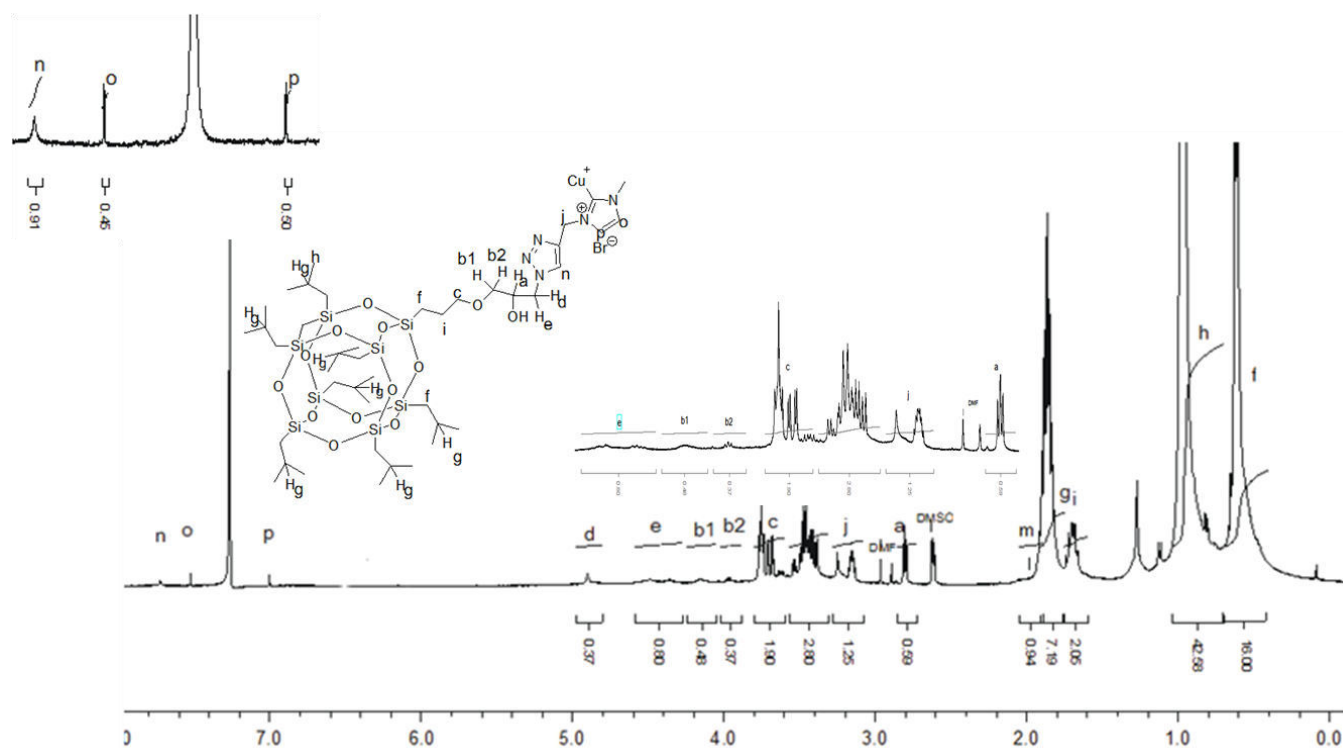


Figure 4.1.10: ^1H NMR spectrum of Cu (I)-imidazoliumhydringlycidylisobutyl POSS complex(**35b**).

MALDI-TOF analysis was also conducted, to prove the chemical identity of azidohydrinisobutyl POSS(**30**), hexynylhydrinisobutyl POSS(**33a**), and 1-methylimidazoliumhydringlycidylisobutyl POSS(**33b**). The molecular weight of compounds **30**, **33a** and **33b** is 990.1 g/mol ($M_n = 990.1$ g/mol), 1050.2 g/mol ($M_n = 1050.2$ g/mol) and 1174.5 g/mol ($M_n = 1174.5$ g/mol). The ionization was done with dithranol: **30**: LiTFA/NaTFA in the ratio 100:10:1. The major peak could be assigned to the species ionized with Na^+ ($M. \text{Na}^+, \text{C}_{34}\text{H}_{75}\text{O}_{14}\text{Si}_8\text{N}_3\text{Na}$) (found: 996.3 Da; calculated 996.3 Da). The spectrum of **33a** shows a major and a minor peak as seen in **Figure 4.1.11**. The major peak of **33a** could be assigned to the species ionized with H^+ ($M. \text{H}^+, \text{C}_{40}\text{H}_{85}\text{O}_{14}\text{Si}_8\text{N}_3\text{H}$) (found: 1056.5 Da; calculated: 1056.77 Da). The minor peak was assigned to species ionized with Na^+ ($M. \text{Na}^+, \text{C}_{40}\text{H}_{85}\text{O}_{14}\text{Si}_8\text{N}_3\text{Na}$) (found: 1078.5 Da; calculated: 1077.7 Da).

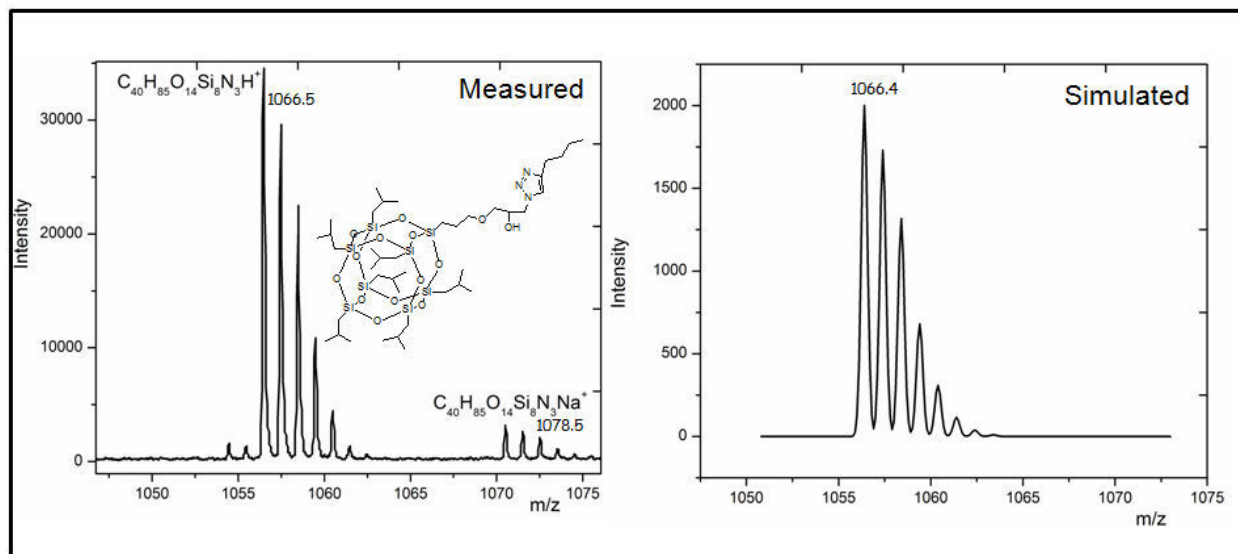
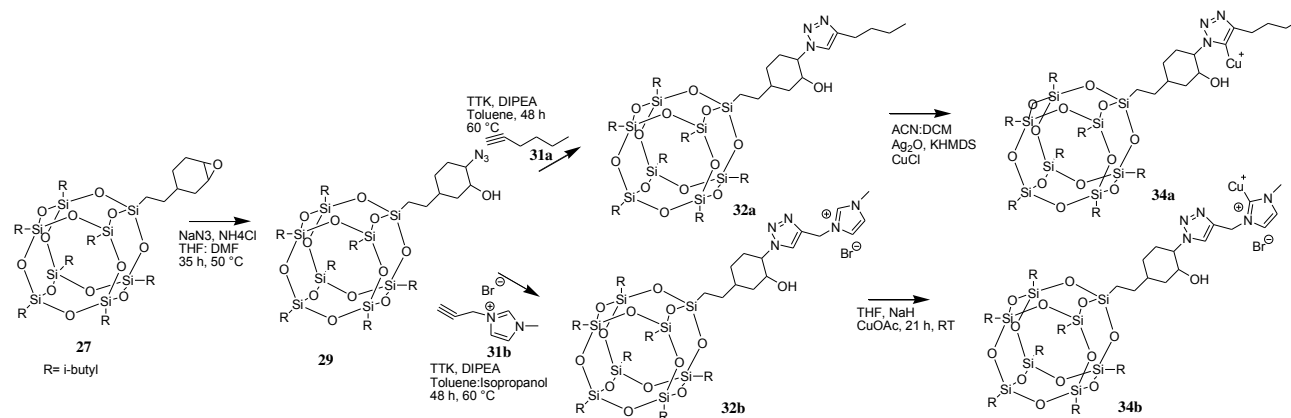


Figure 4.1.11: MALDI-TOF spectrum of hexynylhydridisobutyl POSS33a.

Figure 4.1.7 (see appendix) shows the IR spectra of the different POSS nanomaterials (**30**, **33a**, and **33b**). The IR spectra of **30** have characteristics peaks at 1088.2 cm^{-1} for Si-O-Si stretching, 1675.5 cm^{-1} for CH_2 stretching of cyclohexyl, and 1228.8 cm^{-1} for Si- CH_2 -stretching. The POSS- N_3 peak appears at 2103.8 cm^{-1} , and simultaneously another peak at 3419.12 cm^{-1} belonging to OH stretching. The spectra of **33a**, shows peaks at 1477.3 cm^{-1} for CH_2 stretching, 1092.1 cm^{-1} for Si-O-Si stretching and 3383.7 cm^{-1} for OH stretching in addition to the disappearance of the POSS- N_3 peak. And the peaks for structure **33b** show the same peaks as **33a**.

4.2. Surface modification of epoxy cyclohexylisobutyl POSS for Cu (I) attachment



Scheme 4.2.1: Synthetic representation of epoxy cyclohexylisobutyl POSS modification and subsequent immobilization of Cu (I).

The synthesis of **34a** and **34b** was achieved through a sequence of reaction steps. In the first step, a solution of epoxy cyclohexylisobutyl POSS (**27**) in tetrahydrofuran was added to a solution of sodium azide and ammonium chloride in DMF. In the synthesis of **32a**, azidohydrin cyclohexylisobutyl POSS (**29**), 1-hexyne, tetrakis(acetonitrile)copper(I) hexafluorophosphate, and N,N-diisopropylethylamine were added to a round bottom flask and heated till the reaction reached completion. Similar procedure was followed in the synthesis of **32b** also. In the final step, **32a**, and **32b** were separately reacted with tetrakis(acetonitrile)copper(I) hexafluorophosphate ($\text{Cu}(\text{MeCN})_4\text{PF}_6$) to furnish the products **34a** and **34b**. To remove unreacted copper at the completion of the reaction for compound **34a**, the solution was filtered to remove solid silver oxide followed by the evaporation of the solvent. Further purification was done by dissolving the mixture in minimal amount of dry and degassed toluene (0.1 mL), and precipitating in an equal mixture of dry DMF and acetonitrile (3 mL) to furnish the product **34a**, as a light green solid compound. In the case of compound **34b**, the solvent was removed using rotary evaporator after the completion of the reaction, and the crude product was thereafter washed several times with dry acetonitrile (3 x 5 mL) and dry DMF (3 x 5 mL). The trace of solvent was evaporated to furnish the product **34b** as a light green solid compound.

The ^1H NMR and ^{13}C NMR shown in **Figures 4.2.1** and **4.2.2** (see appendix) confirms the structure of the POSS- N_3 structure. The peaks at 3.12 ppm and 3.50 ppm in ^1H NMR, and the characteristic signals at 69.8 ppm and 52.4 ppm in ^{13}C NMR are assigned to the $-\text{CH}_2$ proton and carbon of cyclohexane combined with $-\text{OH}$ and N_3 groups, respectively, thus confirming the structure of compound **29**. The ^{29}Si NMR also shows four signals belonging to the different silicons and their positions have been properly assigned (see **Figure 4.2.3** in appendix).

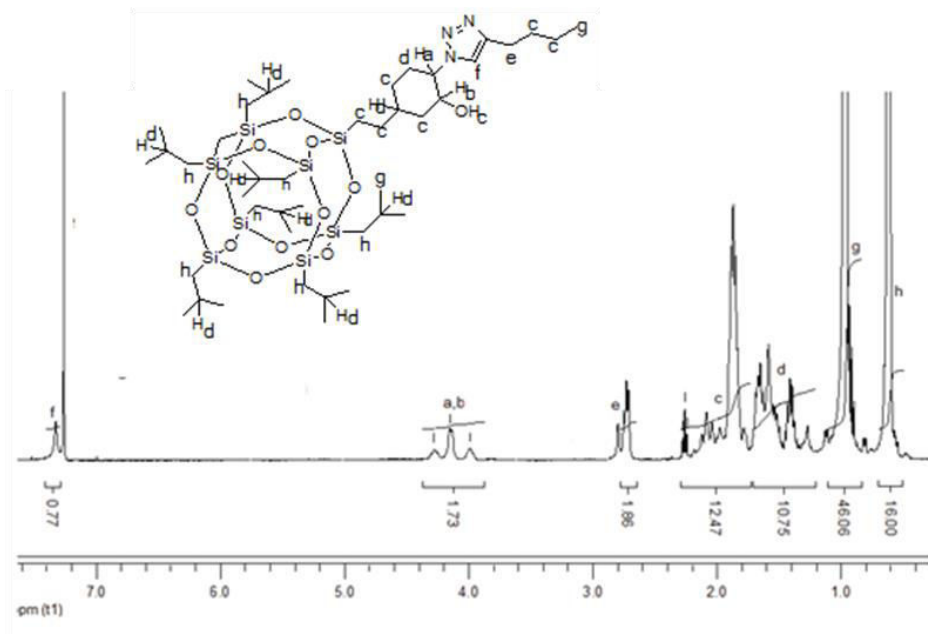


Figure 4.2.4: ^1H NMR spectrum of hexynylhydrincyclohexylisobutyl POSS**32a**.

The characteristic peaks for **32a**(**Figure 4.2.4**) showed the shift of the $-\text{CH}_2$ protons connected to the $-\text{OH}$ and N_3 groups, down field to 4.17 ppm and the appearance of the triazole proton at 7.28 ppm. There is also the presence of the peak at 2.67 ppm assigned to the $-\text{CH}_2$ protons connected to the triazole ring (position “e”). The ^{13}C NMR showed the emergence of the carbon peaks belonging to “o” and “n” at 129 ppm and 126 ppm, coming from the triazole ring. Other peaks have been properly assigned (see appendix **Figure 4.3.5**)

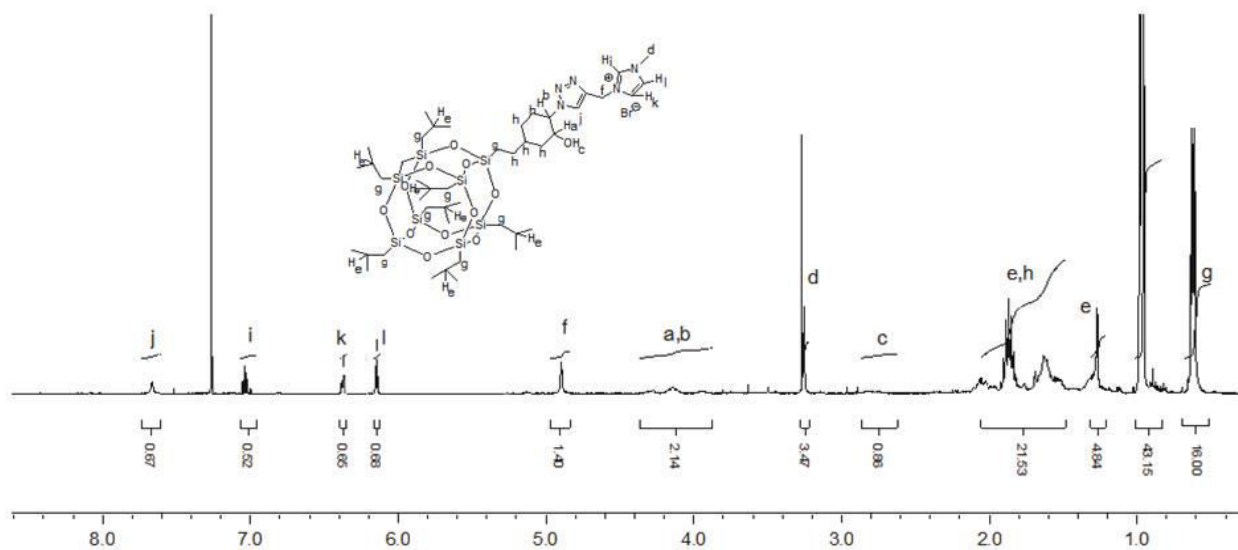


Figure 4.2.7: ^1H spectrum of Cu (I)-imidazoliumcyclohexylisobutyl POSS complex**34b**.

Furthermore, the ^{29}Si NMR (**Figure 4.2.6**, see appendix) shows the silicon peaks at 67.4 ppm, 67.5 ppm, 67.6 ppm, and 67.8 ppm properly assigned to the respective silicon atoms, thus proving the structure of the compound. The peaks from the ^1H NMR of **32b** (**Figure 4.2.7**) have been properly assigned to their respective protons with the proton at position “f” appearing at 4.8 ppm, that of positions “k” and “l” appearing at 6.3 ppm, and 6.1 ppm. The triazole proton (position “j”) appeared at 7.6 ppm and the $-\text{CH}_2$ protons from the $-\text{OH}$ and N_3 groups appearing at 4.8 ppm. All other protons were assigned correctly, thus proving the structure of the desired compound.

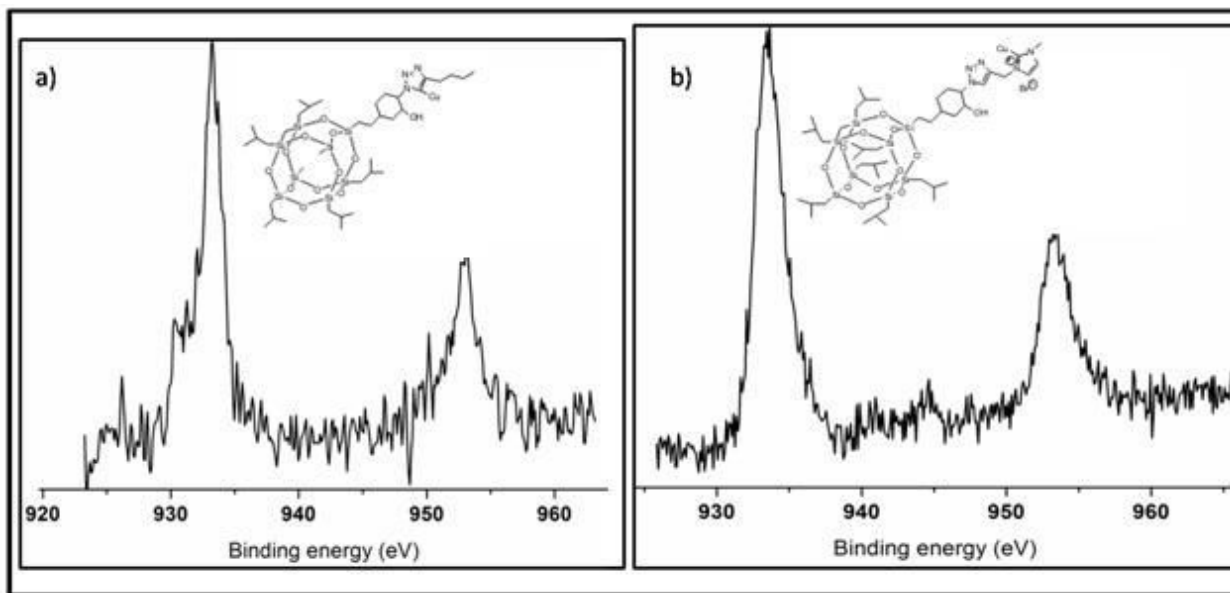


Figure 4.2.8: XPS analysis measured at 200 μ 50W X-ray settings for a) Ep-1H-Cu (**34a**) and b) Ep-1MIM-Cu (**34b**) showing the observable shakeup satellites corresponding to $\text{Cu}(\text{I})$.

The analysis of the Ep-1H-Cu (**34a**) (**Figure 4.2.8a**) sample show the presence of C, N, O, Si, Cu, shown on the survey spectrum. The examination of the $\text{Cu } 2p_{3/2}$ signal show that there is no observable Shake Up satellites present for Cu^0 , whereas the satellites at 932.37 eV and 952.31 eV, corresponds to Cu^{I} .

The analysis of the Ep-1MIM-Cu (**34b**)(**Figure 4.2.8b**) sample show the presence of C, N, O, Si, Cu, shown on the survey spectrum. The examination of the $\text{Cu } 2p_{3/2}$ signal show that there is no observable Shake Up satellites present for Cu^0 , whereas the satellites at 932.37 eV and 952.31 eV, corresponds to Cu^{I} .

Following the MALDI-TOF analysis that was conducted to prove the chemical identity of **29**, **32a** and **32b**, it can be seen from **Figure 4.2.9** that the spectrum displays two major peaks and one minor peak.

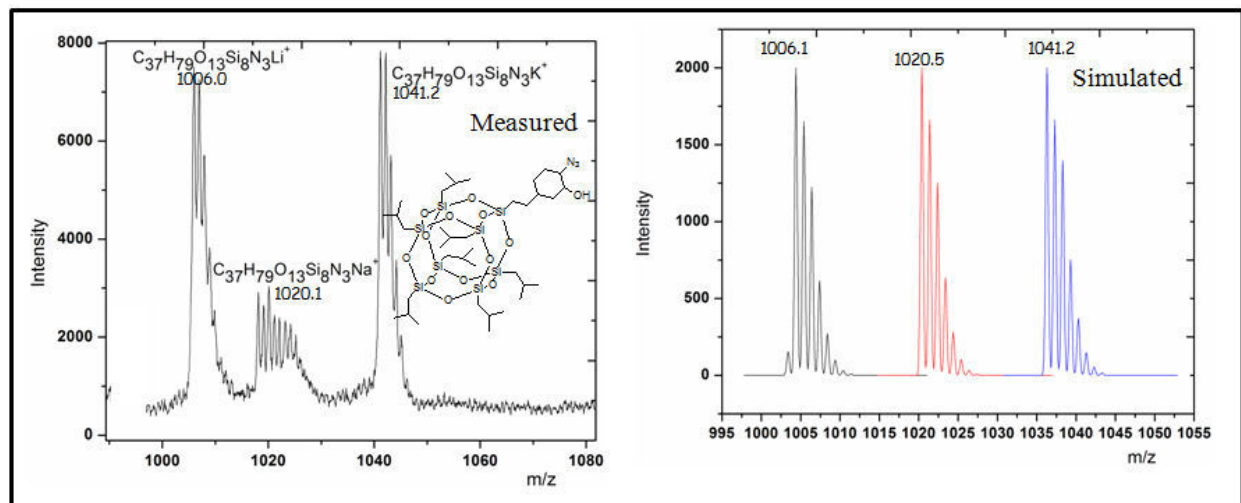


Figure 4.2.9: MALDI-TOFspectrum of azidohydrincyclohexylisobutyl POSS **29**.

The ionization was done with dithranol: **29**: LiTFA/NaTFA in the ratio 100:10:1. The two major peaks could be assigned to the species ionized with Li^+ (M. Li^+ , $\text{C}_{37}\text{H}_{79}\text{O}_{13}\text{Si}_8\text{N}_3\text{Li}$) (found: 1006.0 Da; calculated 1005.1 Da for $n=1$), K^+ (M. K^+ , $\text{C}_{37}\text{H}_{79}\text{O}_{13}\text{Si}_8\text{N}_3\text{K}$) (found: 1041.2 Da; calculated 1041.3 Da for $n=1$), and the minor peak could be assigned to the species ionized with Na^+ (M. Na^+ , $\text{C}_{37}\text{H}_{79}\text{O}_{13}\text{Si}_8\text{N}_3\text{Na}$) (found: 1020.1 Da; calculated 1022.1 Da). The spectrum of **32b** (**Figure 4.2.11**) shows a major series while that of **32a** shows two major peaks and two minor peaks (**Figure 4.2.10**). The ionization of both compounds was done with dithranol: **32a/32b**: NaTFA in the ration 100:10:1. The major peaks of **32b** could be assigned to the species ionized with H^+ (M. H^+ , $\text{C}_{43}\text{H}_{87}\text{O}_{13}\text{Si}_8\text{N}_3\text{H}$) (found: 1066.9 Da; calculated: 1065.9 Da), and Na^+ (M. Na^+ , $\text{C}_{43}\text{H}_{87}\text{O}_{13}\text{Si}_8\text{N}_3\text{Na}$) (found: 1087.9; calculated: 1087.9). The minor peaks were assigned to species ionized with K^+ (M. K^+ , $\text{C}_{43}\text{H}_{87}\text{O}_{13}\text{Si}_8\text{N}_3\text{K}$) (found: 1107.9 Da; calculated: 1106.9 Da), and 2Na^+ (M. 2Na^+ , $\text{C}_{43}\text{H}_{87}\text{O}_{13}\text{Si}_8\text{N}_3\text{2Na}$) (found: 1129.9 Da; calculated: 1128.9 Da).

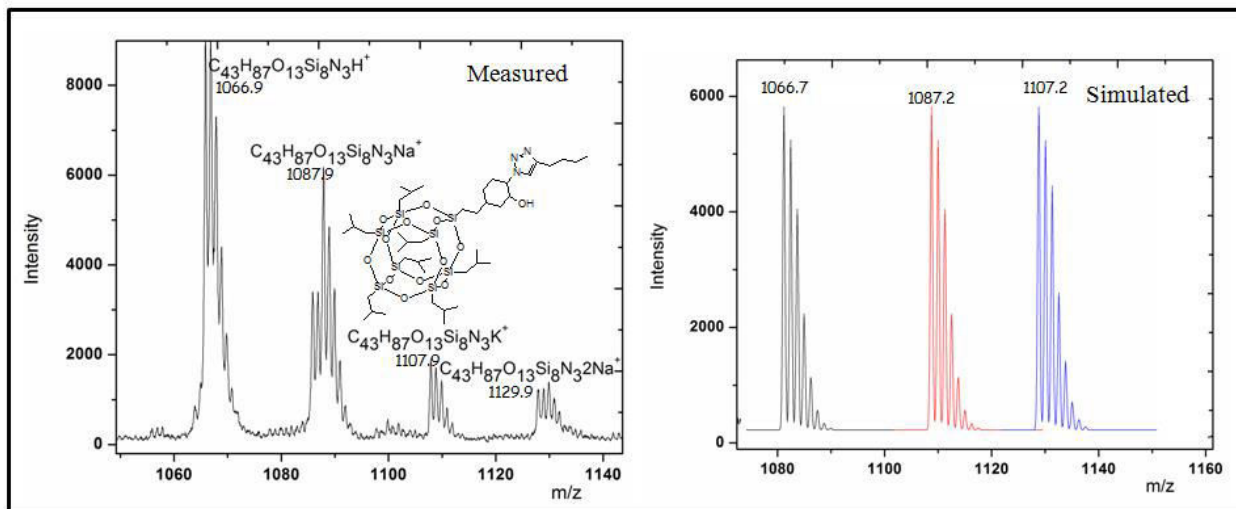


Figure 4.2.10: MALDI-TOF spectrum of hexynylhydrincyclohexylisobutyl POSS32a.

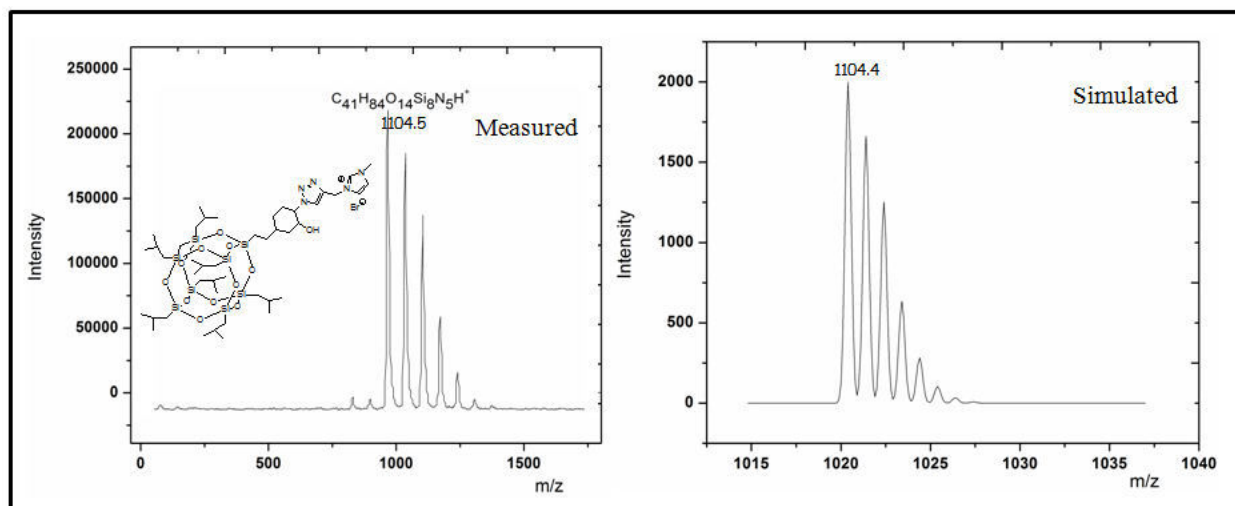


Figure 4.2.11: MALDI-TOF spectrum of 1-methylimidazoliumhydrincyclohexylisobutyl POSS 32b.

Figure 4.2.12 (see appendix) shows the IR spectra of the different POSS nanomaterials (29, 32a, and 32b). The IR spectra of 29 have characteristic peaks at 1090.3 cm^{-1} for Si-O-Si stretching, 1464.8 cm^{-1} for CH_2 stretching of cyclohexyl, and 1228.3 cm^{-1} for Si- CH_2 -stretching. The POSS- N_3 peak appears at 2099.1 cm^{-1} , and simultaneously another peak at 3407.0 cm^{-1} belonging to OH stretching. The spectrum of 32a and 32b show the absence of the azide peak. All other peaks appeared at the same wavelength as 29.

Quantification of Cu present in all POSS nanohybrids was done using flame absorption atomic spectroscopy (FAAS) and TGA (Table 9).

Table 9: Interlayer d-spacing of modified clay materials measured by XRD using Ni filter CuK α radiation in transmission at a sample-detector distance of 9.85 cm.

Entry	Catalyst	Amt of modifier on POSS molecule (mmol/mg) ^a	Amt of Cu (mg of Cu/mg of POSS) ^b	Amt of Cu (mmol of Cu/mg of POSS) ^b
1	Ep-1H-Cu (34a)	0.074 x 10 ⁻³	0.049	0.043 x 10 ⁻³
2	Ep-1MM-Cu (34b)	0.073 x 10 ⁻³	0.023	0.018 x 10 ⁻³
3	OH-1H-Cu (35a)	0.092 x 10 ⁻³	0.054	0.048 x 10 ⁻³

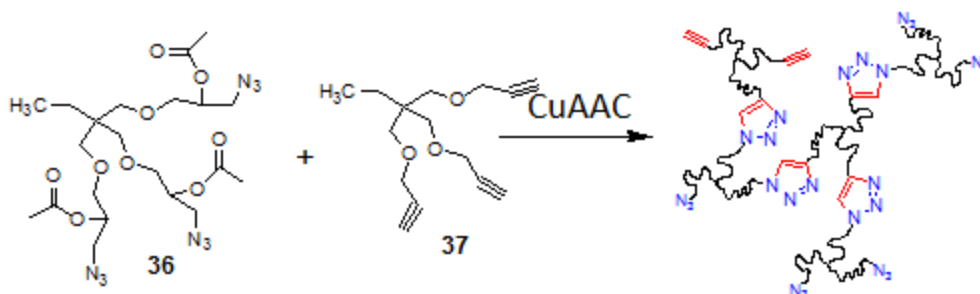
a: Values obtained from TGA. b: Values measured by FAAS.

It can be seen that not all potential sites were stoichiometrically substituted in each POSS molecule. For 1,2,3-triazol-5-ylidenehexynylcyclohexylisobutyl-copper (1) POSS complex, **34a**, only 57.6 % was substituted while 24.7 % of the potential sites were substituted in the case of Cu(1)-imidazoliumcyclohexylisobutyl POSS complex, Ep-1MIM-Cu (**34b**). Also, 51.9 % was substituted for 1,2,3-triazol-5-ylidenehexynylhydrinisobutyl-copper(1) POSS complex, OH-1H-Cu (**35a**). These results suggest that with improved reaction conditions full substitution can be attained, thus enhancing the catalytic effect of these modified catalysts while reducing the reaction time when such catalysts are used to effect “click” crosslinking.

Chapter 5

Performance evaluation of clay and POSS immobilized Cu and Ru catalysts

5.1. Kinetic investigation of Cu (I)-modified clays and POSS using DSC



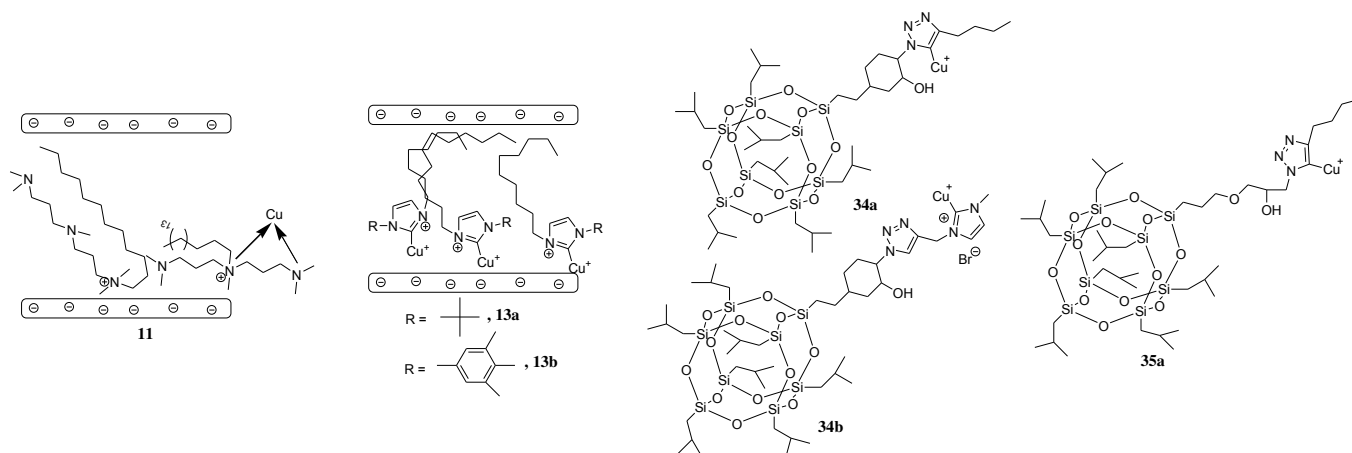
Scheme 5.1.1: Schematic representation for 'click' cross linking reaction.

Differential scanning calorimeter (DSC) was used to investigate the effect of the Cu (I)-modified clay and POSS in the cross linking kinetics of multivalent azides and alkynes in bulk (Synthesis of the multivalent azides and alkynes are shown in subsequent chapters). The important information obtained from DSC were as follows: onset temperature (T_{onset}), peak temperature (T_p), the temperature at which the cross linking reaction ends, the area under the curve (α) and the heat (dH/dt) evolved in the time of curing^{247,248}. The data from the curing process were obtained by means of a NETZSCH 204 F1 Phoenix type differential scanning calorimeter, heated from 20 to 250 °C with different heating rates (5, 10, 15 and 20 K/min) under nitrogen atmosphere. Runs were carried out using an empty pan as the reference with pure indium as standard for calorimetric calibration.

The fundamental principle underscoring the application of DSC technique for curing of multivalent compounds and polymers is that the rate of the kinetic process (da/dt) is proportional to the measured heat flow (ϕ)^{249,250,251}.

$$\frac{da}{dt} = \frac{\phi}{\Delta H}$$

Where ΔH is the enthalpy of the curing reaction.



Scheme 5.1.2: Chemical structures of modified catalysts used for kinetic investigation.

The amount of the inorganic catalysts used (in mmol and mg) was calculated with respect to the FAAS values for each of the inorganic catalyst. 0.01 molar equivalent of all catalyst per functional groups was used. Meanwhile, 1:1 molar ratio of the healing agents (trivalent alkyne (4.4 mg) and trivalent azide 10 mg)) was used. The column in table....having the amount of active catalyst present in DSC measurement was calculated with respect to the measured amount from FAAS. It is important to note that for catalyst **11**, only 50% of the bonded catalyst is actually active as revealed in XPS measurements. Hence, only 50% of 0.65×10^{-3} mmol actually activated the cross linking reactions between the trivalent compounds.

Table..... showing the exact amount of catalyst in mmol and mg used in DSC kinetic studies

S/N	Catalyst	Amt used for DSC studies (mmol)	Amt used for DSC studies (mg)	Amt of active catalyst present in DSC studies (mmol)
1	Ep-c-1H-Cu (34a)	0.76×10^{-3}	1.4	0.061×10^{-3}
2	Ep-1MM-Cu (34b)	0.36×10^{-3}	3.0	0.054×10^{-3}
3	OH-1H-Cu (35a)	0.84×10^{-3}	1.3	0.061×10^{-3}
4	NaMMT-TAL-Cu (11)	1.1×10^{-3}	4.3	0.65×10^{-3}
5	NaMMT-TBIDBr-Cu (13a)	1.1×10^{-3}	2.1	0.11×10^{-3}
6	NaMMT-TMPIDD-Cu (13b)	1.1×10^{-3}	3.4	0.034×10^{-3}

Figure 5.1.1a shows the effect of Cu (I)-modified clay (**13b**) in the ‘click’ reaction between the trivalent alkynes and azides (**36**, **37**) at different heating rates. The area under the curve was integrated to give the heat of reaction(ΔH), generated during the reaction. The heat of the

reaction was found to be 122.6 ± 10 KJ/mol for each functional group. In **Figure 5.1.1b**, the effect of the Cu (I)-modified clay can be clearly seen when compared with the peaks from thermal click reaction, obtained from pristine and surfactant-modified clays without Cu(I). While the peak temperature of the thermally induced click reaction for the pure alkyne and azide, alkyne-azide-nanoclay, and alkyne-azide-organoclay, appears at 133.5, 133.7, and 132.0 °C, the reaction of the cross linking prompted by the catalytically active nanoclays proceeded to completion at a more faster rate evidently seen in the peak temperature appearing at 61.4 °C.

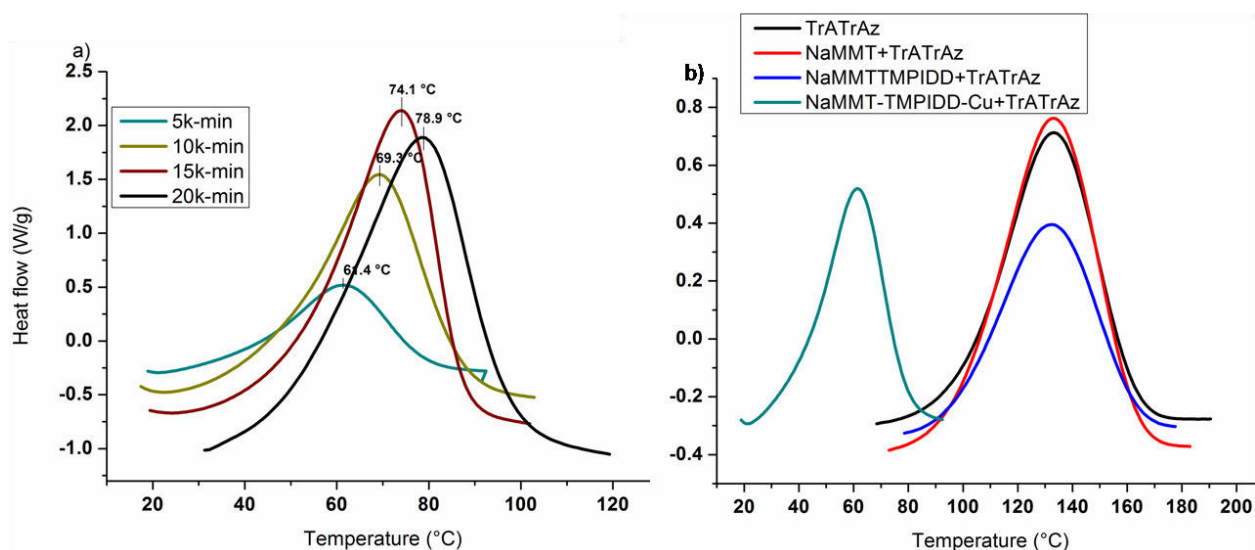


Figure 5.1.1: a) DSC dynamic scan curves for trivalent azide, **36** and alkyne, **37**, systems (with 1 mol% Cu (I)-modified clay catalyst, **13b**, 0.322mg Cu(I) in clay nanoparticle) at different heating rates of 5, 10, 15, and 20 °C/min and b) DSC dynamic scan curves for trivalent alkynes and azides systems (with 1 mol% NaMMT **22**, NaMMT-TMPIDD **12b**, and NaMMT-TMPIDD-Cu **13b**, with trivalent azide, **36**, and alkyne, **37** curve as reference).

This proves the catalytic effect of the Cu(I) bonded nanofiller on the cross linking kinetics of the multivalent alkynes and azides in bulk systems. As has been noted^{247,252,253,254}, increase in the heating rate shows a continuous increase in the peak temperature, increase in onset temperature and a decrease of the cure time (seen in **Figure 5.1.1a**). This trend could be related to the structural factors (a more complete curing at higher heating rates due to the high number of azide and alkyne groups in the reaction), instrumental factors (high initiation temperatures at high heating rates), and kinetic factors²⁴⁷.

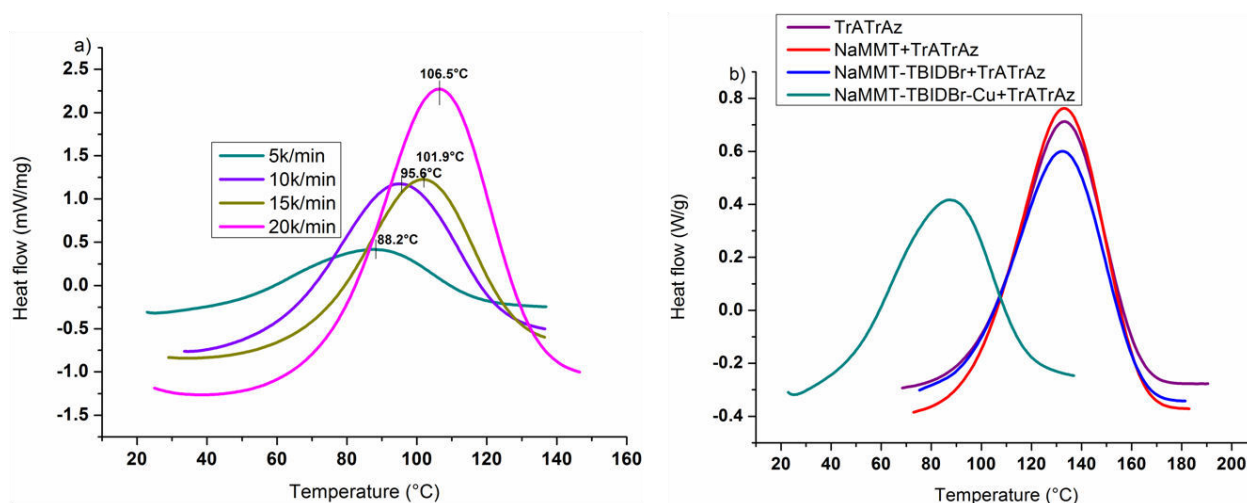


Figure 5.1.2: a) DSC dynamic scan curves for trivalent alkyne, **37** and azide, **36**, systems (with 1 mol% Cu (I)-modified clay catalyst, **13a**, 0.322mg Cu(1) in clay nanoparticle) at different heating rates of 5, 10, 15, and 20 °C/min, and b) DSC dynamic scan curves for trivalent alkynes and azides systems (with 1 mol% NaMMT **22**, NaMMT-TBIDBr **12a**, and NaMMT-TBIDBr-Cu **13a**, with trivalent azide, **36**, and alkyne, **37** curve as reference).

In **Figure 5.1.2a**, the effect of Cu (I)-modified clay, NaMMT-TBIDBr-Cu (**13a**) in the ‘click’ reaction between the trivalent alkynes and azides (TrATrAz) (**36**, **37**) at different heating rates can be seen to be less effective than that of NaMMT-TMPIDD-Cu (**13b**). The heat of reaction, ΔH , generated during the reaction was found to be 108.2 ± 3 KJ/mol for each functional group. The result is unexpected considering the amount of Cu loading, determined by FAAS on the surface of the clay material (**table 5**) when compared with the effect of **13b** in **Figure 5.1.1**. The reason could be due to the fact that the large size of the pendant group in the surfactant restricted complete diffusion of the monomers to areas at the clay galleries where the Cu-carbenes are formed. Basically, the ‘click’ reaction is diffusion-controlled, meaning that the monomers diffuse to regions at the clay galleries where the Cu-carbenes are formed for the ‘click’ reaction to occur. Consequently, the peak temperature of the thermally induced click reaction for the pure trivalent alkyne and azide, alkyne-azide-nanoclay, and alkyne-azide-organoclay, appears at 133.5, 133.7, and 132.9 °C, and the peak temperature of the copper-catalyst reaction appeared at 87.2 °C.

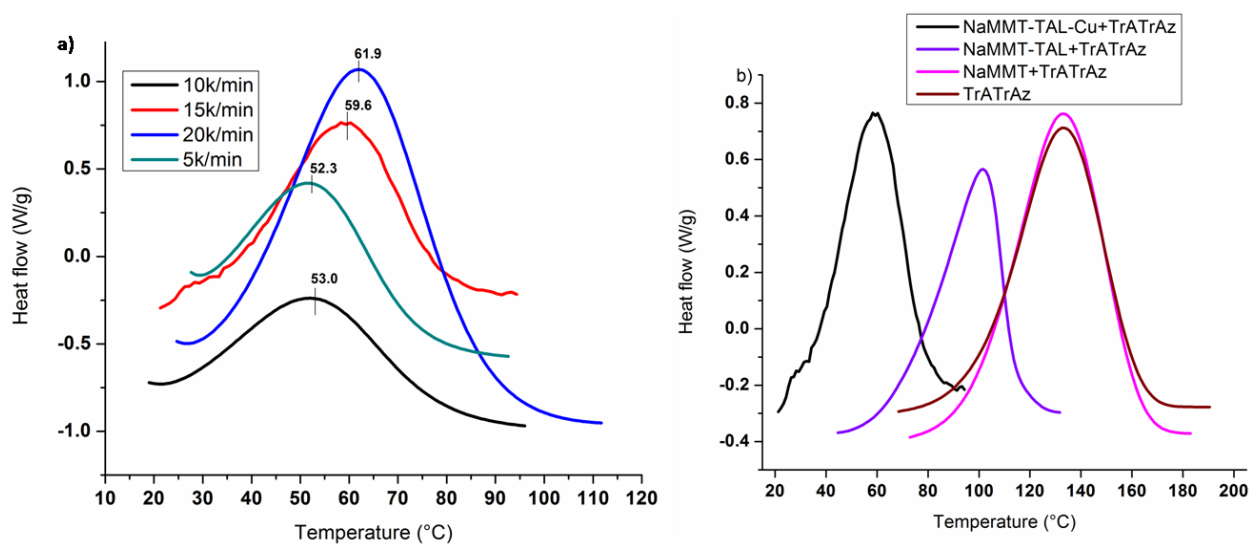


Figure 5.1.3: a) DSC dynamic scan curves for trivalent alkyne, **37** and azide, **36**, systems (with 1 mol% Cu (I)-modified clay catalyst, **11**, 0.59 mg Cu(1) in clay nanoparticle) at different heating rates of 5, 10, 15, and 20 °C/min and b) DSC dynamic scan curves for trivalent alkynes and azides systems (with 1 mol% NaMMT **22**, NaMMT-TAL**10**, and NaMMT-TAL-Cu **11**, with trivalent azide, **36**, and alkyne, **37** curve as reference).

The effect of NaMMT-TAL-Cu, **11** on the cross linking reaction of multivalent alkynes and azides is much more effective even without the presence of Cu-carbenes (**Figure 5.1.3**). Though non-specific with more complexation sites for Cu-carbenes, the TAL-modified clay, **10** seem to affect the kinetics of the reaction by influencing the temperature at which the cross linking takes place when compared with previously discussed organoclays (**12a**, and **12b**) before the attachment of Cu-carbenes. This is obviously due to the presence of amino groups which have been found to encourage cross linking reactions as a result of the hydrogen bonding that exists in the molecule, thus overcoming the issues with temperature and curing time in epoxy systems²⁵⁵. Generally, tertiary amines and other compounds^{254, 256,257} called accelerators are used to accelerate curing of epoxy cross linking at high temperatures even though such accelerators could reduce crosslink density of the network and ultimately decrease the mechanical properties of the epoxy resin²⁵⁸. In their work, Abdolreza et al.²⁵⁵ found that the curing of epoxy systems with special amino compounds took place at a low temperature. There was equally a profound effect on the peak temperature when the copper-modified clay catalyst (**11**) was used (**Figure 5.1.3b**) even with 50% of the active Cu (1) on the surface of the clay material. This further explains the highly effective nature of catalyst **11** in cross linking kinetics which would be relevant industrially.

The heat of reaction, ΔH , generated during the reaction was found to be 136.2 ± 4 KJ/mol for each functional group.

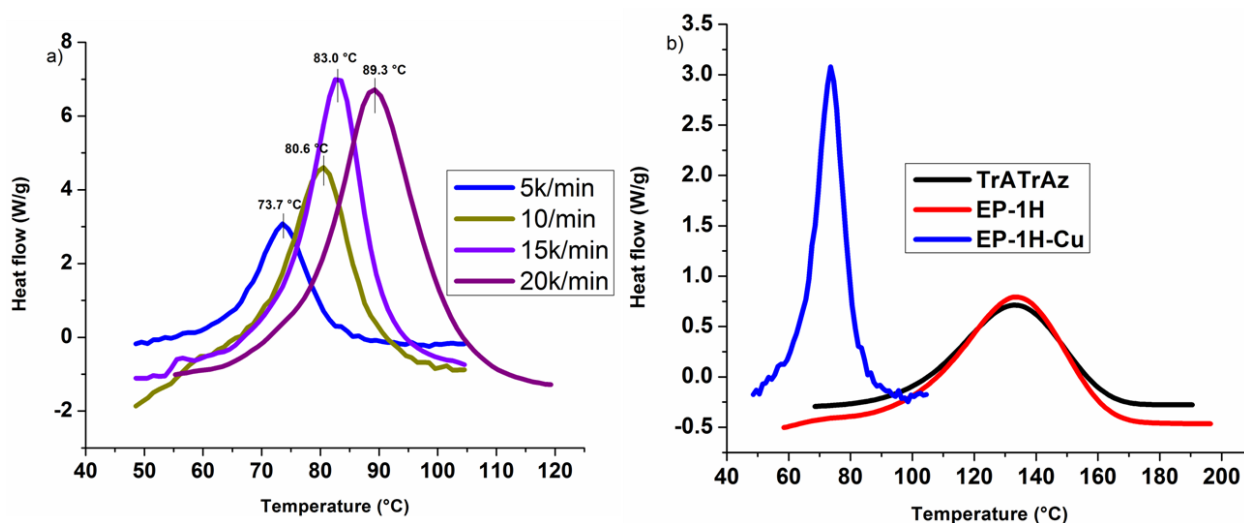


Figure 5.1.4: a) DSC dynamic scan curves for trivalent alkyne, **37** and azide, **36**, systems (with 1 mol% Cu (I)-modified POSS catalyst, **34a**, 0.0686mg Cu(1) in POSS molecule) at different heating rates of 5, 10, 15, and 20 °C/min and b) DSC dynamic scan curves for trivalent alkynes and azides systems (with 1 mol%, Ep-1H **32a**, and Ep-1H-Cu **34a**, with trivalent azide, **36**, and alkyne, **37** curve as reference).

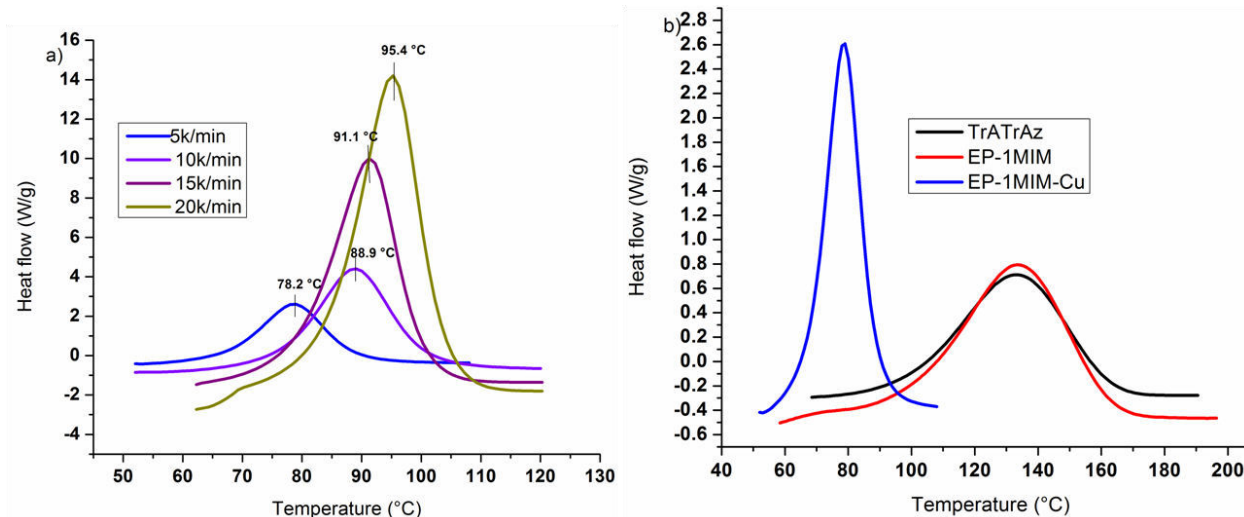


Figure 5.1.5: a) DSC dynamic scan curves for trivalent alkyne, **37** and azide, **36**, systems (with 1 mol% Cu (I)-modified POSS catalyst, **34b**, 0.0322mg Cu(1) in POSS molecule) at different heating rates of 5, 10, 15, and 20 °C/min and b) DSC dynamic scan curves for trivalent alkynes and azides systems (with 1 mol% Ep-1MIM **32b**, and Ep-1MIM-Cu **34b**, with trivalent azide, **36**, and alkyne, **37** curve as reference).

DSC results, in the case of Cu-modified POSS materials show the influence of attached ligand on the catalytic activity of immobilized copper catalysts (Figures 5.1.4, 5.1.5, 5.1.6, Table 7).

Compared to N-heterocyclic carbene-Cu(I)-complex (**34b**), $T_p = 78\text{ }^{\circ}\text{C}$, a higher catalytic activity was observed for triazole-Cu(I) POSS complex (**34a**), $T_p = 73\text{ }^{\circ}\text{C}$.

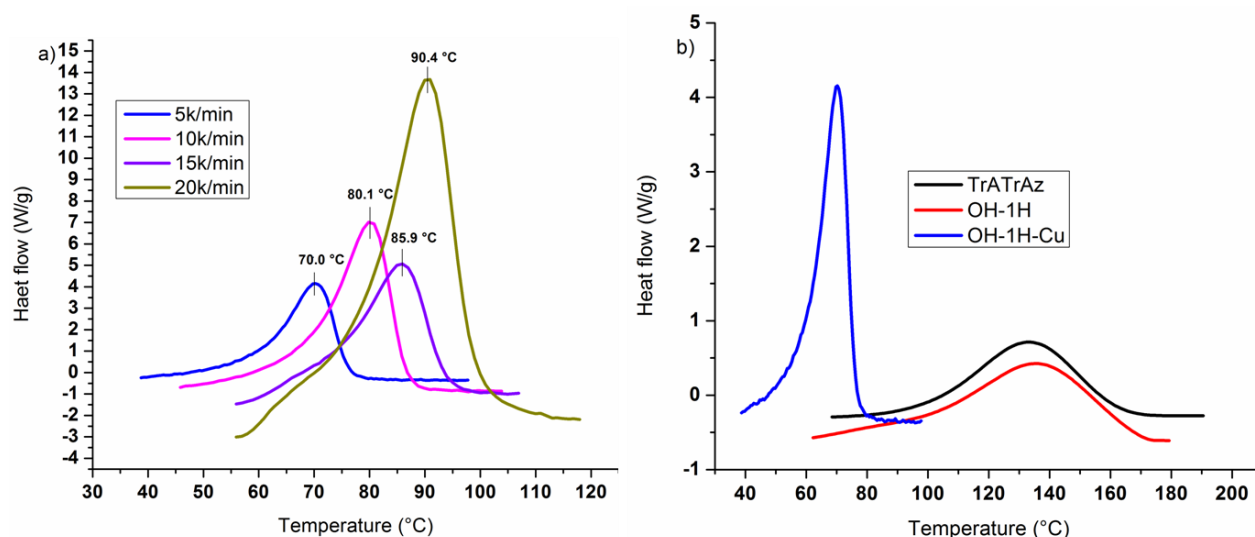


Figure 5.1.6: a) DSC dynamic scan curves for trivalent alkyne, **38** and azide, **36**, systems (with 1 mol% Cu (I)-modified POSS catalyst, **35a**, 0.0702mg Cu(1) in POSS molecule) at different heating rates of 5, 10, 15, and 20 $^{\circ}\text{C}/\text{min}$ and b) DSC dynamic scan curves for trivalent alkynes and azides systems (with 1 mol% OH-1H **33a**, and OH-1H-Cu **35a**, with trivalent azide, **36**, and alkyne, **37** curve as reference).

The results are in agreements with the earlier discussion that the carbene-Cu(I) complexes demonstrate a lower catalytic activity compared to triazole-Cu(I) complex²⁴⁶. The effect of substituted chain flexibility on the catalytic activity of immobilized Cu(I) was also discussed, where flexible chain substituted complex (**35a**) demonstrates a better catalytic performance compared to catalyst with a rigid chain backbone POSS complex(**34a**), where flexible alkyl chain might be creating a more favourable environment around a Cu-complex²⁵⁹.

Table 10: Summary of the activation energies and other kinetic parameters determined by DSC.

S/N	Catalyst	Mol % per FG	Amt of catalyst used/FG (mg Cat/FG)	T _{onset} (°C)	R ²	T _p (°C)	ΔH/FG (KJ/mol)	Activation Energy (KJ/mol)	Reaction Conversion (%)
1	Ep-1H-Cu (34a)	1	0.47	62±4	0.91	73±4	213±3	69±2	50
2	Ep-1H (32a)	1	1.1	113±2	0.92	130±2	236±5	89±2	-
3	Ep-1MIM-Cu (34b)	1	1.0	68±3	0.99	78±3	195±4	68±1	60
4	Ep-1MIM (32b)	1	1.3	104±4	0.99	133±4	208±3	90±1	-
5	OH-1H-Cu (35a)	1	0.43	43±3	0.99	70±3	249±3	57±1	70
6	OH-1H(33a)	1	1.1	60±5	0.99	132±5	258±5	89±2	-

FG: Functional Group.

The enthalpy of the reaction for all Cu-modified POSS materials (**table 10**) seem to be higher than their clay counterpart. This may be due to the structural integrity of POSS materials which makes them thermally highly stable. The cage backbone requires lots of energy to break the bonds.

Figures 5.1.9, and 5.1.10 as well as **Figures 5.1.11, and 5.1.12** (see appendix) show the fractional conversion, α , at variance with the temperature for trivalent alkynes and azides catalyzed with nanoclays (**22**), organoclays (**10, 12a, 12b**), Cu(I)-modified clay fillers (**11, 13a, 13b**), and Cu-modified POSS fillers (**34a, 34b, 35a**) (1 mol%) at different heating rates. It can be observed that the curing curves increases with increasing scan rates. Kinetic parameters were obtained from the curve of the fractional conversion against temperature as well as against time²⁴⁷.

Chapter 6

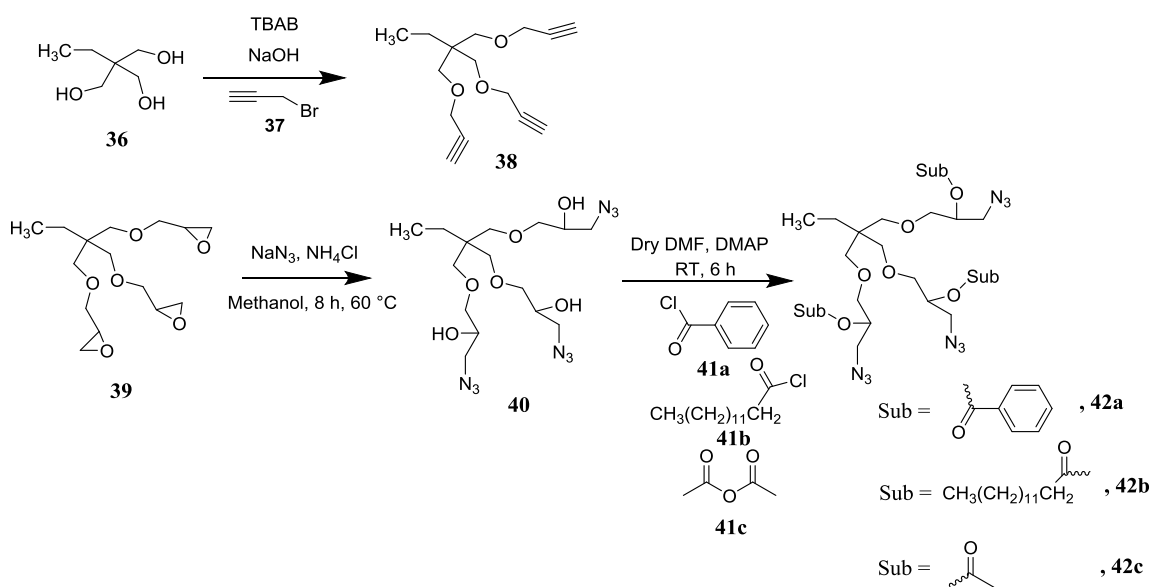
Synthesis and encapsulation of multivalent alkynes and azides for click-based self-healing nanocomposites

6.1. Introduction

Basically, there are two main pathways to material encapsulation depending on the capsule loading. The first method underscores the loading of liquid content in preformed carriers, utilizing different kinds of particles²⁶⁰, mesoporous structures²⁶¹, and natural hollow materials^{262,263,264}. After the loading of the healing agents, additional protective layers which dictate the release and colloidal properties of the capsules are used to cover the carriers. The synthesis of hollow particles²⁶⁵ with a subsequent loading step is at variance to this method. The second method explores the “in situ” polymerization loading and is frequently used for the encapsulation of liquids. Encapsulation by “in situ” polymerization produces microcapsules where the capsule shell walls are formed because of the polymerization of monomers that are added to the encapsulation reactor. It does not require the addition of reactive agents to the core material because polymerization occurs at the continuous phase and under acidic conditions. Initially, there is the formation of a low molecular weight prepolymer which grows in size with time and deposits on the surface of the dispersed core material thereby generating solid capsule shell. The capsules prepared by this method are in the micrometer range and are relatively stable with good dispersion, overcoming the main challenges for designing useful self-healing systems which are a good dispersion (without necessarily functionalizing the surface of the microcapsules) of the capsules in the overall matrix system and an efficient encapsulation of the healing agent. On the other hand, miniemulsion polymerization and solvent evaporation method, is a chemical method as well as a physico-chemical process where capsule shell walls do not require surface functionalization. The encapsulation process is usually efficient with the capsule size in the nanometer range. The capsules are colloidally stable and do not coagulate^{266,267} neither does the preparation of the nanocontainers require any reaction in dispersed media. The internal phase separation that exists between the healing agents and the polymers in miniemulsion engineered the formation of the nanocapsules. While the “in situ” polymerization method can be used to encapsulate both low molecular weight compounds as well as high molecular weights healing agents²⁶⁸, the miniemulsion polymerization method can only be used to encapsulate low molecular weight self healing compounds.

6.2. Synthesis of multivalent alkynes and azides

To obtain compound **40**, trimethylolpropane (**39**) was added to a round bottom flask containing methanol. Ammonium chloride and sodium azide were both added to the reaction flask, afterwards and the overall mixture was heated to reflux for 12 hours. Subsequently, triazidomethylbenzopropane triglycidyl ether (TriAzB, **42a**), triazidomethyloctanopropane triglycidyl ether (TriAzM, **42b**), and triazidomethylacetopropane triglycidyl ether (TriAzAc, **42c**) were all prepared via nucleophilic substitution reaction (**42a** and **42b**) and acetylation reaction (**42c**) independently, through the same procedure. TriAzOH (**39**), and 4-dimethylaminopyridine were placed in three different round bottom flask containing freshly distilled DMF each. The reaction was stirred for a while followed by the addition of acetic anhydride (to obtain **42c**)/merysotyl chloride (to obtain **42b**)/benzoyl chloride (to obtain **42a**) in drops to the reaction mixture at room temperature.



Scheme 6.2.1: Schematic representation of multivalent alkynes and azides synthesized via azidation, nucleophilic, and acetylation reactions.

The synthesis of trimethylethoxyprop-1-yne (**38**) followed the procedure according to literature with slight modification²⁶⁹. Trimethylolpropane was weighed into a dry round bottom flask equipped with a magnetic stirrer and septum. This was followed by the addition of Sodium hydroxide, water, and TBAB. After a while, propargyl bromide was added drop wise over the course of 1 h, and then the temperature was slowly raised, during this time the reaction became homogeneous.

The purity of the compounds **38**, **42a**, **42b**, and **42c** were all confirmed by ^1H NMR with all the peaks properly assigned to corresponding protons.

IR analysis as well as thermogravimetric analysis (see appendix, **Figure 6.2.5** and **Figure 6.2.6**) was done to prove the stability of the compounds and the appearance/disappearance of OH vibrational peaks and the vibrational bends coming from the azide. The results are tabulated in **table 11**.

Table 11: Thermal stability and vibrational peaks of multivalent alkynes and azides measured by IR.

Entry	Compound	OH-vibration (cm^{-1})	Azide bend (cm^{-1})	Td ($^{\circ}\text{C}$)
1	TriAzOH	3430.8	2103.3	204.0
2	TriAzB	-	2096.9	154.5
3	TriAzM	-	2101.9	228.1
4	TriAzAc	-	2102.3	197.9

The table clearly shows that TriAzM is the most stable of all multivalent compounds synthesized.

To further authenticate the purity of the multivalent compounds, ESI-TOF measurement was done using chloroform as the solvent and NaI as the salt. TriAzB (**42a**) flew in the positive mode (**Figure 6.2.7**, see appendix) with one major series showing a molecular weight of 742.2 g/mol which corresponds to the molecular structure $\text{C}_{36}\text{H}_{41}\text{N}_9\text{O}_9\text{H}^+$. The obtained molecular weight is consistent with theoretical calculation. TriAzM (**42b**) flew in the negative mode (**Figure 6.2.8**, see appendix) with one major series showing a molecular weight of 936.2 g/mol which corresponds to the molecular structure $\text{C}_{39}\text{H}_{71}\text{N}_9\text{O}_9\text{I}^-$. Also, TriAzAc (**42c**) flew in the positive mode (**Figure 6.2.9**, see appendix) with one major series showing a molecular weight of 580.2 g/mol which corresponds to the molecular structure $\text{C}_{21}\text{H}_{35}\text{N}_9\text{O}_9\text{Na}^+$. And finally, TriMEP (**38**) flew in the positive mode (**Figure 6.2.10**, see appendix) with one major series having a molecular weight of 271.1 g/mol which corresponds to the molecular structure $\text{C}_{15}\text{H}_{20}\text{O}_3\text{Na}^+$. All obtained molecular weights of the respective trivalent compound are consistent with theoretical calculation, thus proving the purity of the desired compound.

6.3 Encapsulation of trivalent compounds

Microcapsules filled with TriAzAc (**42c**), TriAzM (**42b**), TriAzB (**42a**), TriMEP (**38**), and TriAzAc (**42c**) + TriMEP (**38**) (1:1 molar ratio), with the outer shell composed of poly(urea-formaldehyde) and the inner shell of ethylene maleic anhydride (EMA) copolymer, were successfully prepared by *in situ* polymerization in an oil in water emulsion technique. The *in situ* polymerization technique involves the encapsulation of water immiscible liquids by the reaction of urea with formaldehyde at an acidic pH.

At room temperature distilled water and 2.5 wt% aqueous solution of EMA copolymer were mixed in a glass beaker. EMA copolymer was completely dissolved in distilled water at 100°C until obtaining a perfectly clear solution. Thereafter, the beaker containing the emulsion was suspended in temperature controlled water on a programmable digital stirring hotplate with external temperature immersion probe. The oil-in-water emulsion was kept under stirring with a high shear digital mixer/emulsifier driving a three-bladed, 63.5 mm diameter low shear mixing propeller placed just above the bottom of the beaker. Under agitation, the wall forming materials urea, ammonium chloride and resorcinol were dissolved in the solution. Then, the pH was raised by dropwise addition of NaOH solution. Surface bubbles were eliminated by the addition of two drops of 1-octanol. Then, a slow stream of 50 of healing agent in chloroform was added to form a suspension of fine droplets and allowed to stabilize. After stabilization, formaldehyde was added, keeping pH at a constant value. It is worth noting that no phase separation was observed. The stirring speed was kept constant until the end of the microencapsulation process.

The encapsulation of TriAzOH(**40**) was not successful. This is due to the interaction of the OH groups with the wall forming compound resulting in a high interfacial energy. To overcome this problem, further modifications were made on the OH groups. The modified trivalent azido compounds (**42a**, **42b**, and **42c**) were successfully encapsulated.

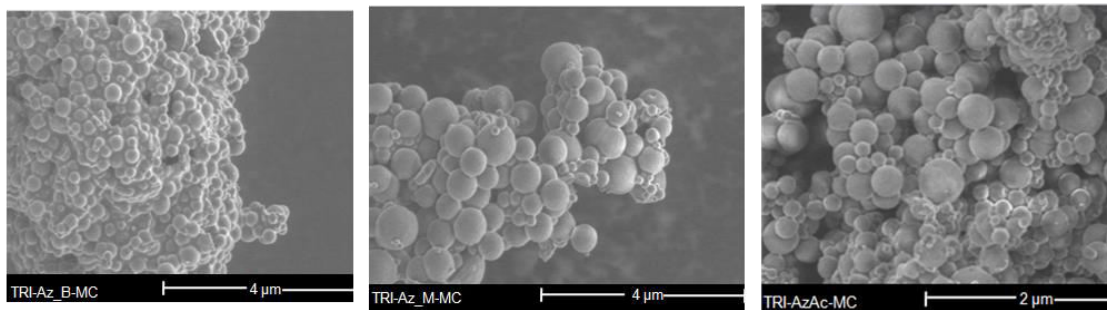


Figure 6.3.2: FE-SEM images of TriAzB (**42a**), TriAzM (**42b**), and TriAzAc (**42c**), measured under gas mode.

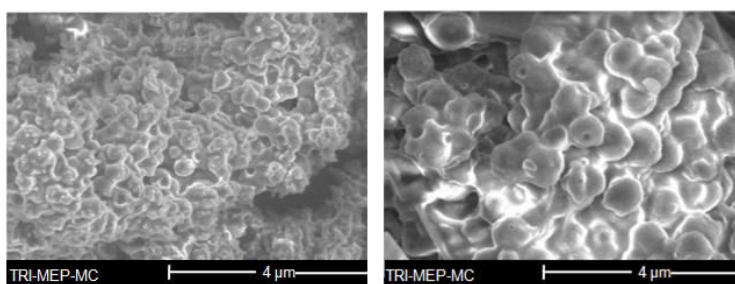


Figure 6.3.3: FE-SEM images of TriMEP (**38**), measure under gas mode.

Attempt was made to encapsulate both the trivalent azide and the trivalent alkyne in one capsule using the same procedure. The encapsulation was successful, however, further analysis made to quantify the amounts of the internal compounds with reference to an internal standard showed that part of the encapsulated trivalent azide (TriAzAc) was deacetylated in the process. Nonetheless, the amounts of each compound was calculated from NMR using naphthalene as internal standard (**table 12**).

Table 12: Amount of encapsulated compounds calculated from ^1H NMR using naphthalene as internal standard.

Sample:	TriMEP	TriAzAc	DiAzAc
Amount:	2.85 mmol/g of microcapsule	0.9 mmol/g of microcapsule	1.3 mmol/g of microcapsule

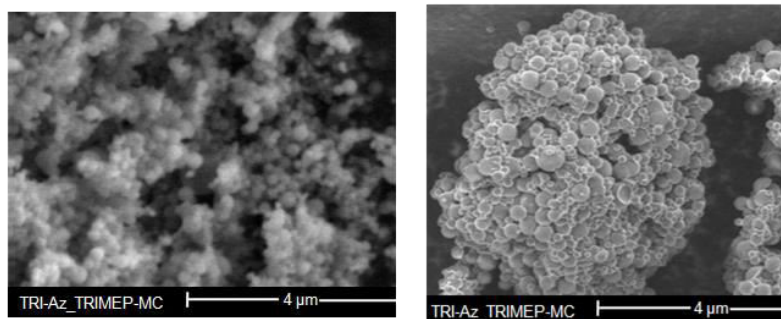


Figure 6.3.4: FE-SEM images of TriMEP (38) +TriAzAc (42c), measured under gas mode.

Thermogravimetric analysis was done to check the thermal stability of the compounds and the microcapsules (see appendix, **Figure 6.3.5**). **Table 13** shows a summary of their thermal stabilities.

Table13: Thermal stabilities of compounds and microcapsules determined by thermogravimetric analysis under nitrogen atmosphere.

S/N	Samples	Td (°C) ^a	Yield (%)	Size (μm) ^c	Stirring speed (rpm)
1	TriAlkTriAzAc-MC	202.6	78.8 ^b	4±2	1500
2	TriAlk-MC	141.3	82.5 ^b	4±1	1500
3	TriAzAc-MC	199.0	56.5 ^b	2±2	1500
4	TriAzM-MC	224.2	74.3 ^b	4±2	1500
5	TriAzB-MC	167.2	86.3 ^b	4±4	1500

a: determined by TGA, b: determined by ¹H NMR, c: determined by FE-SEM.

It is a well established fact that the smaller the capsules, the more transparent the overall material would be from an industrial point of view. On the basis of this fact, therefore, further attempts were made to reduce the size of the microcapsules by adjusting some original synthetic conditions. This is because of the effect smaller sized microcapsules have on the overall mechanical properties of the composites material. Controlling the size of microcapsules also depends on the stirring rate²⁷⁰.

The stability of the capsule was improved significantly (particularly for TriMEP-MC, see appendix, **Figure 6.3.6**) when the amount of the copolymer was increased. All microcapsules seem to reach a maximum stability when the concentration of EMA was 3.0 wt%. Increase amount of EMA afterwards showed a constant value.

Figure 6.3.7 (see appendix) shows the encapsulation efficiency as a function of the EMA concentration. The trivalent alkyne microcapsules (TriMEP-MC) showed the most improvement in capsules stability when the concentration of the surfactant was increased. This is because the

alkyne groups are slightly soluble in the aqueous phase at lower concentrations of EMA, hence making encapsulation a huge task. But when the concentration of EMA is increased the solubility is impaired and encapsulation can be achieved successfully.

Furthermore, **Figure 6.3.8** shows an increase in the encapsulation efficiency for all encapsulated compounds, from 52.2 % to 84.7 % when the concentration of EMA was increased from 0.5, 1.25, 2.5, 3.0, and 4.0 wt%. Urea-formaldehyde that forms the outer shell was driven to the surface of the oil droplets to reduce the total free interfacial energy of the system when the concentration of EMA was increased. Hence, higher concentration of EMA favors the formation of smaller and more stable capsules which is consistent with results from literature for core-to-wall ratio below 5%²⁷¹.

Chapter 7

Experimental Part

7.1. Material

All chemicals and reagents were purchased from Sigma Aldrich, and were used without further purification unless otherwise noted. The solvents used in the synthesis of surface modifying groups and modification of the particles, tetrahydrofuran (THF) and diethyl ether, were used after distillation over sodium and benzophenone²⁷², and dichloromethane (DCM), *N,N*-dimethylformamide (DMF) and pyridine were distilled over CaH₂. Toluene and *n*-hexane were dried according to literature²⁷². The POSS starting materials were gotten from hybrid plastics and the novel synthetic approach for the POSS derivatives were developed. The approach for the synthesis of the multivalent alkynes and azides was developed likewise.

7.2. Measurements.

Characterization of the synthesized surface modifying groups and produced polymers was done by NMR. ¹H-NMR and ¹³C-NMR measurements were performed by using a Varian Gemini 2000 spectrometer. ¹H-NMR analysis of the samples was performed with a 400 MHz instrument while ¹³C-NMR analysis was performed with a 100 MHz instrument. The measurements were performed at room temperature using CDCl₃ as solvent unless otherwise noted.

The molecular weight and the molecular weight distribution of the produced polymers were characterized by using gel permeation chromatography (GPC). The measurements were performed in a Viskotek GPCMax VE 2001 with THF as solvent and a flow rate of 1.00 mL/min, a column temperature of 35°C and a detector temperature of 35°C. Calibration was done with polystyrene standards equipped with two TSK-gel columns (H_{HR}-HGuard+GMH_{HR}-N, bead size: 5 μm, M_w(polyisobutylene) < 4 x 10⁵) and one *ViscoGel HR High Resolution* column (G2500 HR, bead size: 5 μm, M_w(polyisobutylene) < 20000) with a *TDA 302 Triple Detector Array*.

Thermo gravimetric analysis (TGA) was performed to investigate the grafting density of the produced polymer-inorganic composites, by using a Netzsch TG F3 Tarsus instrument. The measurements were conducted under an atmosphere of N₂ with a temperature ranging from

32°C to 900°C with a heating rate of 10 K/min. Netzsch Proteus Analysis software was used to interpret the TGA measurements.

Differential scanning calorimetry (DSC) measurements were performed on a differential scanning calorimeter 204F1/ASC Phoenix from Netzsch. Crucibles and lids made of aluminum were used. Measurements were performed in a temperature range from 0 to 250 °C using heating rates of 5, 10, 15 and 20 K/min. As purge gas a flow of dry nitrogen (20 mL/min) was used for all experiments. For evaluation of data the Proteus Thermal Analysis Software (Version 5.2.1) and OriginPro7 was used. For sample preparation a 1:1 (molar ratio) mixture of the triazide compound (**42c**) and the trialkyne compound (**38**) was placed in a flask (50 mg) and the catalyst (1-2 mol% per functional group) was added to the mixture which was mixed with a spatula and immediately put in a crucible and closed with a pinhole pricked lid. The mixture with the catalyst was put in a freezer at -20 °C and was used in a period of 2 hours for a series of measurements.

Rheological measurements were performed on an oscillatory plate rheometer MCR 101 from Anton Paar (Physica). For all measurements a PP08 measuring system (parallel plated, diameter 8 mm) was used. Measurements were performed at 20 °C, and the sample temperature was regulated by thermoelectric heating and cooling. For evaluation of data the RheoPlus/32 software (V 3.40) and OriginPro7 was used. For sample preparation a 1:1 (molar ratio) mixture of the triazide compound (**42c**) and the trialkyne compound (**38**) was placed in a flask (100 mg) and the catalyst (1 mol% per functional group) was added to the mixture. Subsequently, the reaction mixture was mixed with a spatula and immediately put on the rheometer plate. Measurements were performed with a strain γ of 1.0 % and with an angular frequency ω ranging from 100 to 1 rad/s. A frequency sweep was performed every 5 minutes. The gelation time was determined as crossover of the storage (G') and the loss modulus (G''). Measurements were stopped, when the values of the storage and the loss modulus stayed constant (second decimal place) for at least 60 minutes.

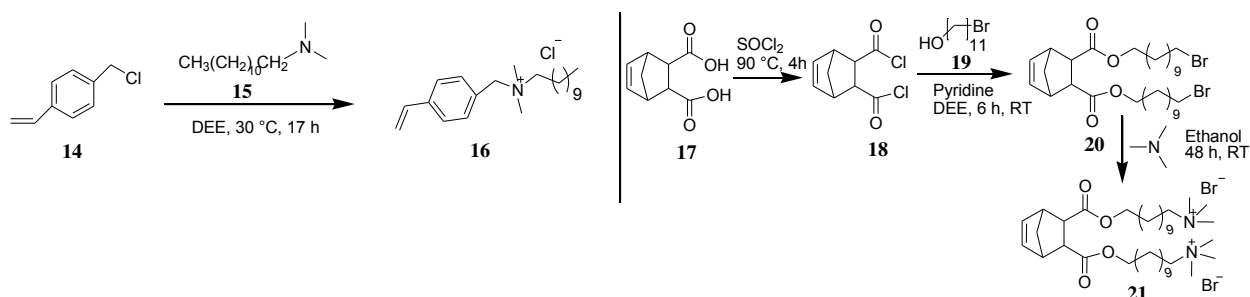
X-ray diffraction patterns have been recorded for powder samples in glass capillaries (\varnothing 1.0 mm) using Ni filtered CuK_α radiation in transmission and an area detector VÅNTEC500 (Bruker) at a sample – detector distance of 9.85 cm.

Matrix-assisted laser desorption/ionization time of flight mass spectrometry (MALDI-TOF MS) measurements were performed on a Bruker Autoflex III Smartbeam equipped with a nitrogen laser (337 nm) and under use of the linear or reflector modus. DCTB (40mg/mL in THF) was used as matrix. All samples were dissolved in either chloroform or acetone (20 mg/mL, HPLC grade, purchased from Sigma Aldrich) and silver trifluoroacetate (1 mg/mL in THF) was added as a salt. The matrix: sample: salt was adjusted to 100:10:1.

TENSILE tests were performed parallel to the extrusion direction on sample bars with length of 50 mm, a thickness of 1 mm, and a gage length of 26 mm using a Zwick universal testing machine (Z010, Zwick/Roell) at room temperature and a testing speed of 10 mm/min (for Young's modulus 1 mm/min). The strain was directly measured in the parallel range of the bars with a sensor arm extensometer. For measurements perpendicular to the extrusion direction specimens of 10 mm length were stamped out and tested using a custom made tensile clamp at a tensile speed of 10 mm/min. Engineering stress (σ) and strain (ϵ) are calculated based on the force and the displacement as well as based on the initial specimen dimensions.

7.3. Modification of nanoclay with VDAC and TAUN and subsequently with Grubbs catalyst.

For the successful attachment of Ru onto the clay surface, surface modification with specific ligands with Ru bonding sites was necessary. Therefore, first the required ligand was synthesized. Their procedure was adopted from literature^{237,238,239}.



Scheme 7.3.1: Step by step reaction pathways for the synthesis of organic modifiers with potential sites for the immobilization of Ru catalyst.

7.3.1. Synthesis of vinylbenzyl dodecyl ammonium chloride 16.

Compound 16 (VDAC) was synthesized according to the procedure from Qutubuddin²³⁷. 4-Vinylbenzylchloride (2 g, 13 mmol), *N,N*-dimethyldodecylamine (3.3 g, 14.3 mmol) and 2,6-di-

t-butyl-*p*-cresol (286 mg, 1.3 mmol) were all placed in a 50 ml flask containing diethylether (3 mL). The mixture was stirred for 17 hours at 30 °C. A colorless precipitate was formed afterwards. The product was washed several times with diethylether and dried under vacuum at room temperature. The product was subsequently purified by re-crystallization from diethylether/acetone (1/10, v/v) with a yield of (92 %, 4.86 g). ¹H-NMR (400 MHz, CDCl₃) δ ppm 7.60 (d, 2H, J = 8.06 Hz, Ar-H), 7.42 (d, 2H, J = 8.04 Hz, Ar-H), 6.69 (dd, 1H, J = 17.59, 10.91 Hz, C=CH₂), 5.79 (d, 1H, J = 17.59 Hz, C=CH₂), 5.34 (d, 1H, J = 10.91 Hz, C=CH₂), 5.06 (s, 2H, CH=CH₂), 3.47 (m, 2H, N-CH₂), 3.29 (s, 6H, N-CH₃), 1.77 (s, 2H, -CH₂-), 1.18-1.22 (m, 18H, -CH₂-), 0.86 (t, 3H, J = 6.76, Hz, -CH₃-); ¹³C-NMR (100 MHz, CDCl₃) δ ppm 139.8, 135.6, 133.5, 126.7, 116.1, 67.1, 63.5, 49.5, 31.8, 29.5, 29.4, 29.3, 29.3, 29.2, 27.4, 26.3, 22.9, 22.6, 14.1.

7.3.2. Synthesis of 5-norbornene-2,3-dicarbonyl dichloride **18**.

The synthesis of **18** was done according to the procedure from Binder et al^{238,239}. A 50 mL dry round-bottom flask equipped with magnetic stirrer bar was flushed with argon and charged with endo, exo-bicyclo (2,2,1)-hept-5-ene-2,3-dicarboxylic acid (2.5 g, 13.73 mmol) and an excess thionyl chloride (8.23 mL, 0.114 mol). The mixture was refluxed for 4 hours at 90 °C and subsequently excess of thionyl chloride was removed under reduced pressure to obtain endo, exo-bicyclo (2,2,1)-hept-5-ene-2,3-dicarboxylic acid chloride (99.9 %, 2.748 g). ¹H-NMR (400 MHz, CDCl₃) δ ppm 6.24 (dd, 1H, J = 5.56, 3.06 Hz, Ar-H), 6.03 (dd, 1H, J = 5.57, 2.80 Hz, Ar-H), 3.34 (d, 1H, J = 4.06 Hz, Ar-H), 3.22 (s, 1H, Ar-H), 3.08 (s, 1H, Ar-H), 2.65 (dd, 1H, J = 4.59, 1.72 Hz, Ar-H), 1.58 (d, 1H, J = 8.79 Hz, Ar-H), 1.43 (m, 1H, Ar-H); ¹³C-NMR (100 MHz, CDCl₃) δ ppm 173.6, 135.1, 52.0, 51.7, 45.5.

7.3.3. Synthesis of 5-norbornene diester **20**.

The procedure for the synthesis of **20** was adopted from Harsha²⁴⁰ with particular reference to that published by Behling²⁴¹. Bromoundecanol (2.25 g, 9.1 mmol) in 1.5 mL of pyridine and 30 ml of diethylether was added dropwise into a flask containing norbornene dicarbonyl chloride **14** in 5 mL of diethylether and the reaction mixture was stirred for 6 hours. Subsequently, the solvent was removed under high vacuum to furnish the product as a dark yellowish liquid (77 %, 2.543 g). ¹H-NMR (400 MHz, CDCl₃) δ ppm 6.27 (dd, 1H, J = 5.47, 3.15 Hz, Ar-H), 6.05 (dd, 1H, J = 5.54, 2.80 Hz, Ar-H), 4.09 (t, 2H, J = 6.68 Hz, O-CH₂), 4.02 (d, 2H, J = 6.66 Hz, O-CH₂),

3.39 (t, 4H, J = 6.87 Hz, -CH₂-), 3.25 (s, 1H, Ar-H), 3.10 (s, 1H, Ar-H), 2.66 (d, 1H, J = 4.47 Hz, Ar-H), 1.84 (q, 4H, J = 6.94 Hz, -CH₂-), 1.26 (m, 36H, -CH₂-); ¹³C-NMR (100 MHz, CDCl₃) δ ppm 137.5, 109.9, 63.1, 52.0, 51.8, 45.6, 34.0, 32.7, 29.5, 29.3, 28.7, 28.1, 25.7.

7.3.4. Synthesis of 5,6-di(11-(n,n,n-trimethylammonium)undecoxycarbonyl)norbornene (TAUN) 21.

Norbornene diester (2.5 g, 5.9 mmol) was mixed with trimethylamine (10 mL, 31-35 % of trimethylamine in ethanol) and stirred for 48 hours under Ar. The reaction mixture was concentrated with rotary evaporator, and the product was dried under dynamic vacuum for 4 days to give a waxy surfactant material **21** (89 %, 8.23 g). ¹H-NMR (400 MHz, CDCl₃) δ ppm 6.26 (s, 1H, Ar-H), 6.1 (s, 1H, Ar-H), 3.70 (q, 4H, J = 7.02 Hz, O-CH₂), 3.59 (m, 5H, N-CH₂), 3.45 (s, 18H, N-CH₃), 3.24 (s, 1H, Ar-H), 3.10 (s, 1H, Ar-H), 2.63 (d, 1H, J = 3.04 Hz, Ar-CH₂), 1.74 (s, 4H, -CH₂-), 1.26 (m, 40H, -CH₂-); ¹³C-NMR (100 MHz, CDCl₃) δ ppm 173.3, 137.4, 66.7, 64.9, 64.6, 62.7, 53.4, 45.5, 32.6, 29.3, 29.2, 28.5, 26.1, 25.8, 23.1.

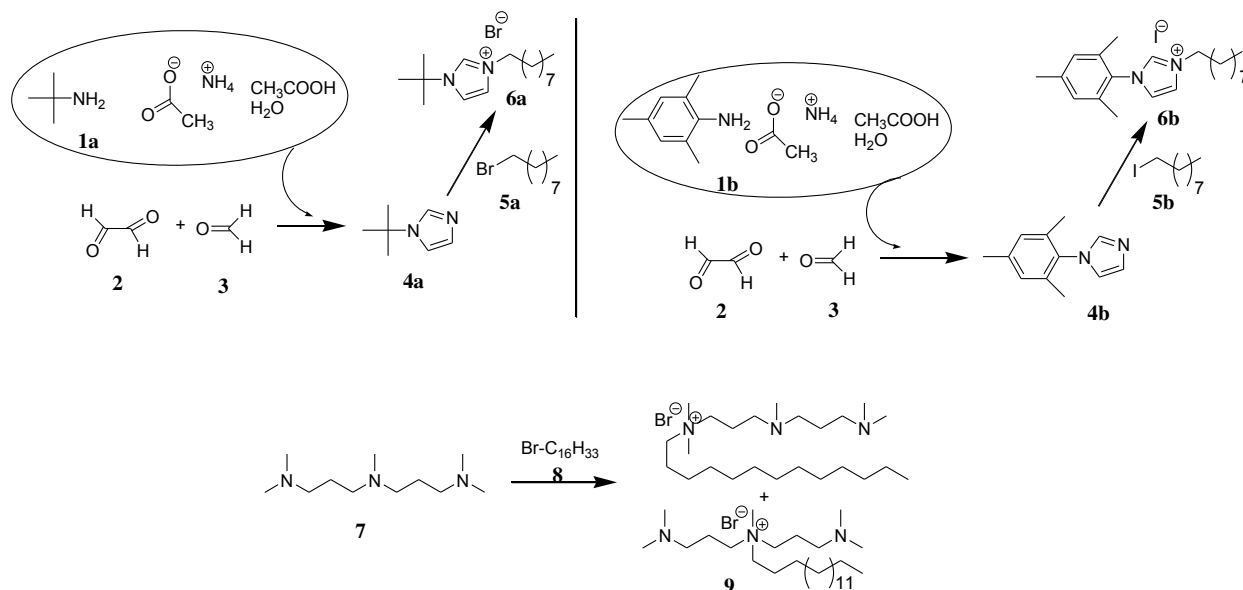
7.3.5. Surface modification of nanoclays with VDAC and subsequent attachment of Ru 23, and 24.

Sodium montmorillonite (1 g, CEC = 82 meq/100 g) was dispersed in 70 °C distilled water (100 mL) and stirred for 1 hour. The solution was allowed to cool slightly (around 40 °C) followed by the addition of 10 % excess of the modifying surfactant in 50 mL of water and 1 % butylated hydroxytoluene as indicator (dissolved in minimal amount of ethanol). The resultant mixture was stirred for further 6 hours. The modified clay was filtered and washed repeatedly with warm distilled water until no chloride ions were detected using 0.1 M AgNO₃ solution. The modified clay was preliminary dried at 75 °C for 12 hours, and further dried at 75 °C after the nanoclay was grounded to particles size of less than 45 μm prior to analysis. Subsequently, the organoclay (0.1 g, 0.064 mmol VDAC/100 mg of clay) was dispersed in degassed DCM (100 mL) and stirred under vortex for 48 hours to swell the clay layers in the solvent. First generation Grubbs catalyst (0.105 g, 0.128 mmol) was added into the mixture and stirred for another 30 minutes, after which the reaction was stopped and the solvent was removed by centrifugation. The G1-modified clay was thoroughly washed with dry DCM (50 mL, three times) to remove unreacted catalyst. The catalyst-modified clay was dried under Ar and thereafter used for kinetic investigations.

7.3.6. Surface modification of nanoclays with TAUN and subsequent attachment of Ru²⁴⁰ 25, and 26. Norbornene surfactant (0.334 g, 0.615 mmol) was mixed with Na MMT clay (0.5 g, 0.41 mmol) in 100 mL distilled water and stirred under reflux for 96 hours to achieve maximum grafting density. The modified clay was recovered by filtration and further dried under vacuum at room temperature for 24 hours. ROMP active organoclay substrate **26**, was prepared by the dispersion of 75 mg of Nmod-MMT in 16 mL of dichloromethane for 4 hours with rigorous stirring at room temperature, and followed by the addition of 50 mg of Grubbs catalyst (first generation) and 200 mg of PCy₃. The mixture was rigorously stirred for 1 hour, and filtered thereafter. The G1-modified clay was thoroughly washed with dry DCM (50 mL, three times) to remove unreacted catalyst. The Ru-modified clay **26** was dried under Ar for 24 hours.

7.4. Synthesis of modifiers for Cu(I) attachment and subsequent attachment of Cu carbenes 6a, 6b, and 9.

In order to successfully attach Cu(I) onto clay surface, the surface of nanoclay had to be modified with organic molecules that have possibilities to bond Cu(I). For this purpose, several modifiers with directional and non-directional bonding sites for Cu(I) were synthesized. Their procedure was adopted from literature^{242,149} with modification.



Scheme 7.4.1: Step by step synthetic route for the successful synthesis of organic modifiers with potential sites for the immobilization of Cu(I).

7.4.1. Synthesis of 1-*tert*-butyl-1*H*-imidazole 4a.

The synthesis of **4a** was according to the procedure from Giovanni²⁴². Glacial acetic acid (10 mL), aqueous formaldehyde (3 mL), and aqueous glyoxal (4.6 mL) were all transferred into a round bottom flask and heated to 70 °C. A solution of glacial acetic acid (10 mL), ammonium acetate in water (3.08 g in 2 mL of water), and *tert*-butyl amine (5.6 mL) was added drop wise over a period of 20 minutes. The solution was allowed to stir continuously for 18 hours. Purification was done by dissolving the crude mixture in NaHCO₃ solution (300 mL). The target product was extracted with chloroform (100 mL, three times) (79.5 % 3.95 g). ¹H-NMR (400 MHz, CDCl₃) δ ppm 7.60 (s, 1H, N-CH), 7.02 (d, 2H, J = 9.32 Hz, -CH=CH-), 1.53 (s, 1H, -CH₃-); ¹³C-NMR (100 MHz, CDCl₃) δ ppm 134.3, 128.9, 116.2, 54.7, 30.5.

7.4.2. Synthesis of 1-(2,4,6-trimethylphenyl)-1*H*-imidazole 4b.

The synthesis of **2b** was done utilizing the procedure from Giovanni²⁴². Glacial acetic acid (10 mL), aqueous formaldehyde (3 mL), and aqueous glyoxal (4.6 mL) were all transferred into a round bottom flask and heated to 70 °C. A solution of glacial acetic acid (10 mL), ammonium acetate in water (3.08 g in 2 mL of water), and mesitylamine (5.6 mL) was added drop wise over a period of 20 mins. The solution was allowed to stir continuously for 18 h. The reaction mixture was cooled down to room temperature and was added drop wise to a stirring solution of NaHCO₃ (300 mL). The target product precipitated. The precipitate was isolated, washed with water several times (100 mL, three times) and dried under air to obtain a brown yellow solid. Recrystallization of crude product using ethyl acetate gave the target product (81.42 %, 4.3 g). ¹H-NMR (400 MHz, CDCl₃) δ ppm 7.43 (s, 1H, N=CH), 7.23 (s, 1H, -CH=CH-), 6.96 (s, 1H, Ar-H), 6.88 (t, 1H, J = 1.19 Hz, -CH=CH-), 2.33 (s, 1H, Ar-CH₃), 1.95 (s, 1H, -CH₃-); ¹³C-NMR (100 MHz, CDCl₃) δ ppm 138.7, 137.4, 135.3, 128.9, 120.0, 20.9, 17.2.

7.4.3. Synthesis of *tert*-butyl-1-dodecylimidazolium bromide 6a.

Tert-butyl-1-dodecylimidazolium bromide **6a** was synthesized by dissolving 1-*tert*-butyl-1*H*-imidazole **4a** (0.5 g, 0.0042 mol) and 1-bromodecane **5a** (1.38 g, 0.0063 mol) in THF and the reaction was heated to 100 °C for 18 hours. The solvent was first cooled to room temperature and decanted and the product dried in vacuum (79 % 1.49 g). ¹H-NMR (400 MHz, CDCl₃) δ ppm 10.70 (s, 1H, N=CH-), 7.48 (t, 1H, J = 1.55 Hz, -CH=CH-), 7.38 (s, 1H, -CH=CH-), 4.46 (t, 2H, J = 7.46 Hz, N-CH₂), 1.72 (s, 9H, -CH₃-), 1.19-1.27 (m, 18H, -CH₂-); ¹³C-NMR (100

MHz, CDCl₃) δ ppm 135.8, 122.0, 119.7, 60.3, 49.9, 31.7, 30.4, 30.1, 29.4, 29.3, 29.1, 29.0, 26.2, 22.5, 14.0.

7.4.4. Synthesis of 1-mesityl-1-dodecylimidazolium iodide **6b**.

For the synthesis of 1-mesityl-1-dodecylimidazolium iodide **6b**, Mesitylimidazole (1 g, 5.37 mmol) **4b**, and 1-iodododecane **5b** (1.91 g, 1.59 ml, 6.44 mmol) were dissolved in THF and heated to 100 °C for 18 hours. The solvent was cooled down to room temperature, decanted and the product dried in vacuum to furnish the product **6b** (98 %, 2.8 g). ¹H-NMR (400 MHz, CDCl₃) δ ppm 10.06 (s, 1H, N=CH-), 7.72 (s, 1H, Ar-H), 7.20 (s, 1H, Ar-H), 7.00 (s, 2H, -CH=CH-), 2.33 (s, 3H, Ar-CH₃), 2.07 (s, 6H, Ar-CH₃), 1.24-1.35 (m, 18H, -CH₂-), 0.87 (t, 3H, J = 6.78 Hz, -CH₃); ¹³C-NMR (100 MHz, CDCl₃) δ ppm 141.5, 137.9, 134.1, 129.9, 122.9, 122.4, 109.9, 50.7, 31.8, 30.4, 29.5, 29.4, 29.3, 29.3, 28.9, 26.0, 22.6, 17.7.

7.4.5. Synthesis of tertiary amino ligand **9**.

The synthesis of the tertiary amino ligand was based on a simple nucleophilic substitution of the bromine atom in 1-bromohexadecane by one amino group. According to the procedure from Stein, et.al¹⁴⁹, *N*^l-(3-(dimethylamino)propyl)-*N*^l,*N*³,*N*³-trimethylpropane-1,3-diamine (10 g, 0.049 mol, 12.0 mL) was added to 12.2 mL of DMF, and with the protection of nitrogen, the mixture was heated to 100 °C. 1-Bromohexadecane (12.3 mmol, 3.75 g, 3.75 mL) was added drop wise (about 10 s per drop) into the mixture and the resultant mixture was stirred for 48 hours at 100 °C. When the reaction was completed, the excess amine was removed by vacuum distillation (50 mbar, 100 °C). ¹H-NMR (400 MHz, CDCl₃) δ ppm 3.48 (d, 6H, J = 16.79 Hz, N-CH₂), 3.42 (s, 2H, N-CH₂), 3.36 (s, 8H, N-CH₂), 3.30 (d, 2H, J = 4.72 Hz, N-CH₂), 3.14 (s, 2H, N-CH₂), 2.34-2.07 (m, 30H, N-CH₃), 1.56 (m, 23H, -CH₂), 1.18 (s, 48H, -CH₂), 0.80 (t, 6H, J = 6.79, -CH₃).

7.4.6. Surface modification of Na MMT with compounds **6a** and **6b** and subsequent attachment of Cu(I) **13a** and **13b**.

The modification of Na MMT with **6a** and **6b** was done according to the procedure from Qutubuddin²⁴⁰ with modification. Na MMT (0.5 g) was dispersed in a 50:50 mixture of water and methanol (50:50 mL) and was heated to 80 °C. The solution was allowed to stir for 1 hour to allow swelling of the clay. **6a** (0.211 g, 0.615 mmol), / **6b** (0.263 g, 0.615 mmol), dissolved in minimal amount of methanol (0.7 mL) was thereafter added at 80 °C and the resultant mixture was allowed to stir for further 5 hours while slowly cooling down to room temperature. The

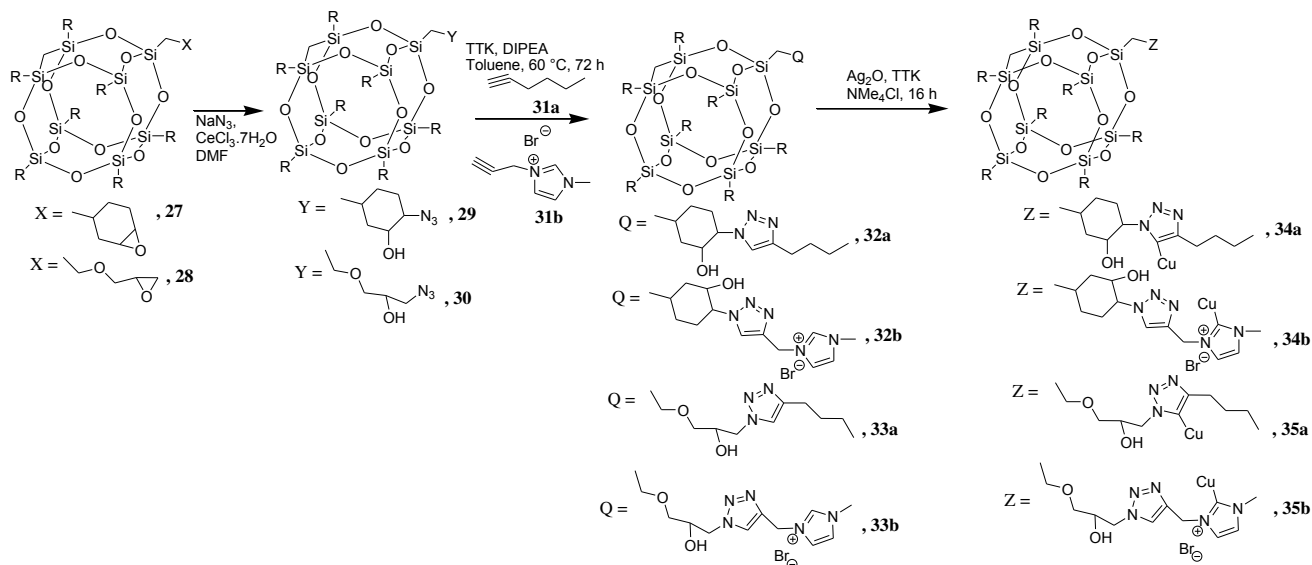
mixture was centrifuged (5000 rpm, 10 mins, 25 °C) and the resultant modified clay was washed several times with methanol (100 mL, three times) and water (100 mL, three times) to remove unreacted modifiers. The modified clay was dried in oven at 70 °C for 24 hours. To achieve successful attachment of Cu(I), the modified clay, **13a** (0.3 g, 0.87 mmol)/ **13b** (0.400 g, 0.176 mmol), was dissolved in dry DMF (5 mL) and stirred for 3 hours at room temperature to allow the clay to swell. Thereafter, tetrakis(acetonitrile)copper(1)hexafluorophosphate (0.423 g, 1.13 mmol-for **8a**, and 0.352 mmol, 0.131g-for **8b**) was added and the resultant solution was allowed to stir for 18 hours. The obtained copper (1)-modified clay was centrifuged (5000 rpm, 10 mins, 25 °C) and washed several times with dry DMF (100 mL, four times) to remove excess copper (I).

7.4.7. Surface modification of Na MMT with **9 and subsequent attachment of Cu(I) **11**.**

Na MMT (0.9 g, 0.74 mmol/0.9 g of clay) was dispersed in 70 °C distilled water (150 mL) and allowed to swell for 1 hour at the same temperature. The solution was cooled down to 40 °C. **5** (1.11 mmol, 0.926 g) was then added to the mixture and the solution was allowed to further stir for 6 hours while slowly cooling down to room temperature. The suspension was centrifuged (5000 rpm, 10 mins, 25 °C) and the organoclay was washed several times with warm water (100 mL, three times) to remove unreacted TAL. The modified clay was dried at 70 °C in a vacuum oven for 48 hours. TAL-Clay **9** (1 g, 0.32 mmol), was dissolved in dry DMF (150 mL) and stirred for 3 hours at room temperature, to allow the clay to swell. Thereafter, tetrakis(acetonitrile)copper(1)hexafluorophosphate (0.416 mmol, 0.155g) was added and the resultant solution was allowed to stir for 18 hours. The obtained copper (1)-modified clay was centrifuged (5000 rpm, 10 mins, 25 °C) and washed several times with dry DMF (100 mL, three times) to remove excess copper.

7.5. Synthesis of Cu- and Ru-modified POSS.

The surface modification of POSS nanomaterials was achieved through a series of reaction steps. The formation of the Ru- and Cu-carbenes on the POSS surface was done according to literature with slight modification.^{246,273,274}



Scheme 7.5.1: Surface modification of different POSS compounds with low molecular weight compounds with potential bonding sites for the immobilization of metal catalyst.

7.5.1. Synthesis of azidohydrincyclohexylisobutyl POSS 29.

A solution of epoxycyclohexylisobutyl POSS (1.0 g, 3.19 mmol) in dry tetrahydrofuran (5 mL) was added to a solution of sodium azide (0.208 g, 3.19 mmol) and ammonium chloride (0.170 g, 3.18 mmol) in dry DMF (5 mL). The mixture was stirred for 35 hours at 50 °C. The solution was then precipitated into 200 mL of water and the product **29** was filtered and vacuum dried at 40 °C for 60 hours (72 %, 0.869 g). ¹H-NMR (400 MHz, CDCl₃) δ ppm 3.49 (dd, 2H, J = 80.88, 42.57 Hz, N-CH₂), 3.13 (t, 1H, J = 6.76 Hz, -CH), 2.13 (m, 1H, OH), 2.06 (m, 1H, -CH), 1.78-1.86 (m, 9H, C-H), 1.67 (m, 1H, -CH), 1.45-1.53 (m, 6H, -CH₂), 0.90-0.98 (m, 42H, -CH₃), 0.55-0.74 (m, 16H, -CH₂); ¹³C-NMR (100 MHz, CDCl₃) δ ppm 69.1, 62.6, 32.2, 30.2, 29.5, 28.9, 27.9, 26.7, 25.6, 24.6, 23.8, 22.47; ²⁹Si-NMR (80 MHz, CDCl₃) δ ppm -67.1, -67.3, -67.7, -67.91.

7.5.2. Synthesis of azidohydrinisobutyl POSS 30.

Sodium azide (0.175 g, 2.7 mmol) was added to a mixture of glycidylisobutyl POSS (0.5 g, 0.54 mmol) and cerium (III) chloride heptahydrate (0.1 g, 0.27 mmol) in a mixture DMF and THF (1:1, 10 mL). The reaction mixture was stirred for 24 hours at 70 °C. The excess solvent was removed by vacuum. The product was redissolved in 80 mL chloroform, washed with water (75 mL, two times) and brine (75 mL, two times) and again with water (100 mL, two times). The organic phase was separated; dried over Na₂SO₄, filtered and the solvent was removed under

reduced pressure. The crude product was purified using column chromatography (R_f value: 0.45, SiO_2 , n-hexane/ethyl acetate, 10:1). $^1\text{H-NMR}$ (400 MHz, CDCl_3) δ ppm 3.95 (m, 1H, -CH), 3.60 (m, 1H, -CH), 3.52 (d, 1H, $J = 5.11$ Hz, -CH), 3.44 (m, 3H, $-\text{CH}_2$), 3.33 (m, 1H, -CH), 1.85 (dd, 7H, $J = 20.12, 6.71$ Hz, -CH), 1.67 (s, 3H, $-\text{CH}_2$, -OH), 0.95 (d, 42H, $J = 6.62$ Hz, $-\text{CH}_3$), 0.60 (d, 16H, $J = 4.32$ Hz, $-\text{CH}_2$); $^{13}\text{C-NMR}$ (100 MHz, CDCl_3) δ ppm 73.6, 71.5, 71.0, 53.4, 25.6, 23.8, 22.8, 22.4, 8.2; $^{29}\text{Si-NMR}$ (80 MHz, CDCl_3) δ ppm -67.4, -67.6, -67.9.

7.5.3. Synthesis of hexynylhydrincyclohexylisobutyl POSS via “click” chemistry 32a.

To a 100 mL one-necked round bottom flask containing 15 mL of toluene was added azidohydrincyclohexylisobutyl POSS $_{29}$ (1 g, 1.0 mmol), 1-hexyne **31a** (0.18 mL, 0.123 g, 1.50 mmol), tetrakis(acetonitrile)copper(I) hexafluorophosphate (0.111 g, 0.3 mmol), *N,N*-diisopropylethylamine (0.2 mmol, 0.025 g). The solution was purged with nitrogen for 45 minutes to remove any trace of oxygen. Thereafter the solution was heated to 60 °C for 48 hours. At the end of the reaction, the solvent was evaporated and crude product was redissolved in chloroform, washed with water (100 mL, three times), brine (100 mL) and again with water (100 mL). The organic phase was separated and dried over Na_2SO_4 . After filtration, the solvent was removed and the product was further purified by column chromatography (Chloroform: methanol, 10:1, R_f value: 0.45) (80.1 %, 0.9 g). $^1\text{H-NMR}$ (400 MHz, CDCl_3) δ ppm 7.32 (s, 1H, TrA-H), 4.12 (t, 2H, $J = 58.84$ Hz, -CH, -CH), 2.74 (dd, 2H, $J = 20.85, 13.47$ Hz, $-\text{CH}_2$), 1.73-2.30 (m, 13H, $-\text{CH}_2$, -OH), 1.20-1.70 (m, 11H, -CH, CH_2), 0.85-1.15 (m, 46H, $-\text{CH}_3$), 0.51-0.70 (m, 16H, $-\text{CH}_2$); $^{13}\text{C-NMR}$ (100 MHz, CDCl_3) δ ppm 128.7, 125.6, 72.9, 53.0, 52.6, 51.9, 35.3, 34.6, 31.8, 31.3, 30.3, 28.9, 27.4, 25.6, 23.8, 22.4, 13.7; $^{29}\text{Si-NMR}$ (80 MHz, CDCl_3) δ ppm -67.4, -67.5, -67.7, -67.8.

7.5.4. Synthesis of 1-methylimidazoliumhydrincyclohexylisobutyl POSS via “click” chemistry 32b.

To a 100 mL one-necked round bottom flask containing a solution of dry toluene and isopropanol (1:1) 15 mL, was added azidohydrincyclohexylisobutyl POSS $_{29}$ (1 g, 1.0 mmol), 1-methylimidazolium ionic liquid **31b** (0.230 g, 1.23 mmol), tetrakis(acetonitrile)copper(I) hexafluorophosphate (0.038 g, 0.102 mmol), *N,N*-diisopropylethylamine (0.102 mmol, 0.014 g). The solution was purged with nitrogen for 45 minutes to remove traces of oxygen. Thereafter the solution was heated to 60 °C for 48 hours. At the end of the reaction, the solvent was evaporated

and the crude product was redissolved in chloroform, washed with water (100 mL, three times), brine (100 mL) and again with water (100 mL). The organic phase was separated and dried over Na_2SO_4 . The solvent was removed and the product was further purified using column chromatography (Chloroform: methanol, 30:1) to give the final product **32b**, with an R_f value of 0.45 (45 %, 0.554 g). $^1\text{H-NMR}$ (400 MHz, CDCl_3) δ ppm 7.66 (s, 1H, TrA-H), 7.03 (t, 1H, J = 6.51 Hz, N=CH-), 6.37 (dd, 1H, J = 4.58, 2.91 Hz, -C=CH-), 6.14 (t, 1H, J = 2.96 Hz, -C=CH-), 4.89 (s, 2H, N- CH_2 -), 4.11 (t, 2H, J = 68.26 Hz, - CH_2), 3.25 (d, 3H, J = 6.23 Hz, N- CH_3), 2.74 (s, 1H, -OH), 1.61-1.93 (m, 22H, - CH_2 -, -CH-), 1.25 (s, 5H, -CH-), 0.95 (d, 43H, J = 7.55 Hz, - CH_3), 0.60 (d, 16H, J = 7.02 Hz, - CH_2).

7.5.5. Synthesis of hexynylhydrinisobutyl POSS via “click” chemistry **33a**.

Azidohydrinisobutyl POSS **30** (2.5 g, 2.7 mmol), 1-hexyne **31a** (0.261 g, 3.2 mmol), TBTA (0.143 g, 0.27 mmol), DIPEA (0.05 mL, 0.27 mmol), $\text{Cu}(\text{MeCN})_4\text{PF}_6$ (0.1 g, 0.27 mmol) were placed into a 50 mL round bottom flask containing 30 mL of dry toluene equipped with a magnetic stir bar. The mixture was purged with nitrogen for 45 minutes. The reaction mixture was heated for 48 hours at 80 °C. The excess solvent was removed with rotary evaporator and the crude product purified using column chromatography (SiO_2 , Chloroform/methanol, 10:1, R_f = 0.34). $^1\text{H-NMR}$ (400 MHz, CDCl_3) δ ppm 7.41 (s, 1H, TrA-H), 4.51 (dd, 1H, J = 14.08, 3.64 Hz, -CH), 4.37 (dd, 1H, J = 14.11, 6.92 Hz, -CH), 4.18 (dd, 1H, J = 10.05, 5.95 Hz, O-CH), 3.44 (m, 3H, O-CH, O- CH_2), 3.35 (dd, 1H, J = 9.63, 6.06 Hz, OH-CH), 2.95 (s, 1H, -OH), 2.73 (t, 2H, J = 7.69 Hz, - CH_2), 1.87 (td, 7H, J = 13.37, 6.70 Hz, -CH), 1.67 (m, 4H, - CH_2), 1.39 (m, 2H, - CH_2), 0.96 (m, 45H, - CH_3), 0.62 (m, 16H, - CH_2); $^{13}\text{C-NMR}$ (100 MHz, CDCl_3) δ ppm 156.3, 122.1, 73.6, 71.3, 69.3, 52.7, 31.4, 30.3, 29.6, 25.6, 23.8, 22.8, 22.4, 22.2, 13.7, 8.3; $^{29}\text{Si-NMR}$ (80 MHz, CDCl_3) δ ppm -67.5, -67.6, -67.8.

7.5.6. Synthesis of 1-methylimidazoliumhydringlycidylisobutyl POSS via “click” chemistry **33b**.

To a 20 mL one-necked round bottom flask containing a solution of dry toluene and isopropanol (1:1) 5 mL, was added azidohydrinisobutyl POSS **30** (0.1 g, 0.103 mmol), 1-propargyl-3-methylimidazole bromide **31b** (0.023 g, 0.124 mmol), tetrakis(acetonitrile)copper(1) hexafluorophosphate (0.0038 g, 0.0103 mmol), *N,N*-diisopropylethylamine (0.0103 mmol, 0.0013 g). The solution was purged with nitrogen for 45 minutes to remove traces of oxygen.

Thereafter the solution was heated to 60 °C for 48 hours. At the end of the reaction, the solvent was evaporated and crude product was redissolved in chloroform, washed with water (20 mL, three times), brine (30 mL) and again with water (20 mL). The organic phase was re-dissolved in methanol to remove unreacted imidazolium compound. The solvent was removed and the product was further purified by column chromatography (Chloroform: methanol, 30:1, R_f value: 0.45) (45 %, 55 mg). ¹H-NMR (400 MHz, CDCl₃) δ ppm 7.59 (s, 1H, TrA-H), 7.24 (d, 1H, J = 7.23 Hz, -CH=CH-), 7.17 (d, 1H, J = 7.36 Hz, -CH=CH-), 5.66 (s, 1H, -CH), 4.88 (s, 1H, -CH), 4.67 (d, 1H, J = 13.59 Hz, -CH), 4.40 (d, 1H, J = 8.70 Hz, O-CH), 4.21 (s, 1H, O-CH), 3.99 (m, 2H, O-CH₂), 3.45 (t, 3H, J = 6.74 Hz, N-CH₃), 3.62 (m, 1H, -CH), 3.52 (d, 2H, J = 5.12 Hz, N-CH₂), 1.98 (s, 1H, -OH), 1.84 (qd, 7H, J = 13.42, 6.71 Hz, -CH), 1.67 (s, 2H, -CH₂), 0.94 (s, 42H, -CH₃), 0.60 (s, 16H, -CH₂).

7.5.7. Synthesis of 1,2,3-triazol-5-ylidene-copper(I) POSS complex 34a.

To a 20 mL round bottom flask containing dry and degassed mixture of acetonitril and dichloromethane (1:1, 2 mL), **32a** (0.050 g, 0.0479 mmol), silver oxide (0.061 g, 0.0264 mmol), and potassium bis(trimethylsilyl)amide (0.0096 g, 0.0479mmol) was added. The mixture was stirred for 15 hours at room temperature under inert environment. Thereafter, copper(I) chloride (0.0084 g, 0.0479 mmol) was added to the mixture was stirred for an additional 6 hours. The reaction was stopped and the solution was filtered to remove the silver oxide solid particles and then the solvent evaporated. To remove the unbound copper, further purification was done by dissolving the mixture in minimal amount of dry and degassed toluene (0.1 mL), and precipitating in an equal mixture of dry DMF and acetonitrile (5 mL) to furnish the product **34a**, as a light green solid compound (31 %, 0.018 g).

7.5.8. Synthesis of Cu(I)-imidazoliumcyclohexylisobutyl POSS complex 34b.

To a 10 mL round bottom flask containing dry THF (5 mL), and sodium hydrid (0.0122 g, 0.507 mmol) was added **32b** (0.200 g, 0.169 mmol). The mixture was stirred for 15 hours at room temperature under inert environment. Thereafter, copper(I) acetate (0.0124 g, 0.101 mmol) was added to the mixture further stirred for an additional 6 hours. At the completion of the reaction, the solvent was removed using rotary evaporator and the crude product was thereafter washed several times with dry DCM (20 mL, three times) and DMF (20 mL, three times). The trace of

solvent was evaporated to furnish the product **34b**, as a light green solid compound (26 %, 0.055 g),

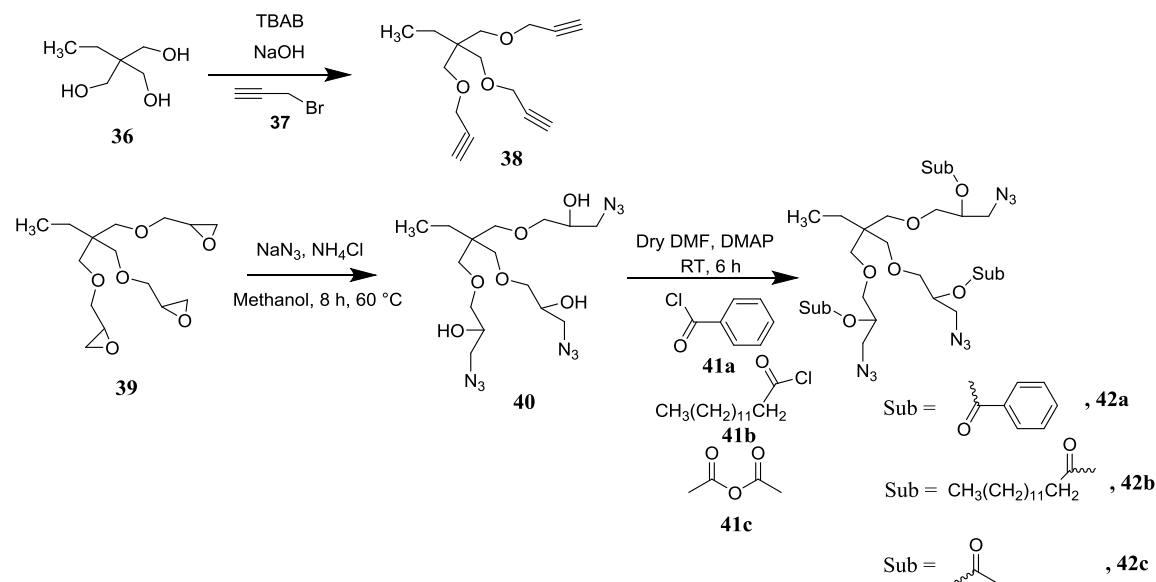
7.5.9. Synthesis of 1,2,3-triazol-5-ylidene-copper(I) POSS complex 35a.

To a 20 mL round bottom flask containing dry and degassed mixture of acetonitril and dichloromethane (1:1, 2 mL), **26a** (0.050 g, 0.0473 mmol), silver oxide (0.060 g, 0.026 mmol), copper chloride (0.0082 g, 0.0621 mmol), and tetramethylammonium chloride (0.0051 g, 0.0473 mmol) were added. The mixture was stirred for 15 hours at room temperature under inert environment. Thereafter, copper(I) chloride (0.0082 g, 0.0473 mmol) was added to the mixture and further stirred for an additional 6 hours. The reaction was stopped and the solution was filtered to remove the silver oxide solid particles followed by the evaporation of the solvent. To remove the unbound copper, further purification was done by dissolving the mixture in minimal amount of dry and degassed toluene (0.1 mL), and precipitating in an equal mixture of dry DMF and acetonitrile (5 mL) to furnish the product **35a**.

7.5.10. Synthesis of Cu (I)-imidazoliumhydringlycidylisobutyl POSS complex 35b.

To a 10 ml round bottom flask containing dry THF (5 mL), was added **28b** (0.100 g, 0.085 mmol), and sodium hydrid (0.0122 g, 0.51 mmol). The mixture was stirred for 15 h at room temperature under inert environment. Thereafter, copper (I) acetate (0.0125 g, 0.102 mmol) was added to the solution and the further stirred for an additional 6 h. The reaction was stopped and the crude product was washed several times with dry DCM. The solution was evaporated to furnish the product **29b**. ¹H-NMR (400 MHz, CDCl₃) δ ppm 7.30 (d, 1H, J = 7.23 Hz, -CH=CH-), 7.10 (d, 1H, J = 7.36 Hz, -CH=CH-), 5.56 (s, 1H, -CH), 4.78 (s, 1H, -CH), 4.67 (d, 1H, J = 13.59 Hz, -CH), 4.32 (d, 1H, J = 8.70 Hz, O-CH), 4.25 (s, 1H, O-CH), 3.91 (m, 2H, O-CH₂), 3.40 (t, 3H, J = 6.74 Hz, N-CH₃), 3.60 (m, 1H, -CH), 3.45 (d, 2H, J = 5.12 Hz, N-CH₂), 1.92 (s, 1H, -OH), 1.74 (qd, 7H, J = 13.42, 6.71 Hz, -CH), 1.56 (s, 2H, -CH₂), 0.90 (s, 42H, -CH₃), 0.54 (s, 16H, -CH₂).

7.6. Synthesis and encapsulation of multivalent alkynes and azides.



Scheme 7.6.1: Schematic representation of multivalent alkynes and azides synthesized via azidation, nucleophilic, and acetylation reactions.

7.6.1. Azidation of trimethylolpropane triglycidyl ether (TriAzOH)²⁷⁵ **40**.

Trimethylolpropane (10 g, 0.033 mol, 8.64 mL) was added to a 250 mL round bottom flask containing 150 mL of methanol. Ammonium chloride (0.165 mol, 8.82 g) and sodium azide (0.165 mol, 10.725 g) were both added to the reaction flask; afterwards the overall mixture was heated to reflux for 12 hours. At the end of the reaction, the solvent was removed under vacuum and the crude product was purified by washing with water (100 mL, three times) and brine (50 mL) and again with water (50 mL, two times), followed by extraction with chloroform (60 mL) to give the product **40** (92 %, 9.2 g). ¹H-NMR (400 MHz, CDCl₃) δ ppm 3.92 (dd, $J = 9.97$, 5.27 Hz, 3H), 3.41 (m, 18H), 3.17 (s, 3H), 1.36 (m, 2H), 0.83 (t, $J = 7.57$ Hz, 3H); ¹³C-NMR (100 MHz, CDCl₃) δ ppm 72.6, 72.3, 69.5, 53.4, 43.3, 23.3, 7.6.

7.6.2. Synthesis of triazidomethylbenzopropane triglycidyl ether **42a**.

42a was synthesized by placing **40** (0.1 g, 0.232 mmol) and 4-dimethylaminopyridine (0.0464 mmol, 0.0056 g) in a 5 mL round bottom flask containing freshly distilled DMF (3 mL). The reaction was stirred for 10 minutes at room temperature, followed by the addition of benzoyl chloride (0.69 mmol, 97.7 mg). The reaction mixture was stirred for 12 hours. After 12 hours, the solvent was removed under vacuum and the crude product was purified by column chromatography. At first, chloroform was used to remove the unreacted benzoyl chloride and

thereafter, chloroform/methanol (20:1, R_f value: 0.25) was used to furnish the product (77 %, 0.152 g). $^1\text{H-NMR}$ (400 MHz, CDCl_3) δ ppm 8.12 (d, 8H, $J = 7.06$ Hz, Ar-H), 7.62 (t, 3H, $J = 7.44$, Ar-H), 7.48 (t, 8H, $J = 7.71$, Ar-H), 3.98 (d, 3H, $J = 5.91$ Hz, O-CH), 3.30-3.70 (m, 18H, O-CH₂), 1.39 (q, 2H, $J = 7.56$, -CH₂), 0.85 (t, 3H, $J = 7.58$ Hz, -CH₃); $^{13}\text{C-NMR}$ (100 MHz, CDCl_3) δ ppm 172.2, 133.7, 130.2, 129.3, 128.4, 71.5, 70.7, 69.4, 50.7, 43.4, 22.9, 7.5. ESI-TOF-MS, measured: 742.13 Da, simulated: 742.14 Da. $[\text{C}_{36}\text{H}_{41}\text{N}_9\text{O}_9+\text{H}]^+$.

7.6.3. Synthesis of triazidomethyloctanopropane triglycidyl ether 42b.

40 (0.1 g, 0.232 mmol) and 4-dimethylaminopyridine (0.0464 mmol, 0.0056 g) were placed in 5 mL round bottom flask containing freshly distilled DMF (3mL). The reaction mixture was stirred for 10 minutes followed by the addition of merysotyl chloride (0.69 mmol, 170 mg) in drops at room temperature. The reaction mixture was then allowed to stir for 12 hours. Upon completion of the reaction, the solvent was removed under vacuum and the crude product was purified by column chromatography using chloroform and methanol (20:1, R_f value: 0.45) (80 %, 0.216 g). $^1\text{H-NMR}$ (400 MHz, CDCl_3) δ ppm 5.08 (s, 3H, O-CH), 3.32-3.68 (3, 21H, O-CH₂), 2.33 (t, 6H, $J = 7.23$ Hz, OOC=CH₂), 1.61 (dd, 6H, $J = 18.47, 11.26$ Hz, -CH₂), 1.26 (m, 60H, -CH₂), 0.88 (t, 12H, $J = 6.86$ Hz, -CH₃); $^{13}\text{C-NMR}$ (100 MHz, CDCl_3) δ ppm 172.9, 71.6, 70.8, 69.5, 51.0, 43.3, 34.2, 31.9, 29.6, 29.4, 29.3, 29.2, 29.1, 24.8, 22.6, 14.0, 7.5. ESI-TOF-MS, measured: 1180.91 Da, simulated: 1180.9 Da $[\text{C}_{57}\text{H}_{101}\text{N}_9\text{O}_9+\text{I}]^-$.

7.6.4. Synthesis of triazidomethylacetopropane triglycidyl ether 42c.

40, (0.1 g, 0.232 mmol) and 4-dimethylaminopyridine (0.0464 mmol, 0.0056 g) were placed in a 5 mL round bottom flask containing freshly distilled DMF (3mL). The reaction mixture was stirred for 10 minutes at room temperature, followed by the addition of acetic anhydride (0.695 mmol, 70.9 mg). The reaction mixture was then allowed to stir for an 1 hour at room temperature, within which the reaction was complete. The solvent was removed under vacuum and the crude product was purified by flash chromatography using chloroform (R_f value: 0.28) (98 %, 0.17 g). $^1\text{H-NMR}$ (400 MHz CDCl_3) δ ppm 5.06 (m, 3H, OC-H), 3.46-3.54 (m, 12H, O-CH₂), 3.27 (s, 6H, N-CH₂), 2.09 (s, 9H, OC-CH₃), 1.35 (d, 2H, $J = 7.58$ Hz, -CH₂), 0.82 (d, 3H, $J = 7.50$ Hz, -CH₃); $^{13}\text{C-NMR}$ (100 MHz, CDCl_3) δ ppm 162.5, 71.6, 69.5, 50.9, 36.4, 31.4, 22.9, 20.9, 7.5. ESI-TOF-MS, measured: 580.19 Da Simulated: 580.24 Da $[\text{C}_{21}\text{H}_{35}\text{N}_9\text{O}_9+\text{Na}]^+$.

7.6.5. Synthesis of 1-(prop-2-ynyloxy)-2,2-bis((prop-2-ynyloxy)methyl)butane **38**.²⁶⁹

Trimethylolpropane **36** (6.71 g, 0.050 mol), under a dry atmosphere of nitrogen, was placed into a dry 100 mL round bottom flask equipped with a magnetic stir bar and septum. Sodium hydroxide (12 g, 0.30 mol), water (2.0 mL), and TBAB (0.80 g, 0.30 mol) were added and the temperature of the solution was adjusted to 25 °C. Propagyl bromide (45.0 g, 80wt% solution in toluene, 0.30 mol) was added drop wise over a course of 1 hour, and then the temperature was slowly raised to 60 deg over the course of 1 h. during this time the reaction became homogeneous. The reaction mixture was stirred at 60 °C for 22 hours. It was then cooled to room temperature and diluted in dichloromethane (150 mL), washed with water (100 mL, five times) and the organic phase was dried over sodium sulphate, filtered and the solvent was evaporated. The product was dried in high vacuum. Further purification was done with column chromatography (chloroform: methanol, 30:1, R_f value: 0.95) (85 %, 43.95 g). ¹H-NMR (400 MHz, CDCl₃) δ ppm 4.11 (d, 6H, J = 2.41 Hz, O-CH₂), 3.39 (s, 6H, O-CH₂), 2.39 (t, 3H, J = 2.38 Hz, -CH), 1.42 (q, 2H, J = 7.58, Hz, -CH₂), 0.87 (t, 3H, J = 7.58 Hz, -CH₃); ¹³C-NMR (100 MHz, CDCl₃) δ ppm 80.1, 73.9, 70.3, 58.5, 42.7, 22.7, 7.4. ESI-TOF-MS, measured: 271.12 Da Simulated: 271.14 Da [C₁₅H₂₀O₃+Na]⁺.

Chapter 8

Summary

In this research, the surface modification of nanofillers (nanoclays and POSS) was achieved through various pathways, followed by the immobilization of metal particles/catalysts (Cu and Ru) onto nanofiller surface. The synthesis and encapsulation of multifunctional azides and alkynes for “click”-based self-healing nanocomposites, was equally done. Attempts were also made to elucidate the potency of the catalyst-modified nanofillers in the cross-linking behavior of the multivalent alkynes and azides (for Cu-modified nanofillers using DSC).

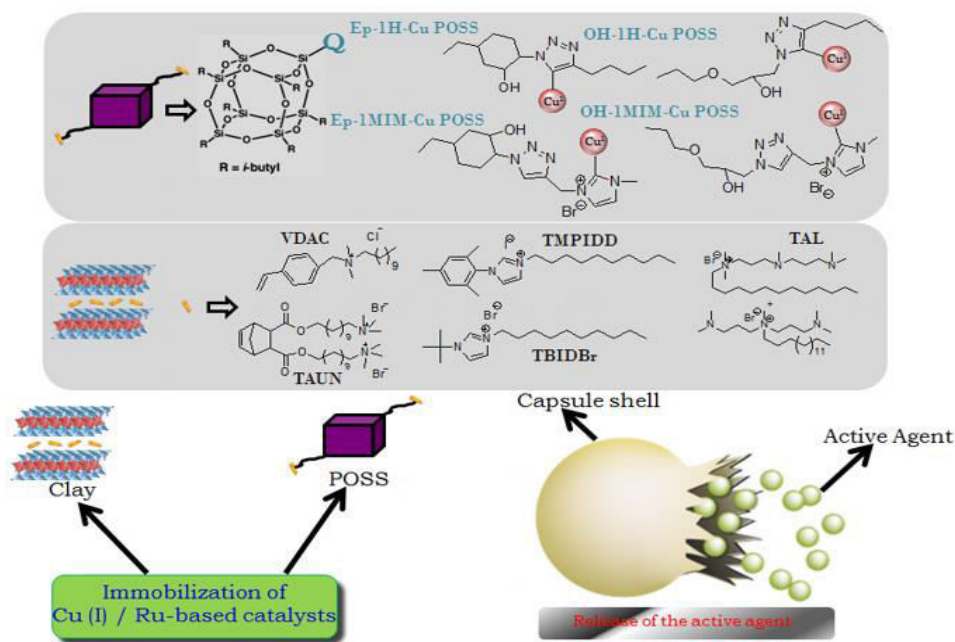
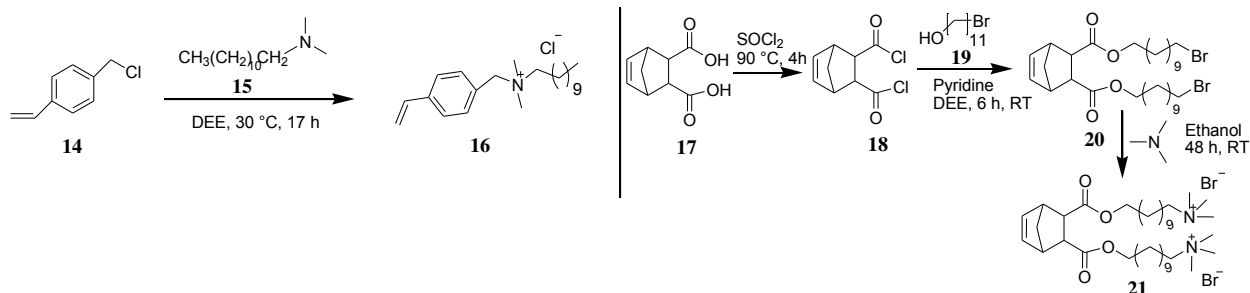


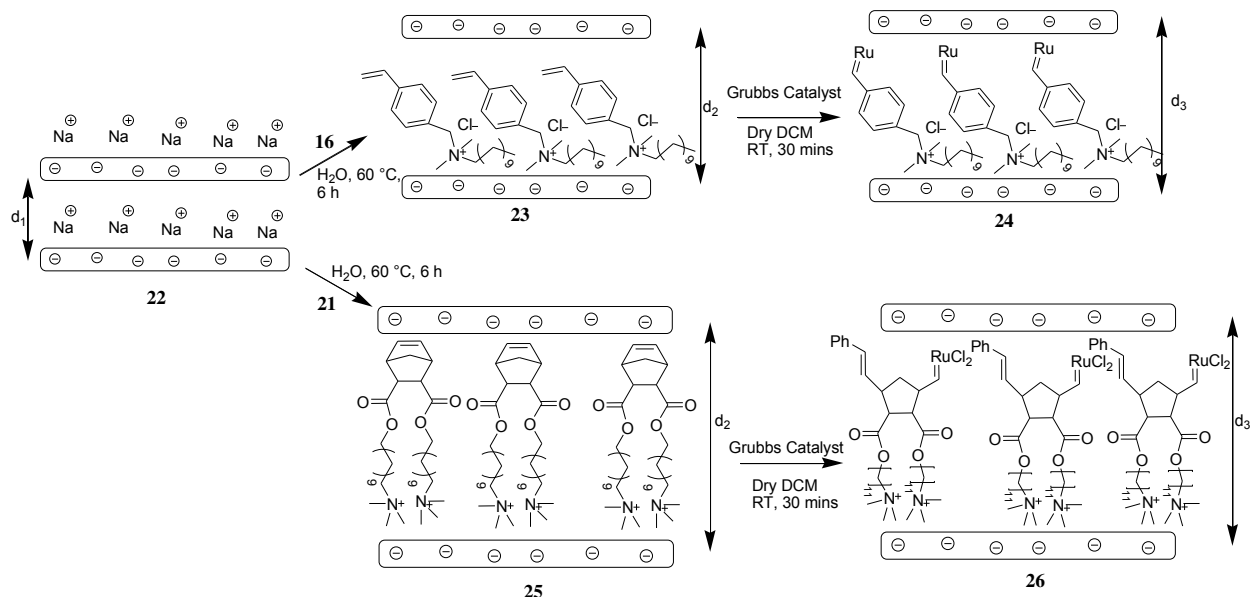
Figure 8.1: General synthetic concept and pathways for the surface modification of clay and POSS, and also the encapsulation of trivalent alkynes and azides.

The first step involved the synthesis of necessary cationically-active organic modifiers with potential sites for the immobilization of Ru-, and Cu-carbenes and subsequent cationic exchange reactions that enables the replacement of the sodium ions present at the interlayer of the clay gallery, to be effectively replaced, relying on Van der Waals forces of attraction to keep the organic molecules bonded to the clay gallery. In achieving this, vinylbenzyl dodecyl chloride and 5,6-di(11-(N,N,N-trimethylammonium)undecoxycarbonyl) norbornene, were successfully synthesized through series of reaction steps (Scheme 8.1)^{237,238,240,241}.



Scheme 8.1: Step by step reaction pathways for the synthesis of organic modifiers with potential sites for the immobilization of Ru catalyst.

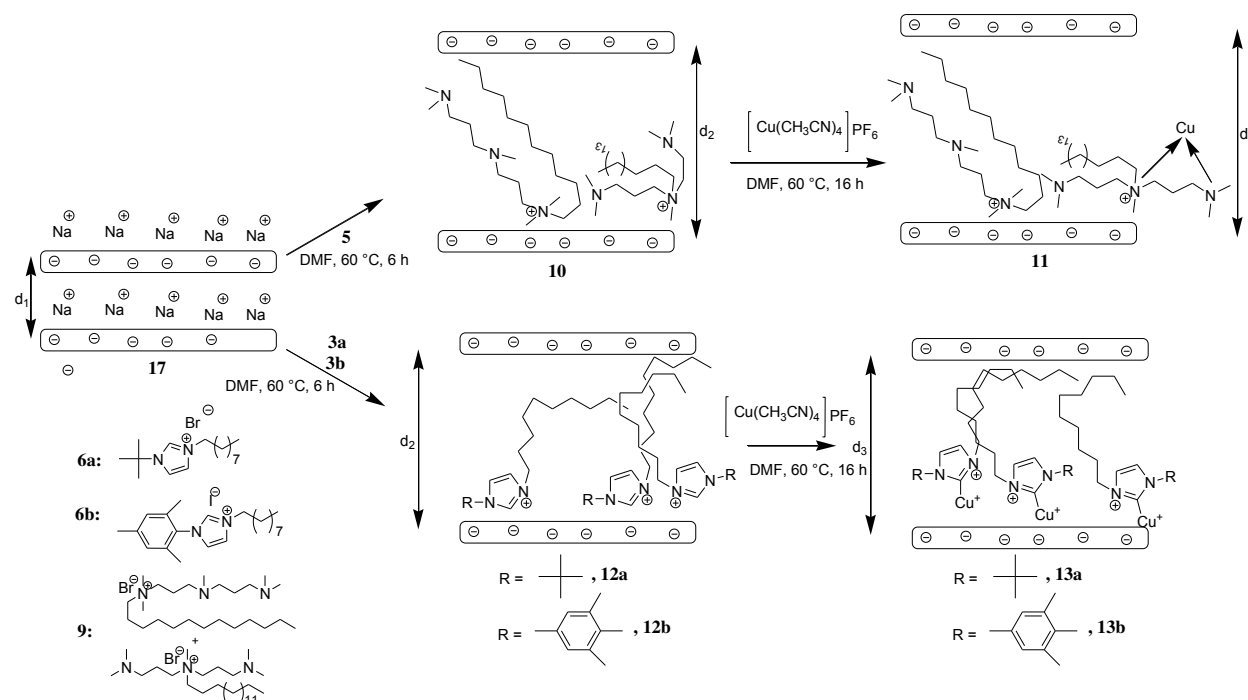
Consequently, the cationic exchange reaction with these cationically-active organic modifiers was done. Several reaction conditions were employed to achieve the organoclay with the highest grafting density (**Scheme 8.2**). And at the end, the reaction condition that gave the best grafting density was selected for further investigations. The modification of nanoclays with these organic molecules gave rise to a completely exfoliated organoclay with an interlayer distance almost doubled of the initial value. This increase of interlayer distance is of immense significance because it overcomes the usual problem of agglomeration of the nano materials, thus making the organoclay dispersible in organic matrix with the possibilities of surface chemistries to be made at the nanometer regime. After the modification of the nanoclays with organic modifiers, subsequent attachment of Ru catalyst on special sites on the organic modifier was made (**Scheme 8.2**)



Scheme 8.2: Synthetic representation for the modification of nanoclays with synthesized organic modifiers with metal-active binding sites followed by the subsequent immobilization of Ru catalyst.

The amount of the Ru-carbenes formed on the surface of the organoclay was determined by FAAS, and from the result obtained, compound **24** had more Ru-carbenes (0.022 mg/mg) than compound **26**. The Ru-modified clay particles was thereafter, used for further cross-linking kinetic studies and formulation of self-healing nanocomposites.

In the same vein, selected organic modifiers with potential bonding sites for copper were synthesized through several reaction steps^{242,246, 273-274, 276}. This was followed by the attachment of Cu (I) (**Scheme 8.3**).

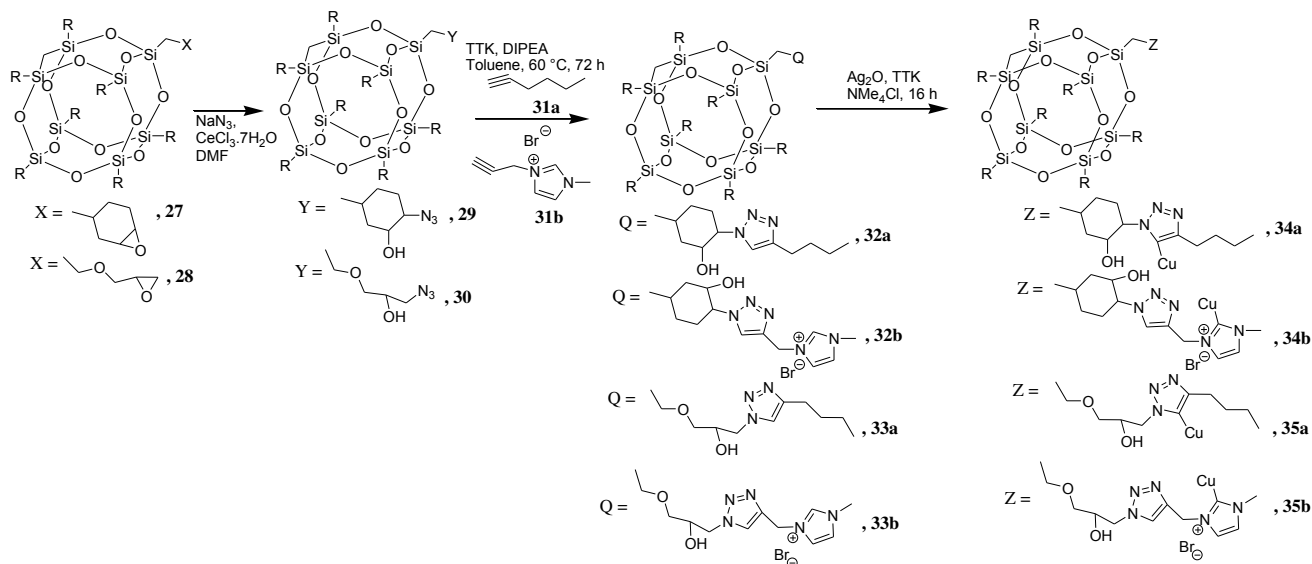


Scheme 8.3: Synthetic representation for the modification of nanoclays with the synthesized organic modifiers for the immobilization of metal catalyst and the subsequent immobilization of Cu(I) onto clay surface.

The amount of the Cu bonded to the surface was determined by FAAS and the results have been reported in the preceding chapters. The catalytic activity of the Cu-modified clay nano particles was determined by DSC using multifunctional azides and alkynes as monomers.

Similar surface modifications were done for POSS. In the light of this, POSS**27**, and **28**, were subjected to surface chemistries in order to create Cu carbenes on the surface²⁴⁶ as seen in **scheme 8.4**. Nevertheless, the creation of Cu carbenes on these POSS materials was achieved

through ionic (Cu carbenes formed on the triazole ring, **34a**, **35a**) and covalent (Cu carbenes formed on the imidazolium ring, **34b**, **35b**) bond formations.



Scheme 8.4: Surface modification of different POSS compounds with low molecular weight compounds with potential bonding sites for the immobilization of metal catalyst.

The Cu carbenes formed by ionic bond formation are labile and can easily be cleaved off at the slightest exposure to air and stored at room temperature. On the contrary, the Cu carbenes formed by covalent bond formation are stronger and more resistant to decomposition when exposed to room temperature, hence, giving them an edge over Cu carbenes formed by ionic bond formation in self-healing applications. The amount of Cu on the surface of the POSS materials was determined by FAAS and the results tabulated below.

Table 14: Amount of Cu on the surface of various POSS catalysts synthesized, as determined by FAAS.

Entry	Compound	Amt of Cu (mg/mg)	Amt of Cu (mmol/mg)
1	Ep-c-1H-Cu	0.049	0.043×10^{-3}
2	Ep-c-1MIM-Cu	0.023	0.018×10^{-3}
3	OH-c-1H-Cu	0.054	0.048×10^{-3}
4	OH-c-1MIM-Cu	0.008	0.006×10^{-3}

In **table 14**, it can be seen that the compound OH-c-1H-Cu (**35a**), had the highest amount of Cu carbene formation. Consequently, the catalytic activity of these Cu-modified POSS materials

was investigated by DSC using multifunctional alkynes and azides, and the results have been discussed in preceding chapters.

8.0. References.

1. Sainz, R.; Small, W. R.; Young, N. A.; Vallés, C.; Benito, A. M.; Maser, W. K.; in het Panhuis, M., Synthesis and Properties of Optically Active Polyaniline Carbon Nanotube Composites. *Macromolecules* **2006**, *39* (21), 7324-7332.
2. Ferreira, A. D. B. L.; Nóvoa, P. R. O.; Marques, A. T., Multifunctional Material Systems: A state-of-the-art review. *Composite Structures* **2016**, *151*, 3-35.
3. Xu, M.; Zhang, T.; Gu, B.; Wu, J.; Chen, Q., Synthesis and Properties of Novel Polyurethane-Urea/Multiwalled Carbon Nanotube Composites. *Macromolecules* **2006**, *39* (10), 3540-3545.
4. Narayana, K. J.; Gupta Burela, R., A review of recent research on multifunctional composite materials and structures with their applications. *Materials Today: Proceedings* **2018**, *5* (2, Part 1), 5580-5590.
5. Gibson, R. F., A review of recent research on mechanics of multifunctional composite materials and structures. *Composite Structures* **2010**, *92* (12), 2793-2810.
6. Fabregat, G.; Teixeira-Dias, B.; del Valle, L. J.; Armelin, E.; Estrany, F.; Alemán, C., Incorporation of a Clot-Binding Peptide into Polythiophene: Properties of Composites for Biomedical Applications. *ACS Applied Materials & Interfaces* **2014**, *6* (15), 11940-11954.
7. Fillery, S. P.; Koerner, H.; Drummy, L.; Dunkerley, E.; Durstock, M. F.; Schmidt, D. F.; Vaia, R. A., Nanolaminates: Increasing Dielectric Breakdown Strength of Composites. *ACS Applied Materials & Interfaces* **2002**, *4* (3), 1388-1396.
8. Zaidi, L.; Kaci, M.; Bruzard, S.; Bourmaud, A.; Grohens, Y., Effect of natural weather on the structure and properties of polylactide/Cloisite 30B nanocomposites. *Polymer Degradation and Stability* **2010**, *95* (9), 1751-1758.
9. Konyshcheva, E.; Blackley, R.; Irvine, J. T. S., Conductivity Behavior of Composites in the La_{0.6}Sr_{0.4}CoO_{3±δ} - CeO₂ System: Function of Connectivity and Interfacial Interactions. *Chemistry of Materials* **2002**, *22* (16), 4700-4711.
10. Da, Z.; Zhou, Z., Applications of Lightweight Composites in Automotive Industries. In *Lightweight Materials from Biopolymers and Biofibers*, American Chemical Society: 2014; Vol. 1175, pp 143-158.
11. Miiinea, L. A.; Sessions, L. B.; Ericson, K. D.; Glueck, D. S.; Grubbs, R. B., Phenylethynylstyrene-Cobalt Carbonyl Block Copolymer Composites. *Macromolecules* **2004**, *37* (24), 8967-8972.
12. Tchernook, A.; Krumova, M.; Tölle, F. J.; Mülhaupt, R.; Mecking, S., Composites from Aqueous Polyethylene Nanocrystal/Graphene Dispersions. *Macromolecules* **2014**, *47* (9), 3017-3021.
13. Liao, L. C. K.; Viswanath, D. S., Thermal Degradation of Poly(vinylbutyral)/Ceramic Composites: A Kinetic Approach. *Industrial & Engineering Chemistry Research* **1998**, *37* (1), 49-57.
14. MacLachlan, M. J.; Ginzburg, M.; Coombs, N.; Raju, N. P.; Greedan, J. E.; Ozin, G. A.; Manners, I., Superparamagnetic Ceramic Nanocomposites: Synthesis and Pyrolysis of Ring-Opened Poly(ferrocenylsilanes) inside Periodic Mesoporous Silica. *Journal of the American Chemical Society* **2000**, *122* (16), 3878-3891.
15. Potts, J. R.; Murali, S.; Zhu, Y.; Zhao, X.; Ruoff, R. S., Microwave-Exfoliated Graphite Oxide/Polycarbonate Composites. *Macromolecules* **2011**, *44* (16), 6488-6495.
16. Dhillon, B. S., A Review on Composite Material Failures. In *Advanced Multilayered and Fibre-Reinforced Composites*, Haddad, Y. M., Ed. Springer Netherlands: Dordrecht, 1998; pp 555-567.
17. Gunjekar, J. L.; Kim, T. W.; Kim, H. N.; Kim, I. Y.; Hwang, S.-J., Mesoporous Layer-by-Layer Ordered Nanohybrids of Layered Double Hydroxide and Layered Metal Oxide: Highly Active Visible Light Photocatalysts with Improved Chemical Stability. *Journal of the American Chemical Society* **2011**, *133* (38), 14998-15007.

18. White, S. R.; Sottos, N. R.; Geubelle, P. H.; Moore, J. S.; Kessler, M. R.; Sriram, S. R.; Brown, E. N.; Viswanathan, S., Autonomic healing of polymer composites. *Nature* **2001**, *409* (6822), 794-797.
19. Bekas, D. G.; Tsirka, K.; Baltzis, D.; Paipetis, A. S., Self-healing materials: A review of advances in materials, evaluation, characterization and monitoring techniques. *Composites Part B: Engineering* **2016**, *87*, 92-119.
20. Döhler, D.; Peterlik, H.; Binder, W. H., A dual crosslinked self-healing system: Supramolecular and covalent network formation of four-arm star polymers. *Polymer* **2015**, *69*, 264-273.
21. Chen, S.; Mahmood, N.; Beiner, M.; Binder, W. H., Self-Healing Materials from V- and H-Shaped Supramolecular Architectures. *Angewandte Chemie International Edition* **2015**, n/a-n/a.
22. Lehn, J.-M., Dynamers: dynamic molecular and supramolecular polymers. *Progress in Polymer Science* **2005**, *30* (8-9), 814-831.
23. Ye, X. J.; Zhang, J.-L.; Zhu, Y.; Rong, M. Z.; Zhang, M. Q.; Song, Y. X.; Zhang, H.-X., Ultrafast Self-Healing of Polymer toward Strength Restoration. *ACS Applied Materials & Interfaces* **2014**, *6* (5), 3661-3670.
24. Guadagno, L.; Vertuccio, L.; Naddeo, C.; Calabrese, E.; Barra, G.; Raimondo, M.; Sorrentino, A.; Binder, W. H.; Michael, P.; Rana, S., Self-healing epoxy nanocomposites via reversible hydrogen bonding. *Composites Part B: Engineering* **2019**, *157*, 1-13.
25. Hong, Y.; Su, M., Multifunctional Self-Healing and Self-Reporting Polymer Composite with Integrated Conductive Microwire Networks. *ACS Applied Materials & Interfaces* **2012**, *4* (7), 3759-3764.
26. Mauldin, T. C.; Leonard, J.; Earl, K.; Lee, J. K.; Kessler, M. R., Modified Rheokinetic Technique to Enhance the Understanding of Microcapsule-Based Self-Healing Polymers. *ACS Applied Materials & Interfaces* **2012**, *4* (3), 1831-1837.
27. Syrett, J. A.; Becer, C. R.; Haddleton, D. M., Self-healing and self-mendable polymers. *Polymer Chemistry* **2010**, *1* (7), 978-987.
28. Pratama, P. A.; Sharifi, M.; Peterson, A. M.; Palmese, G. R., Room Temperature Self-Healing Thermoset Based on the Diels–Alder Reaction. *ACS Applied Materials & Interfaces* **2013**, *5* (23), 12425-12431.
29. Rana, S.; Döhler, D.; Nia, A. S.; Nasir, M.; Wilton, O.; Beiner, M.; Binder, W. H., “Click”-Triggered Self-Healing Graphene Nanocomposites. *Macromolecular Rapid Communications* **2017**, *38* (21).
30. Itoh, S.; Kodama, S.; Kobayashi, M.; Hara, S.; Wada, H.; Kuroda, K.; Shimojima, A., Spontaneous Crack Healing in Nanostructured Silica-Based Thin Films. *ACS Nano* **2017**, *11* (10), 10289-10294.
31. Burattini, S.; Greenland, B. W.; Merino, D. H.; Weng, W.; Seppala, J.; Colquhoun, H. M.; Hayes, W.; Mackay, M. E.; Hamley, I. W.; Rowan, S. J., A Healable Supramolecular Polymer Blend Based on Aromatic π - π Stacking and Hydrogen-Bonding Interactions. *Journal of the American Chemical Society* **2010**, *132* (34), 12051-12058.
32. Hart, L. R.; Nguyen, N. A.; Harries, J. L.; Mackay, M. E.; Colquhoun, H. M.; Hayes, W., Perylene as an electron-rich moiety in healable, complementary π - π stacked, supramolecular polymer systems. *Polymer* **2015**, *69*, 293-300.
33. Burattini, S.; Colquhoun, H. M.; Fox, J. D.; Friedmann, D.; Greenland, B. W.; Harris, P. J. F.; Hayes, W.; Mackay, M. E.; Rowan, S. J., A self-repairing, supramolecular polymer system: healability as a consequence of donor–acceptor π - π stacking interactions. *Chemical Communications* **2009**, (44), 6717-6719.
34. Descalzo, A. B.; Martínez-Máñez, R.; Sancenón, F.; Hoffmann, K.; Rurack, K., The Supramolecular Chemistry of Organic–Inorganic Hybrid Materials. *Angewandte Chemie International Edition* **2006**, *45* (36), 5924-5948.
35. Burattini, S.; Greenland, B. W.; Hayes, W.; Mackay, M. E.; Rowan, S. J.; Colquhoun, H. M., A Supramolecular Polymer Based on Tweezer-Type π - π Stacking Interactions: Molecular Design for Healability and Enhanced Toughness. *Chemistry of Materials* **2011**, *23* (1), 6-8.

36. Neal, J. A.; Mozhdzhi, D.; Guan, Z., Enhancing Mechanical Performance of a Covalent Self-Healing Material by Sacrificial Noncovalent Bonds. *Journal of the American Chemical Society* **2015**, *137* (14), 4846-4850.
37. Mauldin, T. C.; Kessler, M. R., Self-healing polymers and composites. *International Materials Reviews* **Nov 2010**, *55* (6), 317-346.
38. Blaiszik, B. J.; Caruso, M. M.; McIlroy, D. A.; Moore, J. S.; White, S. R.; Sottos, N. R., Microcapsules filled with reactive solutions for self-healing materials. *Polymer* **2009**, *50* (4), 990-997.
39. Keller, M. W.; White, S. R.; Sottos, N. R., A Self-Healing Poly(Dimethyl Siloxane) Elastomer. *Advanced Functional Materials* **2007**, *17* (14), 2399-2404.
40. Yuan, Y. C.; Rong, M. Z.; Zhang, M. Q., Preparation and characterization of microencapsulated polythiol. *Polymer* **2008**, *49* (10), 2531-2541.
41. Liu, X.; Sheng, X.; Lee, J. K.; Kessler, M. R., Synthesis and Characterization of Melamine-Urea-Formaldehyde Microcapsules Containing ENB-Based Self-Healing Agents. *Macromolecular Materials and Engineering* **2009**, *294* (6-7), 389-395.
42. Cho, S. H.; Andersson, H. M.; White, S. R.; Sottos, N. R.; Braun, P. V., Polydimethylsiloxane-Based Self-Healing Materials. *Advanced Materials* **2006**, *18*, 1521-4095.
43. Wazarkar, K.; Patil, D.; Rane, A.; Balgude, D.; Kathalewar, M.; Sabnis, A., Microencapsulation: an emerging technique in the modern coating industry. *RSC Advances* **2016**, *6* (108), 106964-106979.
44. Yamuna, J.; Siva, T.; Kumari, S. S. S.; Sathiyarayanan, S., A smart poly(aniline-formaldehyde) microcapsule based self-healing anticorrosive coating. *RSC Advances* **2016**, *6* (1), 79-86.
45. Khoee, S.; Kachoei, Z., Design and development of novel reactive amine nanocontainers for a self-healing epoxy adhesive: self-repairing investigation using the lap shear test. *RSC Advances* **2015**, *5* (27), 21023-21032.
46. Koh, E.; Kim, N.-K.; Shin, J.; Kim, Y.-W., Polyurethane microcapsules for self-healing paint coatings. *RSC Advances* **2014**, *4* (31), 16214-16223.
47. Huang, M.; Yang, J., Facile microencapsulation of HDI for self-healing anticorrosion coatings. *Journal of Materials Chemistry* **2011**, *21* (30), 11123-11130.
48. Huang, M.; Zhang, H.; Yang, J., Synthesis of organic silane microcapsules for self-healing corrosion resistant polymer coatings. *Corrosion Science* **2012**, *65*, 561-566.
49. McIlroy, D. A.; Blaiszik, B. J.; Caruso, M. M.; White, S. R.; Moore, J. S.; Sottos, N. R., Microencapsulation of a Reactive Liquid-Phase Amine for Self-Healing Epoxy Composites. *Macromolecules* **2010**, *43* (4), 1855-1859.
50. Xiao, D. S.; Yuan, Y. C.; Rong, M. Z.; Zhang, M. Q., Hollow polymeric microcapsules: Preparation, characterization and application in holding boron trifluoride diethyl etherate. *Polymer* **2009**, *50* (2), 560-568.
51. Shchukin, D. G.; Zheludkevich, M.; Yasakau, K.; Lamaka, S.; Ferreira, M. G. S.; Möhwald, H., Layer-by-Layer Assembled Nanocontainers for Self-Healing Corrosion Protection. *Advanced Materials* **2006**, *18* (13), 1672-1678.
52. Skorb, E. V.; Andreeva, D. V., Layer-by-Layer approaches for formation of smart self-healing materials. *Polymer Chemistry* **2013**, *4* (18), 4834-4845.
53. Yu, X.; Chen, L.; Zhang, M.; Yi, T., Low-molecular-mass gels responding to ultrasound and mechanical stress: towards self-healing materials. *Chemical Society Reviews* **2014**, *43* (15), 5346-5371.
54. Wei, Z.; Yang, J. H.; Zhou, J.; Xu, F.; Zrinyi, M.; Dussault, P. H.; Osada, Y.; Chen, Y. M., Self-healing gels based on constitutional dynamic chemistry and their potential applications. *Chemical Society Reviews* **2014**, *43* (23), 8114-8131.
55. Thakur, V. K.; Kessler, M. R., Self-healing polymer nanocomposite materials: A review. *Polymer* **2015**, *69*, 369-383.

56. Balazs, A. C.; Emrick, T.; Russell, T. P., Nanoparticle Polymer Composites: Where Two Small Worlds Meet. *Science* **2006**, *314* (5802), 1107-1110.
57. Habault, D.; Zhang, H.; Zhao, Y., Light-triggered self-healing and shape-memory polymers. *Chemical Society Reviews* **2013**, *42* (17), 7244-7256.
58. Jordan, J.; Jacob, K. I.; Tannenbaum, R.; Sharaf, M. A.; Jasiuk, I., Experimental trends in polymer nanocomposites—a review. *Materials Science and Engineering: A* **2005**, *393* (1–2), 1-11.
59. Thakur, V. K.; Vennerberg, D.; Madbouly, S. A.; Kessler, M. R., Bio-inspired green surface functionalization of PMMA for multifunctional capacitors. *RSC Advances* **2014**, *4* (13), 6677-6684.
60. Thakur, V. K.; Thakur, M. K.; Raghavan, P.; Kessler, M. R., Progress in Green Polymer Composites from Lignin for Multifunctional Applications: A Review. *ACS Sustainable Chemistry & Engineering* **2014**, *2* (5), 1072-1092.
61. Thakur, V. K.; Kessler, M. R., Synthesis and Characterization of AN-g-SOY for Sustainable Polymer Composites. *ACS Sustainable Chemistry & Engineering* **2014**, *2* (10), 2454-2460.
62. Yan, L.; Dillard, D. A.; West, R. L.; Rubis, K. J.; Gordon, G. V., Strain rate and temperature dependence of a nanoparticle-filled poly(dimethylsiloxane) undergoing shear deformation. *Journal of Polymer Science Part B: Polymer Physics* **2012**, *50* (13), 929-937.
63. Abdullayev, E.; Lvov, Y., Halloysite clay nanotubes as a ceramic "skeleton" for functional biopolymer composites with sustained drug release. *Journal of Materials Chemistry B* **2013**, *1* (23), 2894-2903.
64. Thakur, V. K.; Yan, J.; Lin, M.-F.; Zhi, C.; Golberg, D.; Bando, Y.; Sim, R.; Lee, P. S., Novel polymer nanocomposites from bioinspired green aqueous functionalization of BNNTs. *Polymer Chemistry* **2012**, *3* (4), 962-969.
65. Neikirk, C. C.; Chung, J. W.; Priestley, R. D., Thermomechanical behavior of hydrogen-bond based supramolecular poly(γ -caprolactone)-silica nanocomposites. *RSC Advances* **2013**, *3* (37), 16686-16696.
66. Lin, M.-F.; Thakur, V. K.; Tan, E. J.; Lee, P. S., Dopant induced hollow BaTiO₃ nanostructures for application in high performance capacitors. *Journal of Materials Chemistry* **2011**, *21* (41), 16500-16504.
67. Döhler, D.; Michael, P.; Binder, W., Principles of Self-Healing Polymers. In *Self-Healing Polymers*, Wiley-VCH Verlag GmbH & Co. KGaA: 2013; pp 5-60.
68. Thakur, V. K.; Ding, G.; Ma, J.; Lee, P. S.; Lu, X., Hybrid Materials and Polymer Electrolytes for Electrochromic Device Applications. *Advanced Materials* **2012**, *24* (30), 4071-4096.
69. Xiao, X.; Xie, T.; Cheng, Y.-T., Self-healable graphene polymer composites. *Journal of Materials Chemistry* **2010**, *20* (17), 3508-3514.
70. Li, G.; John, M., A self-healing smart syntactic foam under multiple impacts. *Composites Science and Technology* **2008**, *68* (15–16), 3337-3343.
71. Wu, T.; Chen, B., Autonomous self-healing multiwalled carbon nanotube nanocomposites with piezoresistive effect. *RSC Advances* **2017**, *7* (33), 20422-20429.
72. Guadagno, L.; Sarno, M.; Vietri, U.; Raimondo, M.; Cirillo, C.; Ciambelli, P., Graphene-based structural adhesive to enhance adhesion performance. *RSC Advances* **2015**, *5* (35), 27874-27886.
73. Valentini, L.; Bittolo Bon, S.; Signetti, S.; Pugno, N. M., Graphene-Based Bionic Composites with Multifunctional and Repairing Properties. *ACS Applied Materials & Interfaces* **2016**, *8* (12), 7607-7612.
74. Wu, T.; Chen, B., Synthesis of Multiwalled Carbon Nanotube-Reinforced Polyborosiloxane Nanocomposites with Mechanically Adaptive and Self-Healing Capabilities for Flexible Conductors. *ACS Applied Materials & Interfaces* **2016**, *8* (36), 24071-24078.
75. Wu, S.; Li, J.; Zhang, G.; Yao, Y.; Li, G.; Sun, R.; Wong, C., Ultrafast Self-Healing Nanocomposites via Infrared Laser and Their Application in Flexible Electronics. *ACS Applied Materials & Interfaces* **2017**, *9* (3), 3040-3049.
76. Cordes, D. B.; Lickiss, P. D.; Rataboul, F., Recent Developments in the Chemistry of Cubic Polyhedral Oligosilsesquioxanes. *Chemical Reviews* **2010**, *110* (4), 2081-2173.

77. Alvarado-Tenorio, B.; Romo-Urbe, A.; Mather, P. T., Microstructure and Phase Behavior of POSS/PCL Shape Memory Nanocomposites. *Macromolecules* **2011**, *44* (14), 5682-5692.
78. Su, X.; Guang, S.; Xu, H.; Liu, X.; Li, S.; Wang, X.; Deng, Y.; Wang, P., Controllable Preparation and Optical Limiting Properties of POSS-Based Functional Hybrid Nanocomposites with Different Molecular Architectures. *Macromolecules* **2009**, *42* (22), 8969-8976.
79. Leu, C.-M.; Chang, Y.-T.; Wei, K.-H., Synthesis and Dielectric Properties of Polyimide-Tethered Polyhedral Oligomeric Silsesquioxane (POSS) Nanocomposites via POSS-diamine. *Macromolecules* **2003**, *36* (24), 9122-9127.
80. Markovic, E.; Clarke, S.; Matison, J.; Simon, G. P., Synthesis of POSS-Methyl Methacrylate-Based Cross-Linked Hybrid Materials. *Macromolecules* **2008**, *41* (5), 1685-1692.
81. Joshi, M.; Butola, B. S.; Simon, G.; Kukaleva, N., Rheological and Viscoelastic Behavior of HDPE/Octamethyl-POSS Nanocomposites. *Macromolecules* **2006**, *39* (5), 1839-1849.
82. Xu, Z.; Zhao, Y.; Wang, X.; Lin, T., A thermally healable polyhedral oligomeric silsesquioxane (POSS) nanocomposite based on Diels-Alder chemistry. *Chemical Communications* **2013**, *49* (60), 6755-6757.
83. Namvari, M.; Du, L.; Stadler, F. J., Graphene oxide-based silsesquioxane-crosslinked networks - synthesis and rheological behavior. *RSC Advances* **2017**, *7* (35), 21531-21540.
84. Zhang, M.; Yan, H.; Yuan, L.; Liu, C., Effect of functionalized graphene oxide with hyperbranched POSS polymer on mechanical and dielectric properties of cyanate ester composites. *RSC Advances* **2016**, *6* (45), 38887-38896.
85. Zong, P.; Fu, J.; Chen, L.; Yin, J.; Dong, X.; Yuan, S.; Shi, L.; Deng, W., Effect of aminopropylisobutyl polyhedral oligomeric silsesquioxane functionalized graphene on the thermal conductivity and electrical insulation properties of epoxy composites. *RSC Advances* **2016**, *6* (13), 10498-10506.
86. Li, S.; Qiu, S.; Yu, B.; Tang, G.; Xing, W.; Hu, Y., POSS-functionalized polyphosphazene nanotube: preparation and effective reinforcement on UV-curable epoxy acrylate nanocomposite coatings. *RSC Advances* **2016**, *6* (4), 3025-3031.
87. Yari, H.; Mohseni, M.; Messori, M., A scratch resistant yet healable automotive clearcoat containing hyperbranched polymer and POSS nanostructures. *RSC Advances* **2016**, *6* (79), 76028-76041.
88. Du, Y.; Yu, M.; Chen, X.; Ma, P. X.; Lei, B., Development of Biodegradable Poly(citrate)-Polyhedral Oligomeric Silsesquioxanes Hybrid Elastomers with High Mechanical Properties and Osteogenic Differentiation Activity. *ACS Applied Materials & Interfaces* **2016**, *8* (5), 3079-3091.
89. Appel, W. P. J.; Portale, G.; Wisse, E.; Dankers, P. Y. W.; Meijer, E. W., Aggregation of Ureido-Pyrimidinone Supramolecular Thermoplastic Elastomers into Nanofibers: A Kinetic Analysis. *Macromolecules* **2011**, *44* (17), 6776-6784.
90. Wang, Z.; Pinnavaia, T. J., Nanolayer Reinforcement of Elastomeric Polyurethane. *Chemistry of Materials* **1998**, *10* (12), 3769-3771.
91. López-Manchado, M. A.; Herrero, B.; Arroyo, M., Preparation and characterization of organoclay nanocomposites based on natural rubber. *Polymer International* **2003**, *52* (7), 1070-1077.
92. Lau, K.-t.; Gu, C.; Hui, D., A critical review on nanotube and nanotube/nanoclay related polymer composite materials. *Composites Part B: Engineering* **2006**, *37* (6), 425-436.
93. Isik, I.; Yilmazer, U.; Bayram, G., Impact modified epoxy/montmorillonite nanocomposites: synthesis and characterization. *Polymer* **2003**, *44* (20), 6371-6377.
94. Kim, B. C.; Park, S. W.; Lee, D. G., Fracture toughness of the nano-particle reinforced epoxy composite. *Composite Structures* **2008**, *86* (1-3), 69-77.
95. Liu, W.; Hoa, S. V.; Pugh, M., Organoclay-modified high performance epoxy nanocomposites. *Composites Science and Technology* **2005**, *65* (2), 307-316.

96. Nazem Salimi, M.; Torabi Merajin, M.; Besharati Givi, M. K., Enhanced mechanical properties of multifunctional multiscale glass/carbon/epoxy composite reinforced with carbon nanotubes and simultaneous carbon nanotubes/nanoclays. *Journal of Composite Materials* **2016**.
97. Ha, S. R.; Rhee, K. Y.; Kim, H. C.; Kim, J. T., Fracture performance of clay/epoxy nanocomposites with clay surface-modified using 3-aminopropyltriethoxysilane. *Colloids and Surfaces A: Physicochemical and Engineering Aspects* **2008**, 313–314, 112-115.
98. Qi, B.; Zhang, Q. X.; Bannister, M.; Mai, Y. W., Investigation of the mechanical properties of DGEBA-based epoxy resin with nanoclay additives. *Composite Structures* **2006**, 75 (1–4), 514-519.
99. Lau, K.-t.; Lu, M.; Qi, J.-Q.; Zhao, D.-D.; Cheung, H.-y.; Lam, C.-K.; Li, H.-L., Cobalt hydroxide colloidal particles precipitation on nanoclay layers for the formation of novel nanocomposites of carbon nanotubes/nanoclay. *Composites Science and Technology* **2006**, 66 (3–4), 450-458.
100. Keurentjes, J. J. B.; Fu, J.; Terpstra, I. R.; Garcia, J. M.; van den Ackerveken, G.; Snoek, L. B.; Peeters, A. J. M.; Vreugdenhil, D.; Koornneef, M.; Jansen, R. C., Regulatory network construction in *Arabidopsis* by using genome-wide gene expression quantitative trait loci. *Proceedings of the National Academy of Sciences* **2007**, 104 (5), 1708-1713.
101. Sankaran, K.; Manoharan, P.; Chattopadhyay, S.; Nair, S.; Govindan, U.; Arayambath, S.; Nando, G. B., Effect of hybridization of organoclay with carbon black on the transport, mechanical, and adhesion properties of nanocomposites based on bromobutyl/epoxidized natural rubber blends. *RSC Advances* **2016**, 6 (40), 33723-33732.
102. Nelson, J. K., Dielectric polymer nanocomposites. **2010**.
103. Lan, T.; Kaviratna, P. D.; Pinnavaia, T. J., Mechanism of Clay Tactoid Exfoliation in Epoxy-Clay Nanocomposites. *Chemistry of Materials* **1995**, 7 (11), 2144-2150.
104. Brown, J. M.; Curliss, D.; Vaia, R. A., Thermoset-Layered Silicate Nanocomposites. Quaternary Ammonium Montmorillonite with Primary Diamine Cured Epoxies. *Chemistry of Materials* **2000**, 12 (11), 3376-3384.
105. Kornmann, X.; Lindberg, H.; Berglund, L. A., Synthesis of epoxy–clay nanocomposites: influence of the nature of the clay on structure. *Polymer* **2001**, 42 (4), 1303-1310.
106. Kornmann, X.; Lindberg, H.; Berglund, L. A., Synthesis of epoxy–clay nanocomposites. Influence of the nature of the curing agent on structure. *Polymer* **2001**, 42 (10), 4493-4499.
107. Okada, A.; Usuki, A., The chemistry of polymer-clay hybrids. *Materials Science and Engineering: C* **1995**, 3 (2), 109-115.
108. Rajini, N.; Jappes, J. W.; Rajakarunakaran, S.; Jeyaraj, P., Dynamic mechanical analysis and free vibration behavior in chemical modifications of coconut sheath/nano-clay reinforced hybrid polyester composite. *Journal of Composite Materials* **2013**, 47 (24), 3105-3121.
109. Velmurugan, R.; Mohan, T. P., Room temperature processing of epoxy-clay nanocomposites. *Journal of Materials Science* **2004**, 39 (24), 7333-7339.
110. Bitinis, N.; Hernandez, M.; Verdejo, R.; Kenny, J. M.; Lopez-Manchado, M. A., Recent Advances in Clay/Polymer Nanocomposites. *Advanced Materials* **2011**, 23 (44), 5229-5236.
111. Thellen, C.; Orroth, C.; Froio, D.; Ziegler, D.; Lucciarini, J.; Farrell, R.; D'Souza, N. A.; Ratto, J. A., Influence of montmorillonite layered silicate on plasticized poly(l-lactide) blown films. *Polymer* **2005**, 46 (25), 11716-11727.
112. Bharadwaj, R. K., Modeling the Barrier Properties of Polymer-Layered Silicate Nanocomposites. *Macromolecules* **2001**, 34 (26), 9189-9192.
113. Bhattacharya, M.; Biswas, S.; Bhowmick, A. K., Permeation characteristics and modeling of barrier properties of multifunctional rubber nanocomposites. *Polymer* **2011**, 52 (7), 1562-1576.
114. Lagaron, J. M.; Lopez-Rubio, A., Nanotechnology for bioplastics: opportunities, challenges and strategies. *Trends in Food Science & Technology* **2011**, 22 (11), 611-617.

115. Fukushima, K.; Abbate, C.; Tabuani, D.; Gennari, M.; Camino, G., Biodegradation of poly(lactic acid) and its nanocomposites. *Polymer Degradation and Stability* **2009**, *94* (10), 1646-1655.
116. Alix, S.; Follain, N.; Tenn, N.; Alexandre, B.; Bourbigot, S.; Soulestin, J.; Marais, S., Effect of Highly Exfoliated and Oriented Organoclays on the Barrier Properties of Polyamide 6 Based Nanocomposites. *The Journal of Physical Chemistry C* **2012**, *116* (8), 4937-4947.
117. Mohammadalipour, M.; Masoomi, M.; Ahmadi, M.; Safi, S., Interfacial shear strength characterization of GMA-grafted UHMWPE fiber/epoxy/nano clay hybrid nanocomposite materials. *RSC Advances* **2016**, *6* (48), 41793-41799.
118. Tambach, T. J.; Bolhuis, P. G.; Smit, B., A Molecular Mechanism of Hysteresis in Clay Swelling. *Angewandte Chemie International Edition* **2004**, *43* (20), 2650-2652.
119. Hanczyc, M. M.; Fujikawa, S. M.; Szostak, J. W., Experimental Models of Primitive Cellular Compartments: Encapsulation, Growth, and Division. *Science* **2003**, *302* (5645), 618-622.
120. Hensen, E. J. M.; Smit, B., Why Clays Swell. *The Journal of Physical Chemistry B* **2002**, *106* (49), 12664-12667.
121. An introduction to clay colloid chemistry. By H van Olphen. Interscience Publishers, Div. of John Wiley & Sons, 605 Third Ave., New York 16, N. Y, 1963. xvi + 301 pp. 15.5 × 23 cm. Price \$10. *Journal of Pharmaceutical Sciences* **1964**, *53* (2), 230-230.
122. Sinha Ray, S.; Okamoto, M., Polymer/layered silicate nanocomposites: a review from preparation to processing. *Progress in Polymer Science* **2003**, *28* (11), 1539-1641.
123. Lagaly, G., In Development of Ionic Polymers. **1987**, *2*, 77-140.
124. Wypych, G., Handbook of Fillers. *ChemTec Publishing* **1999**, (2nd ed.).
125. Heinz, H.; Vaia, R. A.; Krishnamoorti, R.; Farmer, B. L., Self-Assembly of Alkylammonium Chains on Montmorillonite: Effect of Chain Length, Head Group Structure, and Cation Exchange Capacity. *Chemistry of Materials* **2007**, *19* (1), 59-68.
126. Makaremi, M.; Jordan, K. D.; Guthrie, G. D.; Myshakin, E. M., Multiphase Monte Carlo and Molecular Dynamics Simulations of Water and CO₂ Intercalation in Montmorillonite and Beidellite. *The Journal of Physical Chemistry C* **2015**.
127. Li, Y.; Wang, X.; Wang, J., Cation exchange, interlayer spacing, and thermal analysis of Na/Ca-montmorillonite modified with alkaline and alkaline earth metal ions. *J Therm Anal Calorim* **2012**, *110* (3), 1199-1206.
128. Swenson, J.; Smalley, M. V.; Hatharasinghe, H. L. M.; Fragneto, G., Interlayer Structure of a Clay-Polymer-Salt-Water System. *Langmuir* **2001**, *17* (13), 3813-3818.
129. Israelachvili, J. N., *Surf. Sci. Ref.* **1992**, *14*, 109-159.
130. Newman, A. C. D., Chemistry of Clays and Clay Minerals: Mineralogical Society. **1987**.
131. (a) Lagaly, G., Interaction of alkylamines with different types of layered compounds. *Solid State Ionics* **1986**, *22* (1), 43-51; (b) Yoon, K.-b.; Sung, H.-d.; Hwang, Y.-y.; Kyun Noh, S.; Lee, D.-h., Modification of montmorillonite with oligomeric amine derivatives for polymer nanocomposite preparation. *Applied Clay Science* **2007**, *38* (1-2), 1-8.
132. Zhu, J.; Qing, Y.; Wang, T.; Zhu, R.; Wei, J.; Tao, Q.; Yuan, P.; He, H., Preparation and characterization of zwitterionic surfactant-modified montmorillonites. *Journal of Colloid and Interface Science* **2011**, *360* (2), 386-392.
133. Vaia, R. A.; Teukolsky, R. K.; Giannelis, E. P., Interlayer Structure and Molecular Environment of Alkylammonium Layered Silicates. *Chemistry of Materials* **1994**, *6* (7), 1017-1022.
134. Vaia, R. A.; Giannelis, E. P., Polymer Melt Intercalation in Organically-Modified Layered Silicates: Model Predictions and Experiment. *Macromolecules* **1997**, *30* (25), 8000-8009.
135. Vaia, R. A.; Giannelis, E. P., Lattice Model of Polymer Melt Intercalation in Organically-Modified Layered Silicates. *Macromolecules* **1997**, *30* (25), 7990-7999.

136. Triantafillidis, C. S.; LeBaron, P. C.; Pinnavaia, T. J., Homostructured Mixed Inorganic–Organic Ion Clays: A New Approach to Epoxy Polymer–Exfoliated Clay Nanocomposites with a Reduced Organic Modifier Content. *Chemistry of Materials* **2002**, *14* (10), 4088-4095.
137. Osman, M. A.; Seyfang, G.; Suter, U. W., Two-Dimensional Melting of Alkane Monolayers Ionically Bonded to Mica. *The Journal of Physical Chemistry B* **2000**, *104* (18), 4433-4439.
138. Manias, E.; Touny, A.; Wu, L.; Strawhecker, K.; Lu, B.; Chung, T. C., Polypropylene/Montmorillonite Nanocomposites. Review of the Synthetic Routes and Materials Properties. *Chemistry of Materials* **2001**, *13* (10), 3516-3523.
139. Glinel, K.; Laschewsky, A.; Jonas, A. M., Ordered Polyelectrolyte “Multilayers”. 4. Internal Structure of Clay-Based Multilayers. *The Journal of Physical Chemistry B* **2002**, *106* (43), 11246-11252.
140. Zhu, J.; He, H.; Zhu, L.; Wen, X.; Deng, F., Characterization of organic phases in the interlayer of montmorillonite using FTIR and ¹³C NMR. *Journal of Colloid and Interface Science* **2005**, *286* (1), 239-244.
141. Umemura, Y.; Shinohara, E., Formation of Langmuir–Blodgett Films of a Clay and a Water-Soluble Alkylammonium Cation. *Langmuir* **2005**, *21* (10), 4520-4525.
142. Osman, M. A.; Rupp, J. E. P.; Suter, U. W., Gas permeation properties of polyethylene-layered silicate nanocomposites. *Journal of Materials Chemistry* **2005**, *15* (12), 1298-1304.
143. He, H.; Frost, R. L.; Xi, Y. f.; Zhu, J., Raman spectroscopic study of organo-montmorillonites. *Journal of Raman Spectroscopy* **2004**, *35* (4), 316-323.
144. Sagitova, E. A.; Donfack, P.; Prokhorov, K. A.; Nikolaeva, G. Y.; Gerasin, V. A.; Merekalova, N. D.; Materny, A.; Antipov, E. M.; Pashinin, P. P., Raman Spectroscopic Characterization of the Interlayer Structure of Na⁺-Montmorillonite Clay Modified by Ditetradecyl Dimethyl Ammonium Bromide. *The Journal of Physical Chemistry B* **2009**, *113* (21), 7482-7490.
145. Munusamy, T.; Ya-Ting, J.; Jiunn-Fwu, L., Enhanced adsorption of inorganic and organic pollutants by amine modified sodium montmorillonite nanosheets. *RSC Advances* **2015**, *5* (26), 20583-20594.
146. Simons, R.; Qiao, G. G.; Powell, C. E.; Bateman, S. A., Effect of Surfactant Architecture on the Properties of Polystyrene–Montmorillonite Nanocomposites. *Langmuir* **2010**, *26* (11), 9023-9031.
147. Lawal, I. A.; Moodley, B., Synthesis, characterisation and application of imidazolium based ionic liquid modified montmorillonite sorbents for the removal of amaranth dye. *RSC Advances* **2015**, *5* (76), 61913-61924.
148. Ahrens, S.; Peritz, A.; Strassner, T., Tunable Aryl Alkyl Ionic Liquids (TAAILs): The Next Generation of Ionic Liquids. *Angewandte Chemie International Edition* **2009**, *48* (42), 7908-7910.
149. Qian, Y.; Liu, W.; Park, Y. T.; Lindsay, C. I.; Camargo, R.; Macosko, C. W.; Stein, A., Modification with tertiary amine catalysts improves vermiculite dispersion in polyurethane via in situ intercalative polymerization. *Polymer* **2012**, *53* (22), 5060-5068.
150. Metz, S.; Anderson, R. L.; Geatches, D. L.; Suter, J. L.; Lines, R.; Greenwell, H. C., Understanding the Swelling Behavior of Modified Nanoclay Filler Particles in Water and Ethanol. *The Journal of Physical Chemistry C* **2015**, *119* (22), 12625-12642.
151. Sinha Ray, S.; Yamada, K.; Okamoto, M.; Ueda, K., Polylactide-Layered Silicate Nanocomposite: A Novel Biodegradable Material. *Nano Letters* **2002**, *2* (10), 1093-1096.
152. (a) Helmreich, R. F., Epoxy Resins. Their Applications and Technology. *Journal of the American Chemical Society* **1958**, *80* (4), 1012-1012; (b) Jin, F.-L.; Li, X.; Park, S.-J., Synthesis and application of epoxy resins: A review. *Journal of Industrial and Engineering Chemistry* **2015**, *29*, 1-11.
153. Langemeier, P.; Scheuer, C., Big challenges: the role of resin in wind turbine rotor blade development. *Reinforced Plastics* **2010**, *54* (1), 36-39.
154. (a) Raimondo, M.; Russo, S.; Guadagno, L.; Longo, P.; Chirico, S.; Mariconda, A.; Bonnaud, L.; Murariu, O.; Dubois, P., Effect of incorporation of POSS compounds and phosphorous hardeners on

- thermal and fire resistance of nanofilled aeronautic resins. *RSC Advances* **2015**, *5* (15), 10974-10986; (b) Yeh, J.-M.; Huang, H.-Y.; Chen, C.-L.; Su, W.-F.; Yu, Y.-H., Siloxane-modified epoxy resin–clay nanocomposite coatings with advanced anticorrosive properties prepared by a solution dispersion approach. *Surface and Coatings Technology* **2006**, *200* (8), 2753-2763; (c) Cheng, Q. F.; Wang, J. P.; Wen, J. J.; Liu, C. H.; Jiang, K. L.; Li, Q. Q.; Fan, S. S., Carbon nanotube/epoxy composites fabricated by resin transfer molding. *Carbon* **2010**, *48* (1), 260-266.
155. Wang, L.; Tan, W., Multicolor FRET Silica Nanoparticles by Single Wavelength Excitation. *Nano Letters* **2006**, *6* (1), 84-88.
156. Mark, J. E., Some Interesting Things about Polysiloxanes. *Accounts of Chemical Research* **2004**, *37* (12), 946-953.
157. Brick, C. M.; Ouchi, Y.; Chujo, Y.; Laine, R. M., Robust Polyaromatic Octasilsesquioxanes from Polybromophenylsilsesquioxanes, BrxOPS, via Suzuki Coupling. *Macromolecules* **2005**, *38* (11), 4661-4665.
158. Pescarmona, Paolo P.; van der Waal, Jan C.; Maschmeyer, T., Fast, High-Yielding Syntheses of Silsesquioxanes Using Acetonitrile as a Reactive Solvent. *European Journal of Inorganic Chemistry* **2004**, *2004* (5), 978-983.
159. Laine, R. M.; Roll, M. F., Polyhedral Phenylsilsesquioxanes. *Macromolecules* **2011**, *44* (5), 1073-1109.
160. Burns, A.; Ow, H.; Wiesner, U., Fluorescent core-shell silica nanoparticles: towards "Lab on a Particle" architectures for nanobiotechnology. *Chemical Society Reviews* **2006**, *35* (11), 1028-1042.
161. Laine, R. M., Nanobuilding blocks based on the [OSiO_{1.5}] (x = 6, 8, 10) octasilsesquioxanes. *Journal of Materials Chemistry* **2005**, *15* (35-36), 3725-3744.
162. J. Feher, F.; Terroba, R.; W. Ziller, J., Base-catalyzed cleavage and homologation of polyhedral oligosilsesquioxanes. *Chemical Communications* **1999**, (21), 2153-2154.
163. Quadrelli, E. A.; Basset, J.-M., On silsesquioxanes' accuracy as molecular models for silica-grafted complexes in heterogeneous catalysis. *Coordination Chemistry Reviews* **2010**, *254* (5-6), 707-728.
164. Ervithayasuporn, V.; Tomeechai, T.; Takeda, N.; Unno, M.; Chaiyanurakkul, A.; Hamkool, R.; Osotchan, T., Synthesis and Characterization of Octakis(3-propyl ethanethioate)octasilsesquioxane. *Organometallics* **2011**, *30* (17), 4475-4478.
165. Mya, K. Y.; Gose, H. B.; Pretsch, T.; Bothe, M.; He, C., Star-shaped POSS-polycaprolactone polyurethanes and their shape memory performance. *Journal of Materials Chemistry* **2011**, *21* (13), 4827-4836.
166. Wang, X.; Ervithayasuporn, V.; Zhang, Y.; Kawakami, Y., Reversible self-assembly of dendrimer based on polyhedral oligomeric silsesquioxanes (POSS). *Chemical Communications* **2011**, *47* (4), 1282-1284.
167. Wu, S.; Hayakawa, T.; Kikuchi, R.; Grunzinger, S. J.; Kakimoto, M.-a.; Oikawa, H., Synthesis and Characterization of Semiaromatic Polyimides Containing POSS in Main Chain Derived from Double-Decker-Shaped Silsesquioxane. *Macromolecules* **2007**, *40* (16), 5698-5705.
168. Lin, H.-C.; Kuo, S.-W.; Huang, C.-F.; Chang, F.-C., Thermal and Surface Properties of Phenolic Nanocomposites Containing Octaphenol Polyhedral Oligomeric Silsesquioxane. *Macromolecular Rapid Communications* **2006**, *27* (7), 537-541.
169. Ghanbari, H.; Cousins, B. G.; Seifalian, A. M., A Nanocage for Nanomedicine: Polyhedral Oligomeric Silsesquioxane (POSS). *Macromolecular Rapid Communications* **2011**, *32* (14), 1032-1046.
170. Ervithayasuporn, V.; Wang, X.; Kawakami, Y., Synthesis and characterization of highly pure azido-functionalized polyhedral oligomeric silsesquioxanes (POSS). *Chemical Communications* **2009**, (34), 5130-5132.

171. Roll, M. F.; Kampf, J. W.; Laine, R. M., Crystalline Hybrid Polyphenylene Macromolecules from Octaalkynylsilsesquioxanes, Crystal Structures, and a Potential Route to 3-D Graphenes. *Macromolecules* **2011**, *44* (9), 3425-3435.
172. Kuo, S.-W.; Chang, F.-C., POSS related polymer nanocomposites. *Progress in Polymer Science* **2011**, *36* (12), 1649-1696.
173. Xue, Y.; Wang, H.; Yu, D.; Feng, L.; Dai, L.; Wang, X.; Lin, T., Superhydrophobic electrospun POSS-PMMA copolymer fibres with highly ordered nanofibrillar and surface structures. *Chemical Communications* **2009**, (42), 6418-6420.
174. Xue, Y.; Wang, H.; Zhao, Y.; Dai, L.; Feng, L.; Wang, X.; Lin, T., Magnetic Liquid Marbles: A "Precise" Miniature Reactor. *Advanced Materials* **2010**, *22* (43), 4814-4818.
175. Yadav, S. K.; Mahapatra, S. S.; Yoo, H. J.; Cho, J. W., Synthesis of multi-walled carbon nanotube/polyhedral oligomeric silsesquioxane nanohybrid by utilizing click chemistry. *Nanoscale Research Letters* **2011**, *6* (1), 122.
176. (a) Alves, F.; Scholder, P.; Nischang, I., Conceptual Design of Large Surface Area Porous Polymeric Hybrid Media Based on Polyhedral Oligomeric Silsesquioxane Precursors: Preparation, Tailoring of Porous Properties, and Internal Surface Functionalization. *ACS Applied Materials & Interfaces* **2013**, *5* (7), 2517-2526; (b) Edwards, S. J.; Valkenier, H.; Busschaert, N.; Gale, P. A.; Davis, A. P., High-Affinity Anion Binding by Steroidal Squaramide Receptors. *Angewandte Chemie International Edition* **2015**, *54* (15), 4592-4596.
177. Alves, F.; Nischang, I., A simple approach to hybrid inorganic-organic step-growth hydrogels with scalable control of physicochemical properties and biodegradability. *Polymer Chemistry* **2015**, *6* (12), 2183-2187.
178. Xue, Y.; Liu, Y.; Lu, F.; Qu, J.; Chen, H.; Dai, L., Functionalization of Graphene Oxide with Polyhedral Oligomeric Silsesquioxane (POSS) for Multifunctional Applications. *The Journal of Physical Chemistry Letters* **2012**, *3* (12), 1607-1612.
179. Chen X1, D. M., Ono K, Mal A, Shen H, Nutt SR, Sheran K, Wudl F., A thermally re-mendable cross-linked polymeric material. *Science* **2002**, *1* (295), 1698-702.
180. Lee, M. W.; Hu, X.; Li, L.; Yue, C. Y.; Tam, K. C.; Cheong, L. Y., PP/LCP composites: effects of shear flow, extensional flow and nanofillers. *Composites Science and Technology* **2003**, *63* (13), 1921-1929.
181. Zhou, S.; Wu, L.; Sun, J.; Shen, W., The change of the properties of acrylic-based polyurethane via addition of nano-silica. *Progress in Organic Coatings* **2002**, *45* (1), 33-42.
182. Guo, H.; Meador, M. A. B.; McCorkle, L.; Quade, D. J.; Guo, J.; Hamilton, B.; Cakmak, M.; Sprowl, G., Polyimide Aerogels Cross-Linked through Amine Functionalized Polyoligomeric Silsesquioxane. *ACS Applied Materials & Interfaces* **2011**, *3* (2), 546-552.
183. Zhang, Q.; He, H.; Xi, K.; Huang, X.; Yu, X.; Jia, X., Synthesis of N-Phenylaminomethyl POSS and Its Utilization in Polyurethane. *Macromolecules* **2011**, *44* (3), 550-557.
184. Dasari, A.; Yu, Z.-Z.; Mai, Y.-W.; Cai, G.; Song, H., Roles of graphite oxide, clay and POSS during the combustion of polyamide 6. *Polymer* **2009**, *50* (6), 1577-1587.
185. Kim, K.-M.; Ouchi, Y.; Chujo, Y., Synthesis of organic-inorganic star-shaped polyoxazolines using octafunctional silsesquioxane as an initiator. *Polymer Bulletin* **2003**, *49* (5), 341-348.
186. Kim, K.-M.; Keum, D.-K.; Chujo, Y., Organic-Inorganic Polymer Hybrids Using Polyoxazoline Initiated by Functionalized Silsesquioxane. *Macromolecules* **2003**, *36* (3), 867-875.
187. Zhao, C.; Yang, X.; Wu, X.; Liu, X.; Wang, X.; Lu, L., Preparation and characterization of poly(methyl methacrylate) nanocomposites containing octavinyl polyhedral oligomeric silsesquioxane. *Polymer Bulletin* **2008**, *60* (4), 495-505.
188. Fattahi, P.; Borhan, A.; Abidian, M. R., Microencapsulation of Chemotherapeutics into Monodisperse and Tunable Biodegradable Polymers via Electrified Liquid Jets: Control of Size, Shape, and Drug Release. *Adv. Mater.* **2013**, *25* (33), 4555-4560.

189. She, Z.; Wang, C.; Li, J.; Sukhorukov, G. B.; Antipina, M. N., Encapsulation of Basic Fibroblast Growth Factor by Polyelectrolyte Multilayer Microcapsules and Its Controlled Release for Enhancing Cell Proliferation. *Biomacromolecules* **2012**, *13* (7), 2174-2180.
190. Amali, A. J.; Sharma, B.; Rana, R. K., Assembly of Multiple Components in a Hybrid Microcapsule: Designing a Magnetically Separable Pd Catalyst for Selective Hydrogenation. *Chem. Eur. J.* **2014**, *20* (38), 12239-12244.
191. Horecha, M.; Kaul, E.; Horechyy, A.; Stamm, M., Polymer microcapsules loaded with Ag nanocatalyst as active microreactors. *Journal of Materials Chemistry A* **2014**, *2* (20), 7431-7438.
192. Augustin, M. A.; Hemar, Y., Nano- and micro-structured assemblies for encapsulation of food ingredients. *Chemical Society Reviews* **2009**, *38* (4), 902-912.
193. Dinsmore, A. D.; Hsu, M. F.; Nikolaidis, M. G.; Marquez, M.; Bausch, A. R.; Weitz, D. A., Colloidosomes: Selectively Permeable Capsules Composed of Colloidal Particles. *Science* **2002**, *298* (5595), 1006-1009.
194. Kim, S.-H.; Nam, J.; Kim, J. W.; Kim, D.-H.; Han, S.-H.; Weitz, D. A., Formation of polymersomes with double bilayers templated by quadruple emulsions. *Lab on a Chip* **2013**, *13* (7), 1351-1356.
195. Shum, H. C.; Zhao, Y.-j.; Kim, S.-H.; Weitz, D. A., Multicompartment Polymersomes from Double Emulsions. *Angewandte Chemie International Edition* **2011**, *50* (7), 1648-1651.
196. Henderson, I. M.; Paxton, W. F., Salt, Shake, Fuse—Giant Hybrid Polymer/Lipid Vesicles through Mechanically Activated Fusion. *Angewandte Chemie International Edition* **2014**, *53* (13), 3372-3376.
197. Ma, Y.; Dong, W.-F.; Hempenius, M. A.; Mohwald, H.; Julius Vancso, G., Redox-controlled molecular permeability of composite-wall microcapsules. *Nat Mater* **2006**, *5* (9), 724-729.
198. Kaufman, G.; Boltyanskiy, R.; Nejati, S.; Thiam, A. R.; Loewenberg, M.; Dufresne, E. R.; Osuji, C. O., Single-step microfluidic fabrication of soft monodisperse polyelectrolyte microcapsules by interfacial complexation. *Lab on a Chip* **2014**, *14* (18), 3494-3497.
199. De Cock, L. J.; De Koker, S.; De Geest, B. G.; Grooten, J.; Vervaet, C.; Remon, J. P.; Sukhorukov, G. B.; Antipina, M. N., Polymeric Multilayer Capsules in Drug Delivery. *Angewandte Chemie International Edition* **2010**, *49* (39), 6954-6973.
200. De Koker, S.; Hoogenboom, R.; De Geest, B. G., Polymeric multilayer capsules for drug delivery. *Chemical Society Reviews* **2012**, *41* (7), 2867-2884.
201. Windbergs, M.; Zhao, Y.; Heyman, J.; Weitz, D. A., Biodegradable Core–Shell Carriers for Simultaneous Encapsulation of Synergistic Actives. *Journal of the American Chemical Society* **2013**, *135* (21), 7933-7937.
202. Cui, J.; van Koeveden, M. P.; Müllner, M.; Kempe, K.; Caruso, F., Emerging methods for the fabrication of polymer capsules. *Advances in Colloid and Interface Science* **2014**, *207*, 14-31.
203. Mak, W. C.; Cheung, K. Y.; Trau, D., Influence of Different Polyelectrolytes on Layer-by-Layer Microcapsule Properties: Encapsulation Efficiency and Colloidal and Temperature Stability. *Chemistry of Materials* **2008**, *20* (17), 5475-5484.
204. Parker, R. M.; Zhang, J.; Zheng, Y.; Coulston, R. J.; Smith, C. A.; Salmon, A. R.; Yu, Z.; Scherman, O. A.; Abell, C., Electrostatically Directed Self-Assembly of Ultrathin Supramolecular Polymer Microcapsules. *Advanced Functional Materials* **2015**, *25* (26), 4091-4100.
205. Jyothi, N. V. N.; Prasanna, P. M.; Sakarkar, S. N.; Prabha, K. S.; Ramaiah, P. S.; Srawan, G. Y., Microencapsulation techniques, factors influencing encapsulation efficiency. *Journal of Microencapsulation* **2010**, *27* (3), 187-197.
206. Andrade, B.; Song, Z.; Li, J.; Zimmerman, S. C.; Cheng, J.; Moore, J. S.; Harris, K.; Katz, J. S., New Frontiers for Encapsulation in the Chemical Industry. *ACS Applied Materials & Interfaces* **2015**, *7* (12), 6359-6368.
207. Sindoro, M.; Jee, A.-Y.; Granick, S., Shape-selected colloidal MOF crystals for aqueous use. *Chemical Communications* **2013**, *49* (83), 9576-9578.

208. Sindoro, M.; Yanai, N.; Jee, A.-Y.; Granick, S., Colloidal-Sized Metal–Organic Frameworks: Synthesis and Applications. *Accounts of Chemical Research* **2014**, *47* (2), 459-469.
209. Sun, C.-Y.; Qin, C.; Wang, X.-L.; Su, Z.-M., Metal-organic frameworks as potential drug delivery systems. *Expert Opinion on Drug Delivery* **2012**, *10* (1), 89-101.
210. Hartmann, M., Ordered Mesoporous Materials for Bioadsorption and Biocatalysis. *Chemistry of Materials* **2005**, *17* (18), 4577-4593.
211. Tarn, D.; Ashley, C. E.; Xue, M.; Carnes, E. C.; Zink, J. I.; Brinker, C. J., Mesoporous Silica Nanoparticle Nanocarriers: Biofunctionality and Biocompatibility. *Accounts of Chemical Research* **2013**, *46* (3), 792-801.
212. Pluth, M. D.; Raymond, K. N., Reversible guest exchange mechanisms in supramolecular host-guest assemblies. *Chemical Society Reviews* **2007**, *36* (2), 161-171.
213. (a) Teixeira, R. F. A.; van den Berg, O.; Nguyen, L.-T. T.; Fehér, K.; Du Prez, F. E., Microencapsulation of Active Ingredients Using PDMS as Shell Material. *Macromolecules* **2014**, *47* (23), 8231-8237; (b) Shulkin, A.; Stöver, H. D. H., Photostimulated Phase Separation Encapsulation. *Macromolecules* **2003**, *36* (26), 9836-9839.
214. Bon, S. A. F.; Chen, T., Pickering Stabilization as a Tool in the Fabrication of Complex Nanopatterned Silica Microcapsules. *Langmuir* **2007**, *23* (19), 9527-9530.
215. Esser-Kahn, A. P.; Odom, S. A.; Sottos, N. R.; White, S. R.; Moore, J. S., Triggered Release from Polymer Capsules. *Macromolecules* **2011**, *44* (14), 5539-5553.
216. Poe, S. L.; Kobašlija, M.; McQuade, D. T., Mechanism and Application of a Microcapsule Enabled Multicatalyst Reaction. *Journal of the American Chemical Society* **2007**, *129* (29), 9216-9221.
217. Stadler, B.; Price, A. D.; Chandrawati, R.; Hosta-Rigau, L.; Zelikin, A. N.; Caruso, F., Polymer hydrogel capsules: en route toward synthetic cellular systems. *Nanoscale* **2009**, *1* (1), 68-73.
218. (a) Benichou, A.; Aserin, A.; Garti, N., Double emulsions stabilized with hybrids of natural polymers for entrapment and slow release of active matters. *Advances in Colloid and Interface Science* **2004**, *108–109*, 29-41; (b) Jana, N. R.; Gearheart, L.; Murphy, C. J., Seed-Mediated Growth Approach for Shape-Controlled Synthesis of Spheroidal and Rod-like Gold Nanoparticles Using a Surfactant Template. *Adv. Mater.* **2001**, *13* (18), 1389-1393.
219. Alexandridis, P., Amphiphilic copolymers and their applications. *Current Opinion in Colloid & Interface Science* **1996**, *1* (4), 490-501.
220. Fickert, J.; Makowski, M.; Kappl, M.; Landfester, K.; Crespy, D., Efficient Encapsulation of Self-Healing Agents in Polymer Nanocontainers Functionalized by Orthogonal Reactions. *Macromolecules* **2012**, *45* (16), 6324-6332.
221. (a) Muñoz-Espí, R.; Qi, Y.; Lieberwirth, I.; Gómez, C. M.; Wegner, G., Surface-Functionalized Latex Particles as Controlling Agents for the Mineralization of Zinc Oxide in Aqueous Medium. *Chem. Eur. J.* **2006**, *12* (1), 118-129; (b) Herrmann, C.; Bannwarth, M. B.; Landfester, K.; Crespy, D., Re-dispersible Anisotropic and Structured Nanoparticles: Formation and Their Subsequent Shape Change. *Macromolecular Chemistry and Physics* **2012**, *213* (8), 829-838.
222. Bathfield, M.; Graillat, C.; Hamaide, T., Encapsulation of High Biocompatible Hydrophobe Contents in Nonionic Nanoparticles by Miniemulsion Polymerization of Vinyl Acetate or Styrene: Influence of the Hydrophobe Component on the Polymerization. *Macromolecular Chemistry and Physics* **2005**, *206* (22), 2284-2291.
223. Li, H.; Li, P.; Yang, Y.; Qi, W.; Sun, H.; Wu, L., Incorporation of Polyoxometalates Into Polystyrene Latex by Supramolecular Encapsulation and Miniemulsion Polymerization. *Macromolecular Rapid Communications* **2008**, *29* (5), 431-436.
224. Crespy, D.; Stark, M.; Hoffmann-Richter, C.; Ziener, U.; Landfester, K., Polymeric Nanoreactors for Hydrophilic Reagents Synthesized by Interfacial Polycondensation on Miniemulsion Droplets. *Macromolecules* **2007**, *40* (9), 3122-3135.

225. Wang, Y.; Jiang, G.; Zhang, M.; Wang, L.; Wang, R.; Sun, X., Facile one-pot preparation of novel shell cross-linked nanocapsules: inverse miniemulsion RAFT polymerization as an alternative approach. *Soft Matter* **2011**, *7* (11), 5348-5352.
226. Torini, L.; Argillier, J. F.; Zydowicz, N., Interfacial Polycondensation Encapsulation in Miniemulsion. *Macromolecules* **2005**, *38* (8), 3225-3236.
227. Bechthold, N.; Tiarks, F.; Willert, M.; Landfester, K.; Antonietti, M., Miniemulsion polymerization: applications and new materials. *Macromol. Symp.* **2000**, *151* (1), 1521-3900.
228. Barrère, M.; Landfester, K., Polyester synthesis in aqueous miniemulsion. *Polymer* **2003**, *44* (10), 2833-2841.
229. Thies, C., *In Drugs and the Pharmaceutical Sciences* **1996**, *73*, 1-19.
230. Ley, S. V.; Ramarao, C.; Lee, A.-L.; Østergaard, N.; Smith, S. C.; Shirley, I. M., Microencapsulation of Osmium Tetroxide in Polyurea. *Organic Letters* **2003**, *5* (2), 185-187.
231. Pears, D. A.; Smith, S. C., *Aldrichim. Acta* **2005**, *38*, 23-33.
232. Sondi, I.; Fedynyshyn, T. H.; Sinta, R.; Matijević, E., Encapsulation of Nanosized Silica by in Situ Polymerization of tert-Butyl Acrylate Monomer. *Langmuir* **2000**, *16* (23), 9031-9034.
233. Ali, M. M.; Stöver, H. D. H., Polymeric Capsules Prepared by in Situ Synthesis and Cross-Linking of Amphiphilic Copolymer by Atom Transfer Radical Polymerization. *Macromolecules* **2003**, *36* (6), 1793-1801.
234. Hossain, M. D.; Kim, W. S.; Hwang, H. S.; Lim, K. T., Role of water on PMMA/clay nanocomposites synthesized by in situ polymerization in ethanol and supercritical carbon dioxide. *Journal of Colloid and Interface Science* **2009**, *336* (2), 443-448.
235. Gorrasi, G.; Tortora, M.; Vittoria, V.; Pollet, E.; Lepoittevin, B.; Alexandre, M.; Dubois, P., Vapor barrier properties of polycaprolactone montmorillonite nanocomposites: effect of clay dispersion. *Polymer* **2003**, *44* (8), 2271-2279.
236. Park, J. H.; Jana, S. C., Mechanism of Exfoliation of Nanoclay Particles in Epoxy-Clay Nanocomposites. *Macromolecules* **2003**, *36* (8), 2758-2768.
237. Fu, X.; Qutubuddin, S., Polymer-clay nanocomposites: exfoliation of organophilic montmorillonite nanolayers in polystyrene. *Polymer* **2001**, *42* (2), 807-813.
238. Binder, W. H.; Pulamagatta, B.; Kir, O.; Kurzhals, S.; Barqawi, H.; Tanner, S., Monitoring Block-Copolymer Crossover-Chemistry in ROMP: Catalyst Evaluation via Mass-Spectrometry (MALDI). *Macromolecules* **2009**, *42* (24), 9457-9466.
239. Pulamagatta, B.; Pankaj, S.; Beiner, M.; Binder, W. H., Hierarchical Nanostructures in Semifluorinated Norbornene Block Copolymers. *Macromolecules* **2011**, *44* (4), 958-965.
240. Kalluru, S. H.; Cochran, E. W., Synthesis of Polyolefin/Layered Silicate Nanocomposites via Surface-Initiated Ring-Opening Metathesis Polymerization. *Macromolecules* **2013**.
241. Behling, R. E.; Williams, B. A.; Staade, B. L.; Wolf, L. M.; Cochran, E. W., Influence of Graft Density on Kinetics of Surface-Initiated ATRP of Polystyrene from Montmorillonite. *Macromolecules* **2009**, *42* (6), 1867-1872.
242. Occhipinti, G.; Jensen, V. R.; Törnroos, K. W.; Frøystein, N. Å.; Bjørsvik, H.-R., Synthesis of a new bidentate NHC-Ag(I) complex and its unanticipated reaction with the Hoveyda-Grubbs first generation catalyst. *Tetrahedron* **2009**, *65* (34), 7186-7194.
243. Jlalía, I.; Elamari, H.; Meganem, F.; Herscovici, J.; Girard, C., Copper(I)-doped Wyoming's montmorillonite for the synthesis of disubstituted 1,2,3-triazoles. *Tetrahedron Letters* **2008**, *49* (48), 6756-6758.
244. Slade, P. G.; Gates, W. P., The swelling of HDTMA smectites as influenced by their preparation and layer charges. *Applied Clay Science* **2004**, *25* (1-2), 93-101.
245. Chusuei, C. C.; Brookshier, M. A.; Goodman, D. W., Correlation of Relative X-ray Photoelectron Spectroscopy Shake-up Intensity with CuO Particle Size. *Langmuir* **1999**, *15* (8), 2806-2808.

246. Nakamura, T.; Terashima, T.; Ogata, K.; Fukuzawa, S.-i., Copper(I) 1,2,3-Triazol-5-ylidene Complexes as Efficient Catalysts for Click Reactions of Azides with Alkynes. *Organic Letters* **2011**, *13* (4), 620-623.
247. Roşu, D.; Mustaţă, F.; Caşcaval, C. N., Investigation of the curing reactions of some multifunctional epoxy resins using differential scanning calorimetry. *Thermochimica Acta* **2001**, *370* (1–2), 105-110.
248. Besset, C.; Binauld, S.; Ibert, M.; Fuertes, P.; Pascault, J.-P.; Fleury, E.; Bernard, J.; Drockenmuller, E., Copper-Catalyzed vs Thermal Step Growth Polymerization of Starch-Derived α -Azide- ω -Alkyne Dianhydrohexitol Stereoisomers: To Click or Not To Click? *Macromolecules* **2010**, *43* (1), 17-19.
249. Roşu, D.; Caşcaval, C. N.; Mustaţă, F.; Ciobanu, C., Cure kinetics of epoxy resins studied by non-isothermal DSC data. *Thermochimica Acta* **2002**, *383* (1–2), 119-127.
250. Málek, J.; amp; x, Kinetic analysis of crystallization processes in amorphous materials. *Thermochimica Acta* **2000**, *355* (1–2), 239-253.
251. Park, B.-D.; Riedl, B.; Hsu, E. W.; Shields, J., Differential scanning calorimetry of phenol-formaldehyde resins cure-accelerated by carbonates. *Polymer* **1999**, *40* (7), 1689-1699.
252. Alzina, C.; Mija, A.; Vincent, L.; Sbirrazzuoli, N., Effects of Incorporation of Organically Modified Montmorillonite on the Reaction Mechanism of Epoxy/Amine Cure. *The Journal of Physical Chemistry B* **2012**, *116* (19), 5786-5794.
253. Thomas, R.; Sinturel, C.; Pionteck, J.; Puliyalil, H.; Thomas, S., In-situ Cure and Cure Kinetic Analysis of a Liquid Rubber Modified Epoxy Resin. *Industrial & Engineering Chemistry Research* **2012**, *51* (38), 12178-12191.
254. Garschke, C.; Parlevliet, P. P.; Weimer, C.; Fox, B. L., Cure kinetics and viscosity modelling of a high-performance epoxy resin film. *Polymer Testing* **2013**, *32* (1), 150-157.
255. Mirmohseni-Namin, A.; Nikafshar, S.; Mirmohseni, F., Increasing toughness and tensile strength of an epoxy-diamine system using an inorganic ultra-accelerator. *RSC Advances* **2015**, *5* (65), 53025-53035.
256. Chow, W. S.; Grishchuk, S.; Burkhart, T.; Karger-Kocsis, J., Gelling and curing behaviors of benzoxazine/epoxy formulations containing 4,4'-thiodiphenol accelerator. *Thermochimica Acta* **2012**, *543*, 172-177.
257. Shimbo, M.; Nakaya, T.; Takahama, T., Effects of tertiary amine accelerators on curing of epoxide resins. *Journal of Polymer Science Part B: Polymer Physics* **1986**, *24* (9), 1931-1941.
258. V. Strehmel; K. Deltshewa; H"ausler, K.-G.; K. Schr"oter, *Angew. Makromol. Chem.*, **1994**, *220*, 99-109.
259. Asano, K.; Matsubara, S., Effects of a Flexible Alkyl Chain on a Ligand for CuAAC Reaction. *Organic Letters* **2010**, *12* (21), 4988-4991.
260. Zheludkevich, M. L.; Serra, R.; Montemor, M. F.; Ferreira, M. G. S., Oxide nanoparticle reservoirs for storage and prolonged release of the corrosion inhibitors. *Electrochemistry Communications* **2005**, *7* (8), 836-840.
261. Borisova, D.; M"ohwald, H.; Shchukin, D. G., Mesoporous Silica Nanoparticles for Active Corrosion Protection. *ACS Nano* **2011**, *5* (3), 1939-1946.
262. Abdullayev, E.; Lvov, Y., Clay nanotubes for corrosion inhibitor encapsulation: release control with end stoppers. *Journal of Materials Chemistry* **2010**, *20* (32), 6681-6687.
263. Abdullayev, E.; Price, R.; Shchukin, D.; Lvov, Y., Halloysite Tubes as Nanocontainers for Anticorrosion Coating with Benzotriazole. *ACS Applied Materials & Interfaces* **2009**, *1* (7), 1437-1443.
264. Fix, D.; Andreeva, D. V.; Lvov, Y. M.; Shchukin, D. G.; M"ohwald, H., Application of Inhibitor-Loaded Halloysite Nanotubes in Active Anti-Corrosive Coatings. *Advanced Functional Materials* **2009**, *19* (11), 1720-1727.

265. Wang, Y.; Angelatos, A. S.; Caruso, F., Template Synthesis of Nanostructured Materials via Layer-by-Layer Assembly†. *Chemistry of Materials* **2008**, *20* (3), 848-858.
266. Schaeffel, D.; Staff, R. H.; Butt, H.-J.; Landfester, K.; Crespy, D.; Koynov, K., Fluorescence Correlation Spectroscopy Directly Monitors Coalescence During Nanoparticle Preparation. *Nano Letters* **2012**, *12* (11), 6012-6017.
267. Staff, R. H.; Schaeffel, D.; Turshatov, A.; Donadio, D.; Butt, H.-J.; Landfester, K.; Koynov, K.; Crespy, D., Particle Formation in the Emulsion-Solvent Evaporation Process. *Small* **2013**, *9* (20), 3514-3522.
268. Gragert, M.; Schunack, M.; Binder, W. H., Azide/Alkyne-“Click”-Reactions of Encapsulated Reagents: Toward Self-Healing Materials. *Macromolecular Rapid Communications* **2011**, *32* (5), 419-425.
269. Gorman, I. E.; Willer, R. L.; Kemp, L. K.; Storey, R. F., Development of a triazole-cure resin system for composites: Evaluation of alkyne curatives. *Polymer* **2012**, *53* (13), 2548-2558.
270. Brown, E. N.; Kessler, M. R.; Sottos, N. R.; White, S. R., In situ poly(urea-formaldehyde) microencapsulation of dicyclopentadiene. *Journal of Microencapsulation* **2003**, *20* (6), 719-730.
271. Lee, S. J.; Rosenberg, M., Microencapsulation of theophylline in whey proteins: effects of core-to-wall ratio. *International Journal of Pharmaceutics* **2000**, *205* (1), 147-158.
272. Hadjichristidis, N.; Iatrou, H.; Pispas, S.; Pitsikalis, M., Anionic polymerization: High vacuum techniques. *J. Polym. Sci. Part A Polym. Chem.* **2000**, *38* (18), 3211-3234.
273. Nolte, C.; Mayer, P.; Straub, B. F., Isolation of a Copper(I) Triazolide: A “Click” Intermediate. *Angewandte Chemie International Edition* **2007**, *46* (12), 2101-2103.
274. Donnelly, K. F.; Petronilho, A.; Albrecht, M., Application of 1,2,3-triazolylienes as versatile NHC-type ligands: synthesis, properties, and application in catalysis and beyond. *Chemical Communications* **2013**, *49* (12), 1145-1159.
275. Shaygan Nia, A.; Rana, S.; Döhler, D.; Osim, W.; Binder, W. H., Nanocomposites via a direct graphene-promoted “click”-reaction. *Polymer* **2015**, *79*, 21-28.
276. Warsink, S.; Chang, I. H.; Weigand, J. J.; Hauwert, P.; Chen, J.-T.; Elsevier, C. J., NHC Ligands with a Secondary Pyrimidyl Donor for Electron-Rich Palladium(0) Complexes. *Organometallics* **2010**, *29* (20), 4555-4561.

Eidesstattliche Erklärung

Ich versichere hiermit, dass ich die vorliegende Arbeit mit dem Thema: „Surface modification of nanofillers and encapsulation of healing agents for ROMP- and “click”-based self-healing polymer nanocomposites“ selbständig verfasst und keine anderen als die angegebenen Hilfsmittel benutzt habe. Die Stellen, die anderen Werken dem Wortlaut oder dem Sinn entnommen wurden, habe ich in jedem Einzelnen Fall durch Angabe der Quelle als Entlehnung kenntlich gemacht. Diese Arbeit wurde von mir in gleicher oder ähnlicher Form an keiner anderen Prüfungsbehörde vorgelegt.

Datum.....

Unterschrift des Antragstellers.....


Rochusstraße102

53123 Bonn

Tel.: 0172 – 672 1874

E-Mail:osim.wilton@yahoo.com

Lebenslauf

Persönliche Daten

Geburtsdatum, -ort	22.03.1983, Usumutong/Nigeria
Familienstand	verheiratet
Staatsangehörigkeit	nigerianisch
Einreise nach Deutschland	Oktober 2010
Aufenthaltstitel	Aufenthaltserlaubnis, Arbeitsaufnahme gestattet

Berufspraxis

10/2011 – 05/2018

Chemiker - Polymerchemie

Martin-Luther-Universität Halle-Wittenberg

- Entwicklung und Produktion von Mizellen als lang zirkulierende Arzneimittelabgabeträger
- Entwicklung von Formulierungen zur Langzeitstabilisierung der Drug Delivery-Systeme (beispielsweise mittels Gefriertrocknung)
- Detaillierte physikochemische Charakterisierung der kolloidalen Wirkstoffträger
- Synthese und Analyse neuer und bestehender Polymerzusammensetzungen
- Umfangreiche Erfahrung in der Synthese, Funktionalisierung und Konjugation chemischer Substanzen
- Dokumentation
- Endgruppenmodifikation von Polyisobutylen für Arzneimittelabgabeanwendungen
- Durchführung einer Studie über die Selbstorganisation von hydrophilen und amphiphilen modifizierten Nanopartikeln sowie proteins mit Langmuir-Blugget
- Durchführung eines Projekts zur Charakterisierung von Verbundwerkstoffen nach Anwendung von TGA und DSC.

02/2009 – 10/2010

Persönlicher Assistent des Landesbeauftragten für Gesundheit, Calabar/Nigeria

Federal Ministry of Health, Calabar/Nigeria

- Durchführung von Projekten im Bereich Gesundheitspolitik
- Organisation interner Vorgänge
- Vertragsdokumentation
- Vorbereitung und Koordination von Sitzungen
- Strategieentwicklung

Rochusstraße102

53123 Bonn

Tel.: 0172 – 672 1874

E-Mail:osim.wilton@yahoo.com

Promotion

07/2018

Ph.D. in Polymer Materials Science

Martin-Luther-Universität, Halle-Wittenberg

Dissertation: Surface modification of nanofillers and encapsulation of healing agents for ROMP- and „Click“-based self – healing composites

Studium

10/2018-01/2019

SAP Anwender PPM

Alfatraining Bildungszentrum

Bonn/Germany

Voraussichtlicher Abschluss:

SAP Anwender PPM

09/2018-10/2018

Project Management

Alfatraining Bildungszentrum

Bonn/Germany

Abschluss: Deutsche Gesellschaft für Projectmanagement.

Seit 05/2018

Project Management

Institute of Management - The Learning People

London/UK

Voraussichtlicher Abschluss:

Certified Associate Project Manager

10/2010 – 09/2012

Masterstudiengang Polymer Material Science

Martin-Luther-Universität, Halle-Wittenberg

Abschluss: Master of Science

Thesis: Synthesis and surface modification of polymer-functionalized MoS₂ nanoparticles for the stabilization of Pickering emulsion.

Projekt Thema: Synthesis and characterization of hydrophobic, hydrophilic and amphiphilic nanoparticles for drug delivery purposes.

01/2009–06/2009

Diplomstudiengang Aviation Management

College of Aviation and Management Studies,

Calabar/Nigeria

Abschluss: Advanced Diploma

09/2000 – 08/2005

Bachelorstudiengang Industriechemie

University of Calabar/Nigeria

Abschluss: Bachelor of Science

Rochusstraße102

53123 Bonn

Tel.: 0172 – 672 1874

E-Mail:osim.wilton@yahoo.com

Volontariat

09/2006 – 09/2007

Nachhilfelehrer für Physik, Chemie, Mathematik

Seed of Life College, Ibadan/Nigeria

Pacesetters College, Ibadan/Nigeria

09/2005 –10/2010

Project Manager

Sami Dave Global Foundation, Calabar/Nigeria

Ehrenamt

Seit 01/2018

Leiter des Projekts S.T.O.P

- Beratung und Unterstützung der jungen Generation, Lebensziele herauszufinden und erfolgreich umzusetzen

Seit 08/2018

Gemeindekoordinator Evangelische Gemeinde Köln-Kalk

- Betreuung der Gemeindeglieder

Seit 2012

Leiter des Musikprojekts „The Vessels“

- Heranführung von Kindern an World Music zur Integration
- Fundraising für die Unterstützung eines Waisenhauses in Halle/Saale

Schulbildung

1993 - 1999

Community Secondary School Itigidi/Nigeria

Abschluss: West African Examination Counsel (WAEC)

Sonstige Kenntnisse

Sprachen

Englisch

Muttersprache

Deutsch

B 1

IT

Origin Pro, Corel Draw, Chem Office, SciFinder, ISIS Draw, Materials Studio

Windows

MS Office

Führerschein

Klasse B, PKW vorhanden

Social Media

www.linkedin.com/in/wilton-osim-96416638

www.xing.com

Dr. Wilton Osim

Rochusstraße102

53123 Bonn

Tel.: 0172 – 672 1874

E-Mail:osim.wilton@yahoo.com

Bonn im January 2019

A handwritten signature in black ink, appearing to be 'W. Osim', written on a white background.

Kompetenzprofil Dr. Wilton Osim

Analyseverfahren

NMR, GPC, APM, SEC, TEM, SAXS, DSC, MALDI-TOF, WAXS, XRD, TGA, HPLC, UV-VIS, IR, Raman Spectroscopy, FE-SEM, Flame Calorimetry, ESI-TOF, DLS, DMA FTIR, tensile, rheology measurement

Polymerisationsverfahren

Living Carbocationic Polymerization (LCCP), Living Anionic Polymerization, Living Radical Polymerization (NMP, ATRP, RAFT), Ring Opening Metathesis Polymerization (ROMP), Polykondensation and Polyolefin Polymerisationen mit den Ziegler-Natta Katalysatoren

Kunststoffverarbeitung

Extrusion, Blasextrusion, Spritzguss, Blasformverfahren

Besondere Erfolge

- Herstellung, Modifikation und Charakterisierung von Nanopartikeln inkl. selbstheilender Nano-Verbundstoffe und Formulierung von Pickering Emulsionen
- Nachgewiesene Erfolge bei der Ideengebung in Wissenschaft und Industrie
- Erfolgreiche Charakterisierung von nachwachsenden und abbaubaren Polymeren, Verbundstoffen und Blockcopolymeren für Arzneimittelverabreichungen unter Berücksichtigung der Standard - Herstellungsprozesse